ABSTRACT

Title of dissertation: Large N_c Baryons and Baryonic Matter with Heavy Quarks
Prabal Adhikari, Doctor of Philosophy, 2014

Dissertation directed by: Dr. Thomas D. Cohen
Department of Physics
University of Maryland
College Park, MD 20742

In this dissertation, Quantum Chromodynamics (QCD) is explored at finite baryon density in a combined heavy quark and 't Hooft large N_c limit of QCD. Non-relativistic baryons are fully antisymmetric states containing N_c quarks; it was proposed by Witten that baryons can be described through a mean-field picture in which each quark moves in an average potential created by the remaining $N_c - 1$ quarks. A proof of this mean-field picture is constructed here. Additionally, the mean-field baryon problem is also considered in one spatial dimension, where the full relativistic baryon problem has been solved independently by Bringoltz. The ground state properties of single, isolated baryons and baryonic matter in 1+1 dimension is calculated using Witten's mean-field method and compared against the results of the Bringoltz method. Finally, saturated nuclear matter is studied in the combined limit in 3+1 dimensions, where the density of saturated nuclear matter is calculated.

Large N_c Baryons and Baryonic Matter with Heavy Quarks

by

Prabal Adhikari

Dissertation submitted to the Faculty of the Graduate School of the
University of Maryland, College Park in partial fulfillment
of the requirements for the degree of
Doctor of Philosophy
2014

Advisory Committee:
Dr. Thomas D. Cohen, Chair/Advisor
Dr. Paulo Bedaque
Dr. Elizabeth Jane Beise
Dr. Rabindra Mohapatra
Dr. William Walters

Dedication

To my parents.

Acknowledgments

First and foremost, I would like to thank my advisor Dr. Thomas D. Cohen, who has been a great source of guidance and support. His mentorship and constant encouragement made this thesis possible. I would also like to express my sincere gratitude to various members of TQHN: I would firstly like to express my thanks to Dr. Paulo Bedaque, Dr. Xiangdong Ji and Dr. Steven Wallace. I learned numerous ideas through various discussions and courses I took from them. I would also like to thank Dr. Naoki Yamamoto; the many discussions I had with him were enlightening. Finally I want to acknowledge the support of Loretta Robinette, Yuri Kubota and Heather Markle.

The funding for my research came from the Department of Energy (DoE) (Grant No. DEFG02-93ER-40762) and the Department of Physics Graduate Fellowship. My research activities that led to this dissertation would not have been possible without this support.

There have been many other people who have been of great support to me during my graduate school work at the University of Maryland. I would like to thank my brother, Prabin Adhikari, with whom I have had a common interest in physics since a very young age. He has been a great source of inspiration and support throughout my life. I would also like to thank Linda O'Hara and Jane Hessing for their incredible support especially during my early years in Maryland. I would also like to thank my friends Michael Baume and Guilherme Miranda for being there in times of need and times of fun.

I would also like to kindly remember all the teachers and friends at St. Xavier's School (Lalitpur, Nepal), where I spent my early, formative years. These years were truly special and I will never forget them. The dedication of the teachers truly made a difference in my life and for this I will be forever grateful. There are a few teachers I felt a special connection with and therefore, I would especially like to point out Mrs. Vinod Chettri (who taught me English and helped me through various health problems I suffered as a child) and Mr. Soongma Tuladhar (who taught me mathematics).

I would also like to thank all the teachers and friends at Budhanilkantha School (Kathmandu, Nepal), where I completed my A-Levels. The community was truly intellectually stimulating and I cannot emphasize how much I learned in my two years there.

I also want to thank Grinnell College for their financial generosity that allowed me to pursue a world-class undergraduate education. The community at Grinnell was unique and special. I would especially like to thank Dr. Jacob Willig-Onwuachi, my adviser, who supported me not only throughout college but also beyond. His advice has been truly invaluable as I look to begin a new chapter in my life. I would also like to thank Dr. William B. Case, from whom I took my first physics course in college. His lectureship was truly one of the best and most memorable. Finally, I would like to thank all my friends at Grinnell, especially Sheahan Virgin for his friendship and support (that made my transition to the United States easier) and for all the amazing intellectual discussions that were a huge part of our college lives.

Finally, I would like to thank my entire (extended family) including my broth-

ers Prajesh and Prabin, and my sister-in-law, Clare. Most importantly, I would like to thank my parents, who have made an incredible sacrifice over the past nine years. Since childhood, they have constantly dedicated themselves to finding the best education for me and my brothers. Their love, support and sacrifice are truly the reasons why I am here today.

Table of Contents

List of Tables

List of Figures

Chapter 1: Introduction

1.1 Motivation

QCD is the quantum field theory of strong interactions and is believed to explain a wide range of physical phenomena. The phenomena that is of relevance for this dissertation is the problem of infinite nuclear matter and saturated nuclear matter. It is currently not possible to study this problem directly from the QCD Lagrangian. In principle, this Lagrangian explains all physical phenomena involving strong interactions for a large variety of physical settings [1]. However, the problem of nuclear matter is inherently non-perturbative and as such there is no suitable expansion parameter. Therefore, the problem is extremely challenging.

There are numerous methods currently available to study QCD. [2] The first of these methods is lattice QCD [3]. It is the only available method to study QCD directly from the QCD Lagrangian and has been very successful in investigating a number of properties of QCD. For example, lattice QCD can be used to predict the masses of stable hadrons (at least the lightest ones). These include the pions and the baryon octet. Furthermore, it has also been used to characterize phase shifts in hadron scattering processes. As computer capacity increases rapidly with time, the range of predictions based on lattice QCD is expected to increase and

so is their accuracy. However, lattice QCD is dogged by a fundamental problem known as the fermion sign problem [4, 5], which means that there is no hope of solving the nuclear matter problem using current lattice methods. These methods use probabilistic (Monte-Carlo) techniques, which rely on the fermion determinant being positive definite. However, at finite baryon density (relevant for the nuclear matter problem) the fermion determinant takes on complex values and therefore is not positive-definite. Therefore, the probabilistic description necessary for lattice QCD breaks down and consequently the nuclear matter problem cannot be solved on the lattice [6–8].

Alternative methods to study QCD include the use of Effective Field Theories (EFTs). These methods are generally reliable for physical regimes in which there are large scale separations. In such circumstances, the symmetries of the relevant regime can be used to write down an effective lagrangian in a power counting scheme, where higher dimension operators are less relevant compared to low-dimension ones. An example of an EFT is chiral perturbation theory [9], which can be used to systematically study the behaviour of the lightest hadrons, namely the pions. These pions are the Goldstone bosons that arise due to chiral symmetry breaking by the ground state of QCD. Another physical regime, where EFTs are useful is the regime of asymptotically high baryon densities. As noted, no finite baryon density regime can be currently studied on the lattice. But EFT methods have been used to show that in this regime of high baryons densities, color-flavor-locked condensates of color superconductors form [10]. The primary appeal of these EFTs is that they can be used to study physical phenomena in a systematic fashion with corrections that are

controlled and well-understood in a physical way. As such the predictions are not only reliable but also model-independent and therefore apply generally to QCD.

The nuclear matter problem has been historically studied in the context of nuclear models, which are by construction unsystematic and give rise uncontrolled errors. A better approach is to systematically understand the nature of the many-body interactions between nucleons. But even this is incredibly difficult because the nuclear matter problem is non-perturbative (we know that nuclear matter saturates i.e. forms bound states). For example, non-perturbative effects such as the possible formation of weakly bound states such as the deuteron have to be taken into account when studying the problem of nucleon-nucleon scattering.

A method to understand nucleon interactions was proposed by Weinberg [11]. He suggested an effective field theoretic method whereby one first constructs a Lagrangian that captures the low-energy symmetries of QCD. This Lagrangian is then used to generate nucleon-nucleon potentials in a perturbative fashion and used to solve a Lippmann-Schwinger equation, which is known to be inherently non-perturbative. The method has been used quite successfully: for example, low-energy constants of Weinberg's EFT can be fit using scattering phase shifts and mixing parameters in scattering processes. Then further predictions of physical quantities such as delta mass splittings [12] and deuteron binding energies [13] can be made. However, the general problem of nuclear matter is much harder: it requires both qualitative and quantitative understanding of the nature of arbitrary n-body interactions, which is beyond the scope of even Weinberg's EFT.

Given this situation, it is useful to find tractable limits of QCD where analyt-

ical methods are of at least some value and some physical insights may be gained. One such limit of QCD (at finite baryon density) is the heavy quark limit and the 't Hooft large N_c limit of QCD, which when combined together provide a regime where analytical methods can be used to yield information such as baryon masses, interaction energies of baryonic matter (at least for parametrically low densities) and densities at which nuclear matter saturate. This particular combined heavy quark, large N_c limit of QCD is the primary focus of this dissertation.

The dissertation will be organized in the following way:

In the following sections of this chapter, firstly the QCD Lagrangian, its fundamental degrees of freedom and its non-perturbative nature is discussed. Then, a brief description of the 't Hooft large N_c limit of QCD is provided. Here, a brief argument of why large N_c limit of QCD is simplifying is discussed; in particular, the sub-leading role in the N_c power counting scheme played by interactions involving quark loops and non-planar Feynman diagrams is discussed. Finally, the nature of large N_c non-relativistic baryons with a particular focus on the heavy quark mass limit is discussed. The QCD Lagrangian is discussed in section 1.2, large N_c QCD is discussed in section 1.3 and non-relativistic baryons are discussed in section 1.4. Those familiar with this content can omit reading one or more of these sections.

Chapter 2 considers formal arguments that justify the treatment of large N_c baryons using a mean-field approximation [14], which was first considered in Ref. [15] by Witten. He argued that in the 't Hooft large N_c limit, each quark moves in an average color-Coulomb potential that arises due to gluon exchange interactions with

the remaining quarks and constructed a Hamiltonian for the non-relativistic case in three spatial dimension and for the relativistic case in one spatial dimension. The Hamiltonian for the non-relativistic case can be written down in many-body language in terms of one-body and two-body operators. Given that this Hamiltonian cannot be solved exactly, the chapter will discuss how a mean-field approximation with a baryonic, color-singlet, generalized coherent states basis as the variational space proves useful. Using properties of these coherent states, bounds on baryon masses and interaction energies are constructed such that the corrections associated with using a generalized coherent state are sub-leading in the large N_c expansion relative to the size of the observables (namely baryon masses and interaction energies) under consideration are found. The argument made in the chapter is completely general in the sense that it holds for an arbitrary number of baryons in a finite-sized but large box.

Chapter 3 is devoted to an application of the mean-field approximation (developed in the chapter 2) but only in one-spatial dimension [16]. The primary motivation for doing this stems from an independent but fully relativistic treatment of baryons and baryonic matter at leading order in N_c that was developed recently by Bringoltz [17, 18]. This treatment is applicable for arbitrary quark masses and was done in a finite sized box with periodic boundary conditions; remarkably, it was found that the relevant potential in a box is not simply a color-Coulomb potential (as one expects naively) of the form $|x-y|$, with x and y being two-points in the box but $x-y+QL$, with Q being an integer indicating the number of windings around a box of length L. In Chapter 3, it is shown that the the results based on this approach

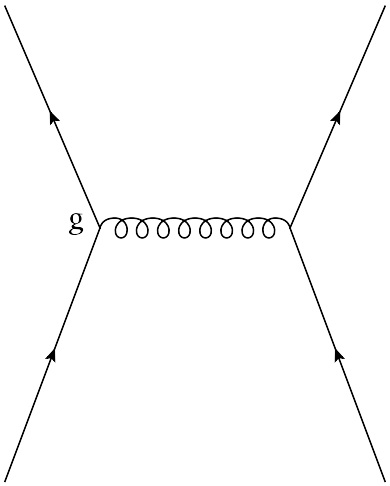

Figure 1.1: Interaction between two quarks via a gluon exchange

are consistent with baryons masses and interaction energies (at parametrically low densities) that were calculated using Witten's mean-field approximation.

Finally in Chapter 4, the problem of saturated nuclear matter in three spatial dimensions [19] is considered. It is shown that nuclear matter saturates at sub-leading order in the N_c expansion with a crystalline structure, which is either hexagonal-close packed or face-centered cubic with baryon densities of $\mathcal{O}\left(\frac{1}{(\ln N_c)^3}\right)$. The leading order interaction of baryons (in the same spin-flavor structure) is through the Pauli exclusion principle and is repulsive, whereas the sub-leading interaction is via the exchange of scalar glueballs, which is attractive. The nature of Pauli interaction is such that its strength becomes exponentially small with increasing baryon separation and the glueball interaction, even though sub-leading, is able to overcome the Pauli repulsion since the glueball interaction is longer-ranged. Here, it shown that these interactions lead to the binding of baryons into a self-saturated crystal.

1.2 QCD Lagrangian

QCD, as discussed previously, describes a very rich array of phases and physical phenomena and the Lagrangian that encodes all this information is written in terms of the fundamental degrees of freedom, which are the quarks, Ψ and the gluons, A.

$$\mathcal{L}_{\rm QCD} = -\frac{1}{4g^2}{\rm Tr}\ F_{\mu\nu}F^{\mu\nu} + \sum_{\rm f}\bar{\Psi}_{\rm f}\left(i\gamma^\mu D_\mu + \gamma^0\mu_{\rm f} - m_{\rm f}\right)\Psi_f\ , \tag{1.1}$$

where the covariant derivative, $D_\mu = \partial_\mu - iA_\mu$, with $A_\mu = A^a_\mu T^a$, with T^a, where $a = 1,\ 2,\ \cdots,\ 8$ are traceless 3×3 Hermitian matrices. Note that Latin characters are used to denote the color indices and Greek characters to denote the Dirac indices. The index f in $\Psi_{\rm f}$ denotes the various quark flavors - which could be up, down, strange, top, bottom or charm with $m_{\rm f}$ being the masses the various quark flavors. However, the color and Dirac indices have been suppressed from $\Psi_{\rm f}$. $\mu_{\rm f}$ is the chemical potential of quarks with flavor quantum number f and F is the gluon field strength tensor, which is defined as

$$F^a_{\mu\nu} \equiv \partial_\mu A^a_\nu - \partial_\nu A^a_\mu + g f^{abc} A^b_\mu A^c_\nu\ , \tag{1.2}$$

with f^{abc} being the structure constants of $SU(3)$ color.

The various interactions between quarks and gluons in QCD can be deduced from the Lagrangian. The most fundamental of these interactions is depicted in Fig. 1.1. It is the interaction between two quarks, which is mediated by the gluons, with g being the strength of the coupling between a quark and a gluon. This interaction is analogous to the interaction between electrons (that carry electromagnetic charges) via a photon exchange. However, the mediating particles in QCD, the glu-

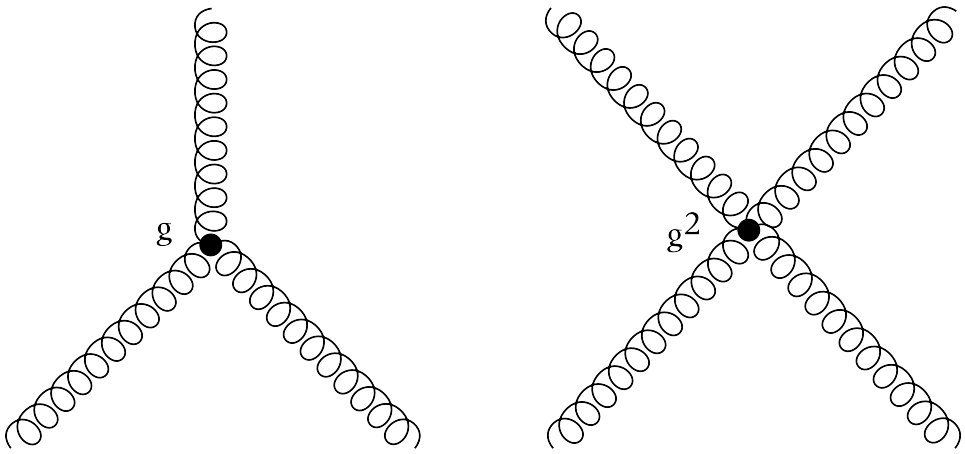

Figure 1.2: The diagram on the left depicts a three-gluon interaction, which has a vertex of order g and the diagram on the right depicts a four-gluon interaction, which has a vertex of order g^2

ons, also carry a color charge and as a result can interact among themselves. This is quite unlike QED, where photons carry no electromagnetic charge and hence do not interact with each other. There are two possible ways in which gluons interact: as depicted in Fig. 1.2, they either interact through a three-gluon vertex, which has a strength of size g or through four-gluon interaction, where the vertex is of strength g^2.

While the basic interactions of QCD can be easily understood in terms of Feynman diagrams, it is generally impossible to derive first principle results for low momentum observables from QCD owing to the strength of the coupling constant g, which can be derived using renormalization group flow. Only the result is presented

here [20]; it is as follows:

$$g^2(Q) = \frac{g^2(\mu)}{1 + \frac{1}{16\pi^2}\left(\frac{11}{3}N_c - \frac{2}{3}N_f g^2 \log\left(\frac{Q^2}{\mu}\right)\right)} \tag{1.3}$$

with $g(\mu)$ representing the strength of the quark-gluon coupling constant at momentum scale μ, N_c representing the number of colors, which is 3 for the real world and N_f the number of quark flavors, which is believed to be 6 in the real world. There is a regime where as $Q \to \infty$, $g \to 0$ logarithmically and quarks behave as if they are free. This behavior is known as *asymptotic freedom* and in this particular regime QCD can be studied perturbatively. This regime includes, for example, high-energy scattering processes. Additionally, certain aspects of high temperature QCD, where a quark-gluon plasma is expected to exist also seems tractable perturbatively. However, much of the hadronic world including the problem of cold nuclear matter is in a regime of small baryon densities. g is not a small parameter and therefore the problem cannot be treated non-perturbatively.

As mentioned in the motivation section, there are alternative methods of studying QCD, either through the use of effective field theory methods or through the use of lattice QCD, which are both inadequate to study the nuclear matter problem. There are no available EFTs to understand the many-body interactions of the nuclear matter problem and certain observables of lattice QCD is dogged by the infamous fermion sign problem. This means that while lattice QCD can be performed at finite temperatures and finite isospin density, the finite baryon density regime is not tractable. It cannot be accessed because current lattice based methods (i.e. the path integral approach) rely on probabilistic approaches which break down at

finite baryon density. The problem is such that for the foreseeable future, computing resources cannot overcome it.

Given that non-perturbative QCD at finite baryon density can neither be solved analytically nor numerically, it is useful to find ways to get insight into the problem by considering a more tractable limit of QCD, known as the 't Hooft large N_c limit. Formally, this is the limit where $N_c \to \infty$ with the quantity $g^2 N_c$ held fixed to be of $\mathcal{O}(N_c^0)$. This limit is considered in Section 1.3.

1.2.1 Color Confinement

Before proceeding to study the large N_c limit, it is useful to point out an important property of low-energy QCD, which will be assumed to hold for the rest of this dissertation, namely that of *color confinement*. While at high-energies quarks behave as if they are free, free quarks have never been observed in nature. In fact, they are always found to be confined (at least in the low energy regime) within color-singlet states such as baryons and mesons. For the case of arbitrarily heavy quarks, there is some interesting evidence for confinement from lattice QCD. It is observed that the strength of the potential between a fundamental quark source and an anti-fundamental quark source becomes linear with increasing separation implying that it would take an infinite amount of energy to separate a quark anti-quark pair and therefore impossible. The behaviour is more complicated generally in QCD for relativistic quark-anti-quark pairs or other color-singlet configurations. But it is expected that as a fundamental quark source and an anti-fundamental

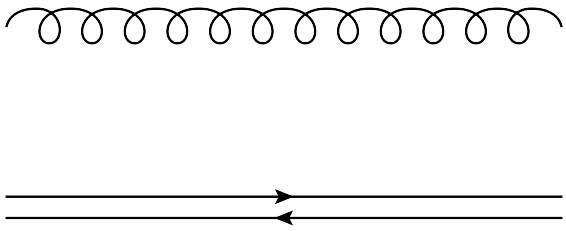

Figure 1.3: The 'tHooft double line notation for gluons

quark source is pulled apart flux-tubes (which are basically strings made of gluons) form, which eventually break leading to the formation of additional quark-antiquark pairs.

In the context of the problem of baryon and baryonic matter, it will be assumed in this dissertation that cold nuclear matter is a color-singlet state. More specifically, only a subspace of color-singlet states with some baryon number B (in the Fock space of all possible non-relativistic states) will be considered.

1.3 Large N_c QCD

In the 't Hooft large N_c limit of QCD [21–24], the quantity $g^2 N_c$ is held fixed as N_c is increased such that the coupling constant, g, scales as $\sqrt{\frac{1}{Nc}}$. For large enough N_c, g is small. In order to illustrate the simplifications that arise in the 't Hooft large N_c limit, vacuum polarization diagrams of gluons, which are the gauge bosons that mediate color forces between quarks, will be considered. In particular, there are two important simplifications that arise in the 't Hooft large N_c limit. They are as follows:

1. Only planar vacuum polarization diagrams contribute at leading order in the N_c

expansion.

2. Vacuum polarization diagrams with quark loops contribute only at sub-leading orders in the N_c expansion. In particular, they are at most of $\mathcal{O}\left(\frac{1}{N_c}\right)$.

In order to illustrate these simplifications, it is useful to draw a 't Hooft diagram in addition to a Feynman diagram. 't Hooft diagrams were first used by Gerardus 't Hooft, who invented the large N_c limit, and further invented the diagrams as a means way of understanding color-flow in interactions between quarks, anti-quarks and gluons. In this diagram, quark fields, q^a, are indicated by a single line with an arrow pointing forward. The index a runs from 1 to N_c. Antiquark fields, $\bar{q}_a$, come with a lower color index and is represented by a line with an arrow pointing in the backward direction. Gluons fields are different in that they are not in the fundamental and anti-fundamental representation like the quarks and anti-quarks repectively, but in the adjoint representation of the color-group. They are denoted by A^a_b with each of the indices going from 1 to N_c. They are represented using double lines (see Fig. 1.3); this is sensible since in color space, gluons transform in a manner analogous to a quark-anti-quark bilinear. In other words, both a quark-anti-quark bilinear and gluons have two color indices.

1.3.1 Planar Diagrams

It is helpful to consider gluon vacuum polarization diagrams in order to understand the first simplication. The first diagram (Fig. 1.4) consists of two three-gluon

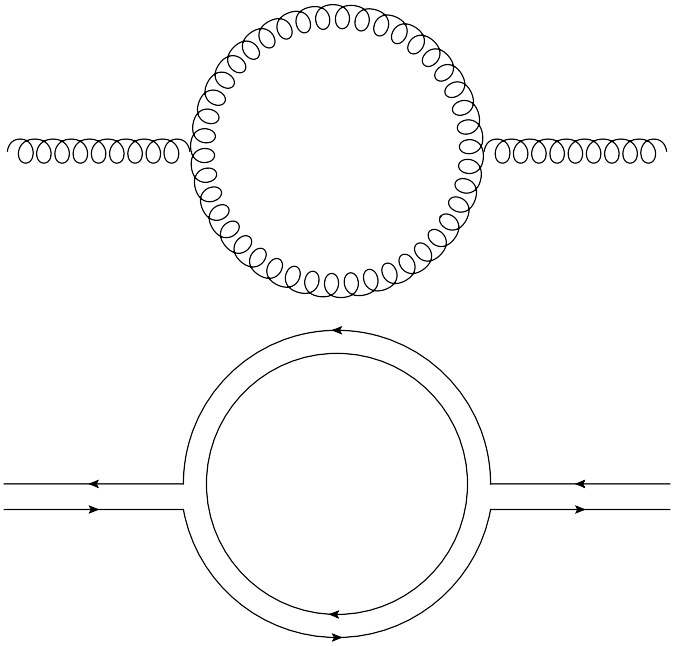

Figure 1.4: The simplest gluon polarization diagram

interaction vertices and a one-gluon loop. Using the 't Hooft diagram, it is easy to see that there is a single color loop in the diagram. This loop contributes at $\mathcal{O}(N_c)$ and the two vertices, each contribute at $\mathcal{O}\left(\frac{1}{\sqrt{N_c}}\right)$. Therefore, the diagram is of $\mathcal{O}(N_c^0)$.

Next, a slightly more complicated vacuum polarization diagram in Fig. 1.5 will be considered. It is a one-particle irreducible gluon polarization diagram involving two gluon loops instead of one as in the previous case. Since, the diagram consists of four three-gluon vertices and two color loops, it contributes at $\mathcal{O}(N_c^0)$, which is the same order as that of the first diagram.

Next, a one-particle irreducible gluon polarization diagram with three gluons loops is considered. The diagram illustrated in Fig. 1.6 consists of six three-gluon vertices and three color loops. Therefore, it contributes again at $\mathcal{O}(N_c^0)$.

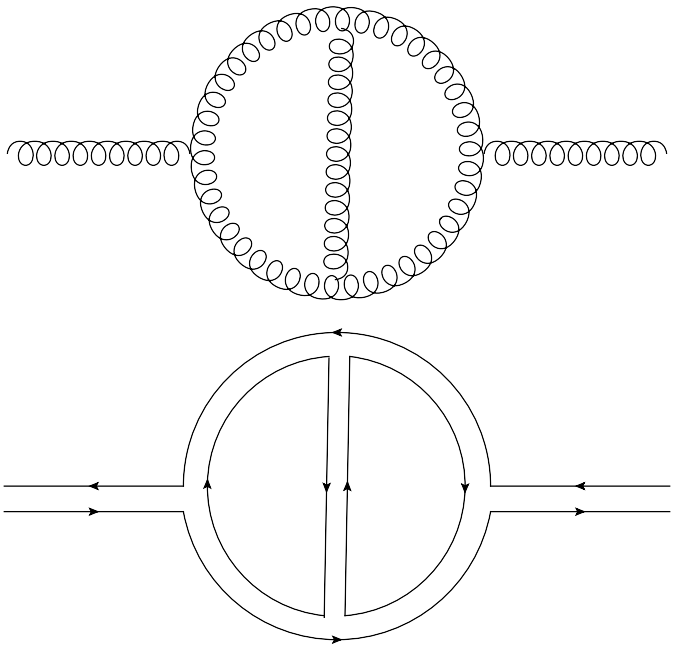

Figure 1.5: A one-particle irreducible two-loop gluon polarization diagram

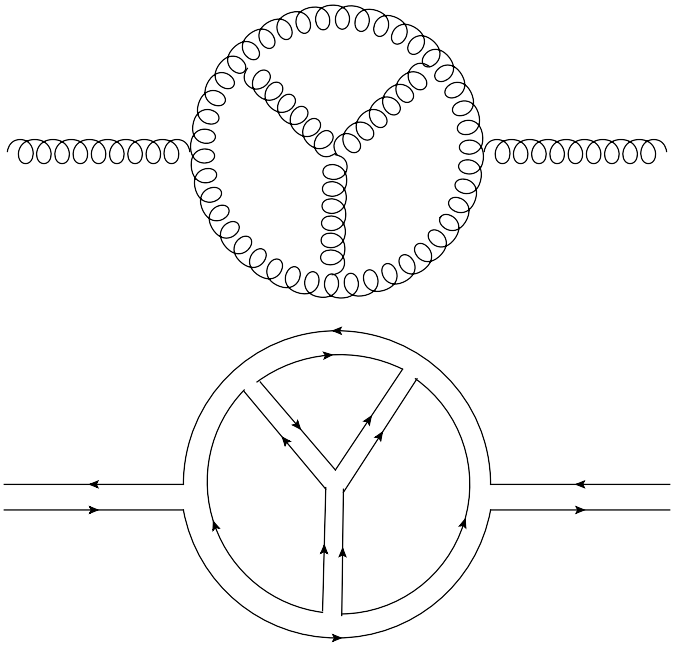

Figure 1.6: A one-particle irreducible three-loop gluon polarization diagram

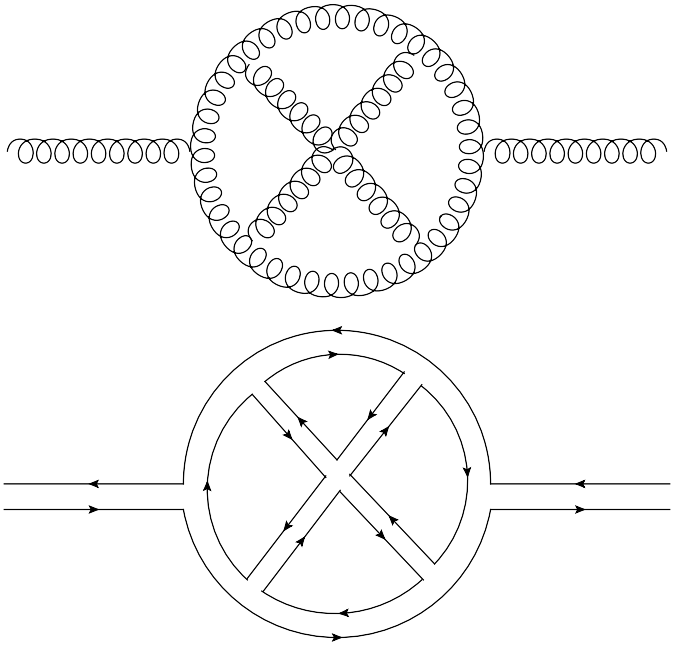

Figure 1.7: A one-particle irreducible four-loop gluon polarization diagram with a four-gluon vertex

The final planar diagram considered (see Fig. 1.7) is a one-particle irreducible gluon polarization diagram with four gluon loops and a four-gluon vertex, which comes with a factor of g^2 instead of g for three-gluon vertices. Since the diagram consists of four loops, six three-gluon vertices and a four-gluon vertex, the total contribution of this diagram is again $\mathcal{O}(N_c^0)$.

From the four examples of planar diagrams illustrated above it is clear that for each additional loop (which is of $\mathcal{O}(N_c)$) that is added while maintaining one-particle-irreducibility of the diagrams, there is an additional factor of $\mathcal{O}(g^2)$, which is picked up due to the addition of two-vertices for every loop that is added to the gluon-polarization diagram. Indeed, it can be shown to all orders in g^2 that all such planar diagrams with only gluons (one-particle irreducible or not), contribute

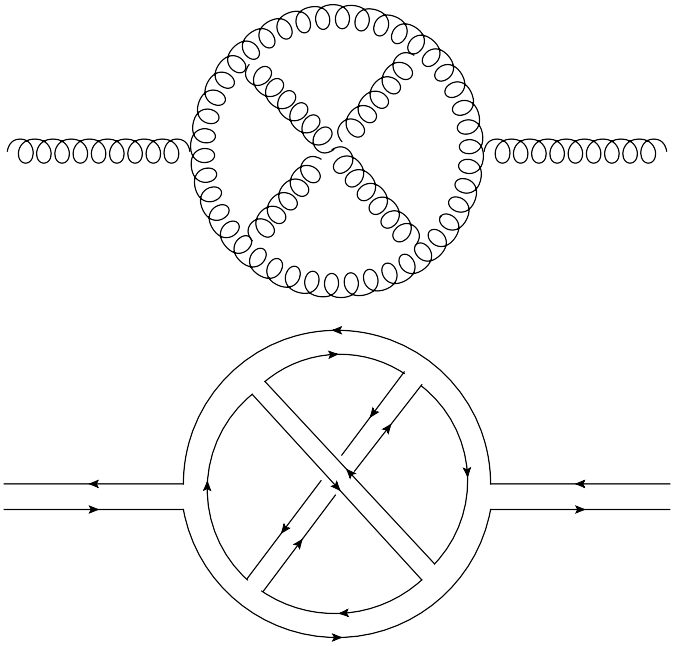

Figure 1.8: A non-planar gluon polarization diagram

exactly at $\mathcal{O}(N_c^0)$.

1.3.2 Non-planar diagrams

Only planar diagrams have been considered so far. Next, a modification of Fig. 1.7 is made such that the four-gluon vertex is removed and the diagram becomes non-planar. The modification gets rid of the four-gluon coupling of $\mathcal{O}(g^2)$ but also reduces the number of color loops from four to one, hence reducing the order of the diagram by N_c^3. By virtue of the fact that the diagram now only has six three-gluon vertices and a single color loop, the diagram is of $\mathcal{O}\left(\frac{1}{N_c^2}\right)$. As such, it only contributes at a sub-leading order in the N_c expansion relative to the planar diagram. While only a single example of a non-planar diagram contributing at sub-leading order in the N_c expansion has been considered, it is not difficult to see that the

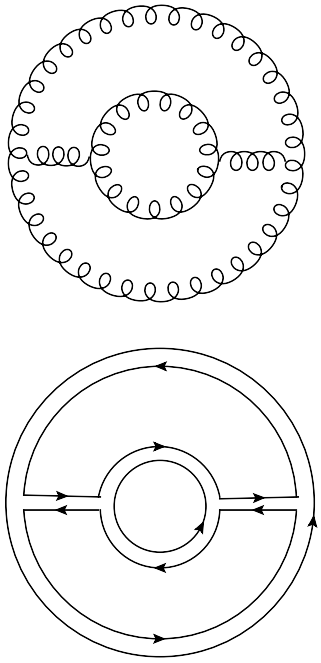

Figure 1.9: A gluon polarization diagram with no quark loops

result is far more general, a proof of which is discussed in Ref. [21].

1.3.3 Diagrams with Quark Loops

A second simplification of the 't Hooft large N_c limit is that diagrams with quark loops contribute at sub-leading order relative to diagram with only gluon loops. In order to illustrate this point, consider two gluon polarization diagrams of Figs. 1.9 and 1.10. The diagram in Fig. 1.10 is the same as the diagram in Fig. 1.9 but with one of the gluon loops being replaced by a quark loop. It is straightforward to see that the diagram with the quark loop is down by $\mathcal{O}\left(\frac{1}{N_c}\right)$ compared to the one with only gluon loops, the reason being that the quark loop in the middle only carries a single color while a gluon loop would have carried N_c different colors.

It is clear from the discussion above that large N_c QCD is considerably simpler than QCD with $N_c = 3$ because gluons play a dominant role in the interaction between any two quarks and also that gluon diagrams that are non-planar play a sub-leading role. However, this is not to say that large N_c QCD can be fully solved in three dimensions. While coupling constant, g is small in the 't Hooft large N_c limit, there are an infinite number of diagrams at each order that need to be summed. However, there are no known methods of doing so in three spatial dimensions.

It turns out, however, the one spatial dimension version of large N_c QCD can been solved [17, 18, 21, 22] for both the meson spectrum and baryon masses as a function of the constituent quark masses (including baryonic matter interaction energies). The reason for this is that gluons do not propagate in one spatial dimension and by an appropriate choice of gauge, gluon-gluon interaction vertices are absent.

1.4 Non-Relativistic Baryons at Large N_c QCD

It is well-known that non-relativistic baryons are totally antisymmetric (i.e. fermionic) states with N_c fundamental quarks, where each of the N_c quarks belongs to a distinct color state different from all the other quarks. In other words, baryons (including baryonic matter) are color-singlets [25–27].

Non-relativistic baryons in N_c color QCD are similar to the 3-color world in that they are color-singlet states with the states being anti-symmetric with respect color and symmetric with respect to the remaining degrees of freedom including flavor, spin and space. However, the obvious difference is the fact that in large N_c

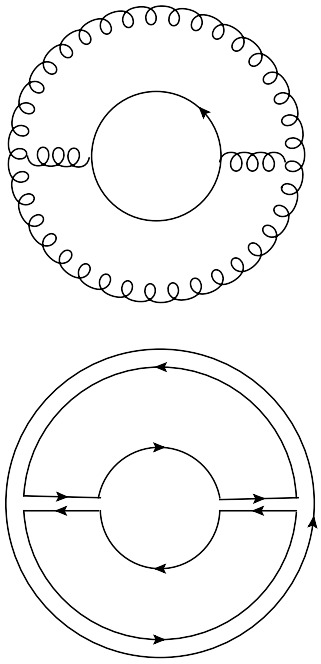

Figure 1.10: A gluon polarization diagram with a single quark loop but otherwise equivalent to Fig. 1.9

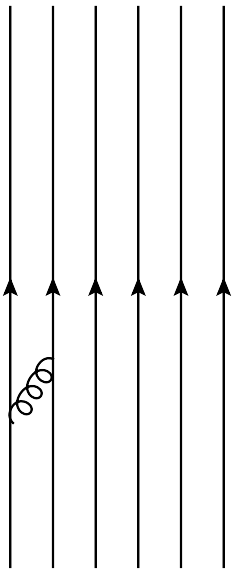

Figure 1.11: A single gluon exchange interaction in a baryon

QCD, baryons are composed of N_c quarks, N_c is only three in the real world. This distinction leads to a physical picture for baryons at large N_c, which is not true for the three-color world, namely the N_c scaling of the masses of large N_c baryons and the applicability of mean-field theory, which will be pursued in the following sections. These ideas were first suggested by Witten [15] and in this section only his heuristic arguments suggesting the N_c scaling of baryon masses is considered.

1.4.1 N_c scaling of baryon mass

In this subsection, arguments first given by Witten in Ref [15] exhibiting that baryon masses scale as N_c will be presented. But before proceeding with that argument, Feynman diagrams that contribute to baryon masses will be considered.

1.4.1.1 Divergence of Baryonic Feynman Diagrams

The first diagram is a single gluon exchange diagram of Fig. 1.11. The diagram consists of two quark-gluon vertices which from the QCD Lagrangian is of $\mathcal{O}(g^2)$. However, there is also a combinatoric contribution that arises due to the fact that the single gluon exchange may occur between any of $\frac{N_c(N_c-1)}{2}$ possible pairs of quarks. In the large N_c limit, there are $\mathcal{O}(N_c^2)$ pairs, which combined with the fact that the vertices contribute an $\mathcal{O}(g^2)$ means that this diagram contributes at $\mathcal{O}(N_c)$.

However, a diagram with two-gluon exchange contributes at a higher order than the single-exchange diagram. In Fig 1.12, is a two-gluon exchange diagram. This diagram has four quark-gluon vertices, which are of total order g^4. The combinatorics are such that there are a possible $\frac{N_c(N_c-1)(N_c-2)(N_c-3)}{4!}$ sets of four quarks, assuming that each quark can only undergo at most a single gluon exchange. In effect, therefore the diagram contributes at $\mathcal{O}(N_c^4 g^4) = \mathcal{O}(N_c^2)$.

Therefore, with an increasing number of gluon exchanges, the Feynman diagrams become more divergent in N_c power counting. More precisely, for n gluon exchanges, the Feynman diagram contributes at $\mathcal{O}(N_c^{n-2})$ assuming $N_c \gg n$. Therefore, a Feynman diagrammatic analysis is hopeless as far as determining properties of baryons in the large N_c limit is concerned. Naively, one may think that that this means that baryon masses diverge with N_c faster than a power law. However, it turns out that the facts that the Feynman diagrams diverge and that baryon masses scale as N_c are easily reconcilable.

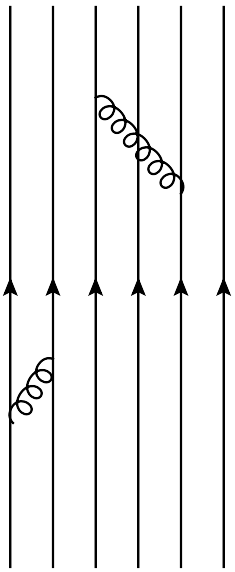

Figure 1.12: A double gluon exchange interaction in a baryon

1.4.1.2 Contributions to Baryon Mass

In order to do so, consider the various contributions to baryon masses in the large N_c limit. As first argued by Witten [15], there are three distinct contributions to the baryon mass, which are as follows:

1. the quark mass, m_q, contribution from N_c quarks
2. the quark kinetic energy, t_q, contribution from N_c quarks, and
3. the potential energy due to the interaction via gluon exchange between quarks.

It is trivial to see that the baryon masses scale as $N_c m_q$ with respect to the baryon mass and $N_c t_q$ with respect to the quark kinetic energy. However, it turns out that the potential energy contribution to the baryon mass also scales with N_c.

Assume that the potential energy associated with one gluon exchange is $g^2 V$,

where V is a $\mathcal{O}(N_c^0)$ contribution. It is natural to expect the potential term then scales as N_c since the potential between two quarks acts between $\frac{N_c(N_c-1)}{2}$ pairs, making the overall contribution to the quark mass from the potential energy to be of $\mathcal{O}(N_c)$. In other words, the baryon mass m_B scales with N_c in the following way:

$$m_B = N_c m_q + N_c t_q + \frac{N_c(N_c-1)}{2}\left(g^2 V\right) = N_c\left(m_q + t_q + \frac{1}{2}V + \mathcal{O}(N_c^0)\right) \ , \quad (1.4)$$

where the fact that g^2 scales as $\frac{1}{N_c}$ in the 't Hooft large N_c limit has been used to obtain the second equality.

Using this fact, it is straightforward to understand the increasing divergence of the gluon-exchange diagrams discussed in the previous subsection. The amplitude of the propagating baryons at time T is given by $\exp(-im_B T)$ with m_B defined above. Noting that the potential term above comes in power of g^2, this amplitude scales in the following way in perturbation theory, with g^2 being the expansion parameter.

$$\begin{aligned}
&\exp(-im_B T) \\
=&\exp(-iN_c(m_q + t_q + g^2 N_c V/2)T) \\
=&\exp(-iN_c(m_q + t_q)T)\exp((g^2 N_c^2 V/2)T) \\
=&\exp(-iN_c(m_q + t_q)T)(1 + \text{term of } \mathcal{O}(g^2 N_c^2) + \text{term of } \mathcal{O}(g^4 N_c^4) + \cdots)
\end{aligned} \quad (1.5)$$

Therefore, in a perturbative expansion in g^2, the higher order diagrams i.e. diagrams involving more gluon exchanges become more divergent in N_c, which is what was observed in the Feynman diagrammatic analysis earlier in the section. However, this divergence is not a problem as long as a full non-perturbative analysis of baryonic properties is performed.

1.4.2 Mean Field Approximation of Heavy Quark Baryons

A means of doing such a non-perturbative analysis was first argued by Witten. It was argued heuristically that in large N_c baryons each quark moves in an average potential created by the remaining $N_c - 1$ quarks.

The fully relativistic mean-field approximation for the large N_c baryons is still quite complicated. Here, only a simpler problem is pursued: namely the case of large N_c baryons in the limit where the quark masses, m_q, are much larger than the QCD scale i.e. $m_q \gg \Lambda_{\rm QCD}$ and therefore, can be described non-relativistically. In this limit a number of important simplifications happen, which are as follows:

1. Since the quarks are heavy, quark loops are suppressed as $\mathcal{O}\left(\frac{1}{m_q}\right)$;

2. Gluon-gluon interactions are suppressed since they are of $\mathcal{O}(g^2)$ and g is small (albeit logarithmically) for large quark masses [1] and

3. Color magnetic effect interactions are suppressed since they are $\mathcal{O}\left(\frac{1}{m_q}\right)$.

1.4.3 Non-Relativistic Hamiltonian for Baryons

These simplifications mean that the non-relativistic Hamiltonian can be written down in many-body language and it is as follows:

$$\begin{aligned}\hat{H} = &\int d^3\vec{x}\ \hat{\psi}_a^\dagger(\vec{x}) \left(m_q - \frac{\vec{\nabla}^2}{2m_q}\right) \hat{\psi}_a(\vec{x}) \\ &+ g^2 T^A_{aa'} T^A_{bb'} \int d^3\ \vec{x} d^3\ \vec{y}\ V(|\vec{x}-\vec{y}|) \hat{\psi}_a^\dagger(\vec{x}) \hat{\psi}_{a'}^\dagger(\vec{y}) \hat{\psi}_{b'}(\vec{y}) \hat{\psi}_b(\vec{x})\ ,\end{aligned} \tag{1.6}$$

[1] As discussed in Ref. [28], in the combined heavy quark mass and large N_c limit, $g^2 N_c \sim \frac{1}{\log(\frac{m_q}{\Lambda_{\rm QCD}})}$, where $\Lambda_{\rm QCD}$ is the scale at which g is of order one.

where the four-Fermi interaction term has being deduced from the QCD Lagrangian. Here, $V(|\vec{x}-\vec{y}|)$ is the color-Coulomb potential, which with V being the color-Coulomb potential [2], which has the following form

$$\begin{aligned} V(|\vec{x}-\vec{y}) &= -\frac{1}{|\vec{x}-\vec{y}|} \text{ in 3 spatial dimensions} \\ V(r) &= +|\vec{x}-\vec{y}| \text{ in 1 spatial dimension.} \end{aligned} \tag{1.7}$$

In Chapter , the three-dimensional version in the context of saturated nuclear matter will be considered and the one-dimensional version will be considered in Chapter 3 in the context of numerically checking results that are derived in Chapter 2. The difference in sign in three and one spatial dimensions arises because the zero of the potential is defined at infinity in three spatial dimensions and at the origin in one spatial dimension.

Also, note that here $T^A = \frac{\lambda^A}{2}$ with λ^A being the large N_c generalization of the Gell-mann matrices the index $A = 1, \cdots N_c^2 - 1$ running over the $N_c^2 - 1$ gluon colors. T^A is traceless and is normalized such that $\mathrm{tr}(\mathrm{T^A T^B}) = \frac{1}{2}\delta^{\mathrm{AB}}$. There is a useful identity for the product of two T^A, which appears in the interaction term in the Hamiltonian above. It is as follows:

$$T^A_{aa'} T^A_{bb'} = \frac{1}{2}\delta_{ab'}\delta_{a'b} - \frac{1}{2N_c}\delta_{aa'}\delta_{bb'}. \tag{1.8}$$

Using the above identity the two different four-heavy-quark interaction terms can be simplified. The first is known as the Fock term and its contribution to the

[2]The Coulombic nature of the potential is somewhat motivated also from lattice QCD involving a heavy quark-anti-quark pair. The corrections to the potential are logarithmic.

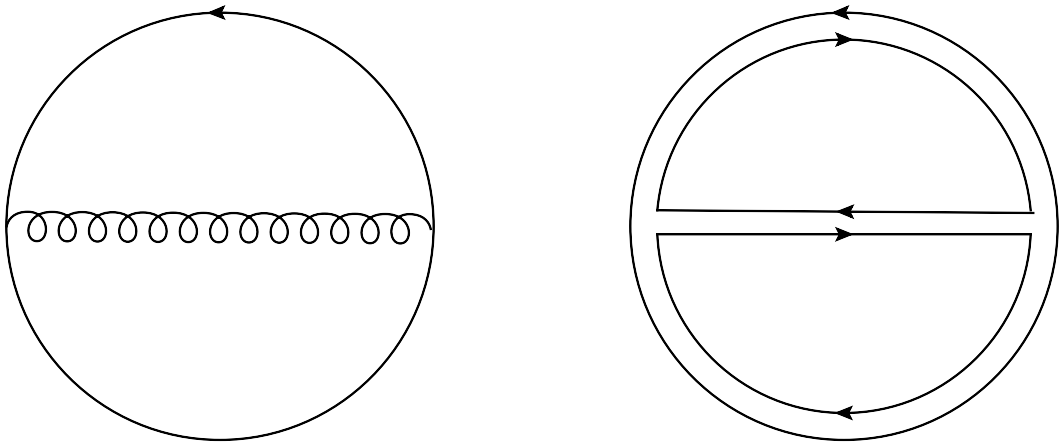

Figure 1.13: Position space Feynman diagram showing the Fock interaction

Hamiltonian is:

$$\begin{aligned}&\frac{g^2}{2}\delta_{ab'}\delta_{a'b}\int d^3\vec{x}d^3\vec{y}\; V(|\vec{x}-\vec{y}|)\hat{\psi}_a^\dagger(\vec{x})\hat{\psi}_{a'}^\dagger(\vec{y})\hat{\psi}_{b'}(\vec{y})\hat{\psi}_b(\vec{x})\\ =&\frac{g^2}{2}\int d^3\vec{x}d^3\vec{y}\; V(|\vec{x}-\vec{y}|)\hat{\psi}_a^\dagger(\vec{x})\hat{\psi}_b^\dagger(\vec{y})\hat{\psi}_a(\vec{y})\hat{\psi}_b(\vec{x})\;,\end{aligned} \tag{1.9}$$

This term represents an interaction where a quark of color a is produced at point $\vec{x}$, quark of color b is produced at point $\vec{y}$ with the color a quark annihilated at point $\vec{y}$ and the color b quark annihilated at point $\vec{x}$. A diagrammatic representation is presented in Fig. 1.13. From the diagram, it is clear that there are two color loops each of $\mathcal{O}(N_c)$ and two vertices of combined $\mathcal{O}(g^2)$. Therefore, the diagram contributes at $\mathcal{O}(N_c)$, which is what one expects if Witten's heuristic argument were correct.

The second term is known as the Hartree term and its contribution to the non-relativistic baryonic Hamiltonian operator is of the form:

$$\begin{aligned}&\frac{g^2}{2N_c}\delta_{aa'}\delta_{bb'}\int d^3\vec{x}d^3\vec{y}\; V(|\vec{x}-\vec{y}|)\hat{\psi}_a^\dagger(\vec{x})\hat{\psi}_{a'}^\dagger(\vec{y})\hat{\psi}_{b'}(\vec{y})\hat{\psi}_b(\vec{x})\\ =&\frac{g^2}{2N_c}\int d^3\vec{x}d^3\vec{y}\; V(|\vec{x}-\vec{y}|)\hat{\psi}_a^\dagger(\vec{x})\hat{\psi}_a^\dagger(\vec{y})\hat{\psi}_b(\vec{y})\hat{\psi}_b(\vec{x})\;.\end{aligned} \tag{1.10}$$

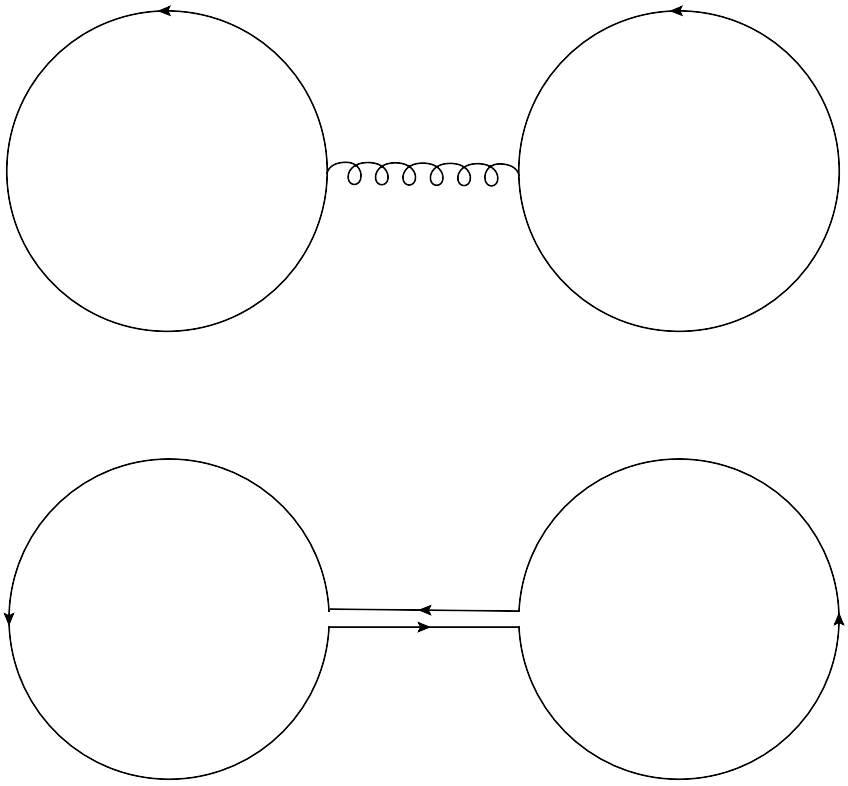

Figure 1.14: Position space Feynman diagram showing the Hartree interaction

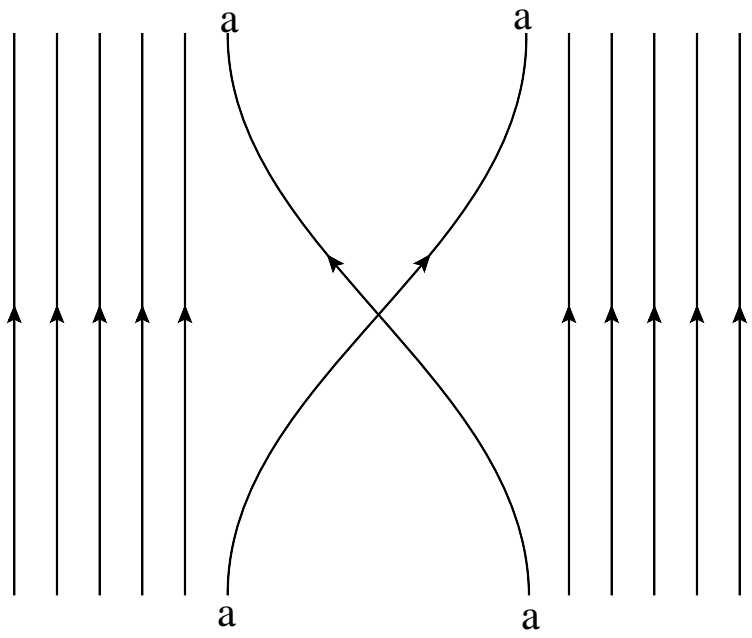

Figure 1.15: A gluonless baryon-baryon interaction via quark exchange

This term represents a quark of color a that is created at point $\vec{x}$ and also annihilated at the same point $\vec{x}$; additionally, another quark of color b is created at point $\vec{y}$ and also destroyed at the same point. The interaction is shown in a (position space) Feynman diagram of Fig. 1.14. Note that while there are two quark-gluon vertices there is only one color-flow loop owing to the fact that the colors are fixed by the two quark loops. Therefore, the diagram is of $\mathcal{O}(g^2) = \mathcal{O}\left(\frac{1}{N_c}\right)$ and the contribution from the Hartree term is suppressed by a relative order of N_c compared to the Fock term. Note that when Witten first considered this argument he assumed that it was actually the Fock term that was suppressed in the large N_c limit and not the Hartree term, as it has been shown here.

1.4.4 Baryon-baryon Interactions

The primary objective of this dissertation is to pursue the problem of cold nuclear matter in the combined large N_c and heavy quark mass limits. So far only gluon exchange interactions within single baryons have been considered. Therefore, to complete the discussion, in this section the leading order interaction between two color-singlet baryons will be considered. However, this is not to imply that nuclear matter is necessarily composed of color-singlet baryons - while the entire quantum many-body state (of nuclear matter) is required by color confinement to be a color-singlet state, it is conceivable that while each baryon may not be a color-singlet, the entire nuclear matter state is. Such states are sometimes referred to as *hidden color states*. These states are only relevant in the context of the heavy quark mass limit or in quark models. The issue of hidden color states will be further pursued in the following two chapters. (Here the sub-leading interactions between baryons that is mediated by scalar glueballs will be ignored. But this issue will be considered in the last chapter, where it is found that nuclear matter saturates at sub-leading order in N_c.)

A further assumption in addition to the absence of hidden color states is necessary for the formation of nuclear matter. Each quark is a spin-1/2 fermion and comes in one of N_f flavors. In the case of the single baryon interaction the issues of spin and flavour were ignored as long as the baryon state is antisymmetric in color and symmetric with respect to space, spin and flavor. However, for the ensuing discussion, only baryons that are all in the same spin-flavor state of which

there are $2N_f$ possibilities, are considered. (Note that in the heavy quark mass limit spin and flavor degrees of freedom are decoupled.) While in general baryons have more complicated structures, including states where spin and flavor are correlated, for now such possibilities are ignored. As will become clear in subsequent chapters, the N_c scaling is not altered when spin-flavor is correctly taken into account.

The first source of interaction between two baryons (in the same spin-flavor state) is through Pauli repulsion. It turns out that this is the leading order interaction in nuclear matter in three spatial dimensions at parametrically low densities which was considered in Ref. [28]. This interaction between baryons occurs through a gluon-less exchange of quarks as depicted in Fig. 1.15. The combinatorics of this interaction is rather simple under the assumption that after the interaction the two baryons remain color-singlets. There are N_c ways to choose a quark from the first baryon that can be exchanged but once this quark is chosen there is only one way to choose a quark from the second baryon. Therefore, this interaction is of $\mathcal{O}(N_c)$.

Finally, consider an interaction involving an exchange of different colored quarks via a gluon exchange, a diagram for which is shown in Fig. 1.16. Note that this interaction "looks" like a meson exchange. There are N_c ways to choose a quark from the first baryon and there are $N_c - 1$ ways to choose a quark of a different color from the second baryon (assuming a single gluon exchange occurs). Therefore, there are $\mathcal{O}(N_c^2)$ ways to choose two quarks, which combined with the fact that a gluon exchange interaction is of $\mathcal{O}(g^2)$ means that the diagram contributes at $\mathcal{O}(N_c)$.

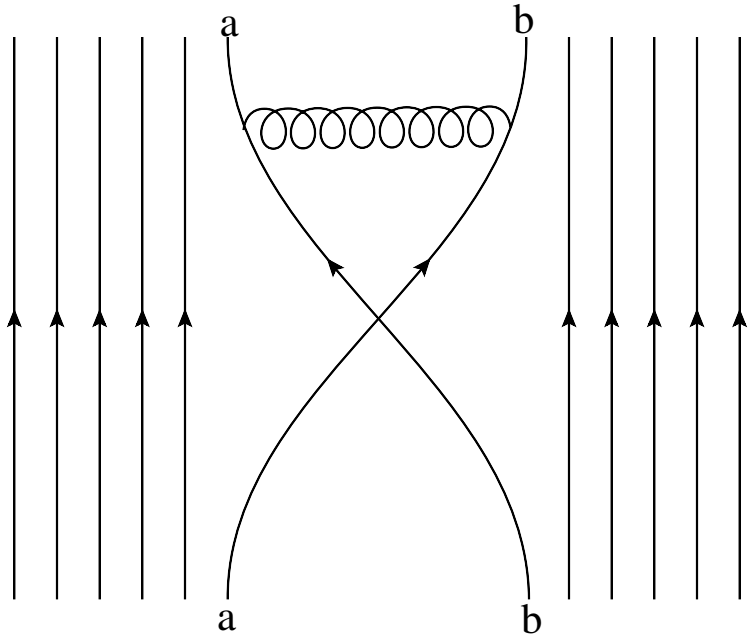

Figure 1.16: A baryon-baryon interaction via gluon and quark exchange

1.4.5 Summary

In this chapter, a number of issues including the difficulties with studying the problem of cold, nuclear matter from within QCD due its non-perturbative nature and due to the fact that lattice QCD is inapplicable due to the fermion sign problem have been discussed. Furthermore, the large N_c limit of QCD and some of its simplifying structure were also discussed. Finally, the behavior of baryons and baryonic interactions in the combined 't Hooft large N_c and heavy quark mass limits of QCD were discussed.

Chapter 2: Validity of Mean-field Approximation for Large N_c Baryons

2.1 Introduction

Two important theoretical issues pertaining to baryons in the combined heavy quark and 't Hooft large N_c limits of QCD are considered in this chapter [29]. The first of these pertain to the validity of the mean-field approximation. As noted in the previous chapter, baryons in the combined heavy quark mass and large N_c limits are expected be completely anti-symmetric, color-singlet states of N_c quarks. Furthermore, Witten [15] argued that baryons and baryonic matter, which is a system of interacting baryons, can be described via a mean-field approximation with each quark moving in an average color Coulomb potential. While the argument seems plausible, it is important to justify that this is actually correct. Remarkably, while the argument was made twenty-five years, it had not been rigorously proven.

This chapter is based on a rigorous argument that is presented in the article of Ref. [14]. The argument relies on choosing a particular variational space of trial states known as *generalized baryonic coherent states*. These states are color-singlet states that carry a baryon charge. They form an over-complete state analogous to Glauber states in quantum optics [30]. Here, the energy functional of baryons is written as integrals over these overcomplete states and it is shown that in the

large N_c limit, the ground state has a finite support over a width of $\mathcal{O}\left(\frac{1}{\sqrt{N_c}}\right)$, which implies that the energy is well-approximated by a single coherent state with corrections to the energy of $\mathcal{O}\left(\frac{1}{N_c}\right)$.

A second theoretical issue that will be considered relates to the role (or lack thereof) played by hidden color states [31–33] in the nuclear matter problem. Witten in his mean-field analysis assumed that baryonic matter is composed of constituent baryons that are also color-singlet states i.e. non-hidden color states. The argument is *ad hoc*. It is conceivable that the baryonic matter ground state is a different type of color-singlet state, namely a hidden color state; it could be a state in which the individual "baryons" are not color-singlet states but the entire state is a color-singlet. Generalized baryonic coherent states, as will be shown later, are Slater determinants states, which are examples of non-hidden color states. It will be shown in this chapter that hidden color states in the heavy quark and large N_c limits play a sub-leading role in the interaction energies of baryonic matter.

2.2 Baryon Hamiltonian

The exact form of the baryon Hamiltonian in the heavy quark mass limit was considered in Chapter 1. Here a form of the Hamiltonian in terms of raising and lowering operators is considered. Particle-hole space [34] instead of position or momentum space is used. The physics is completely independent of the choice of space used to describe the quantum mechanical basis. As was seen previously, the Hamiltonian comprises of one-body operators for the mass and the kinetic energy terms

and two-body operators for the potential term, which encodes the four heavy quark interactions that occur via a color Coulomb potential (Note here that the incoming and outgoing states are being counted separately). The Hamiltonian can be written in term of creation and annihilation operators (i.e. single-quark operators), which satisfy the following anti-commutation relations.

$$\begin{aligned} \{\hat{a}^a_\alpha, \hat{a}^b_\beta\} &= 0 \\ \{\hat{a}^{\dagger a}_\alpha, \hat{a}^{\dagger b}_\beta\} &= 0 \\ \{\hat{a}^a_\alpha, \hat{a}^{\dagger b}_\beta\} &= \delta_{\alpha\beta}\,\delta^{ab}\ . \end{aligned} \tag{2.1}$$

Here, each of the Greek indices represent a set of spin-flavor-space quantum numbers while the Roman indices indicate color. Using these operators, the Hamiltonian assumes the following form:

$$\begin{aligned} \hat{H} &= \hat{M} + \hat{T} + \hat{V} \\ \hat{M} &= \sum_{\alpha} \sum_{a=1}^{N_c} M_Q\, \hat{a}^{\dagger a}_\alpha \hat{a}^a_\alpha \\ \hat{T} &= \sum_{\alpha\beta} \sum_{a=1}^{N_c} t_{\alpha\beta}\, \hat{a}^{\dagger a}_\alpha \hat{a}^a_\beta \\ \hat{V} &= \sum_{\alpha\beta\gamma\delta} \sum_{a=1}^{N_c} \sum_{b=1}^{N_c} \frac{v_{\alpha\beta\gamma\delta}}{N_c}\, \hat{a}^{\dagger a}_\alpha \hat{a}^{\dagger b}_\beta \hat{a}^b_\gamma \hat{a}^a_\delta \end{aligned} \tag{2.2}$$

with $\hat{M}$ being the mass operator, $\hat{T}$ being the kinetic energy operator and $\hat{V}$ being the two-body operators. Note that the quark mass is denoted by m_q. The $t_{\alpha\beta}$ represent kinetic energy coefficients and is $\mathcal{O}(N_c^0)$. Similarly, $v_{\alpha\beta\gamma\delta}$ represents the color-Coulomb potential, which is independent of spin, color and flavor. It is also $\mathcal{O}(N_c^0)$.

2.3 Boundary Conditions

The arguments presented in this chapter regarding the validity of the mean-field approximation is completely general in that it applies not only to single baryons but also to baryonic matter. For both cases, it is important to specify the boundary conditions before specifying the trial coherent states, which will be done in the following section. For the single baryon problem, an infinite space problem will be considered with the choice of wave function only restricted by square integrability. In other words, the wave function can be chosen such that it drops off sufficiently rapidly such that probability that a quark is found anywhere in space is one.

For the case of infinite nuclear matter, one way of imposing boundary conditions is by fixing the baryon charge in a box while varying its volume. In order to study infinite nuclear matter at different densities, formally, the limit with the volume, V and baryon number, B both going to infinity can be taken with the baryon density $\rho = \frac{B}{V}$ fixed.

2.4 Generalized Coherent States

In this section, the variational space of baryonic generalized coherent states will be defined. These will be later used to characterize the ground state energy of the baryons and baryonic matter. These states will allow for the comparison of the exact baryonic ground state (in large N_c QCD with heavy quarks) with the mean-field state first suggested by Witten. The states are generalized coherent

states that carry a baryon charge. The minimum of our baryon (or baryonic matter) Hamiltonian in this space will be found subject to the boundary condition that were described in the previous section.

These generalized coherent states are analogous to the coherent states in that they can be generated via an exponentiated operator acting on some state that is called the reference state. The difference between the operator here and the ones used in quantum optics, namely the Glauber states is that the operator here is that the exponentiated operator is instead of being a single annihilation/creation operator, a color singlet particle-hole operator. This ensures that in the state that is generated, color neutrality is preserved. This fact will be proved later in this section.

In order to construct the most general color-singlet coherent state with baryon charge B and BN_c quarks, it is important to first define a reference state. The primary purpose of this state is to generate all possible states that are color-singlets. It possesses a baryon charge B. This is analogous to the way in which Thouless generated Slater determinants of N-particles [35]. The reference state with baryon charge B is defined as:

$$|\text{ref}, B\rangle = \prod_{h=1}^{B} \prod_{a=1}^{N_c} \hat{a}_h^{\dagger a} |\text{vac}\rangle \ , \tag{2.3}$$

where the hole index h runs from 1 to B, the color index a runs from 1 to N_c and $|\text{vac}\rangle$ is the vacuum state that possesses no baryon charge and has a trivial structure since the theory being considered is non-relativistic. $a_h^{\dagger a}$ is defined as the operator

that creates a quark state with color a in a state h, i.e.

$$\hat{a}_h^{\dagger a}|\text{vac}\rangle = |q_h^a\rangle \ . \tag{2.4}$$

This state is referred to as a hole state, since in the reference state it is occupied so that its dynamics becomes relevant when a_h acts upon it leaving a "hole". Besides the B hole creation operators, $a_h^{\dagger a}$, there are also particle creation operators, which are all the creation operators that are not the hole operators. Analogously, there are also hole and particle annihilation operators and these operators will be use to define all the generalized coherent states starting from the reference state $|\text{ref}, B\rangle$. Below are the anti-commutation relations for the particle and hole operators.

$$\begin{aligned} &\{\hat{a}_p^{\dagger a}, \hat{a}_h^{\dagger b}\} = \{\hat{a}_p^a, \hat{a}_h^{\dagger b}\} = 0 \\ &\{\hat{a}_p^a, \hat{a}_{p'}^{\dagger b}\} = \delta_{pp'}\delta^{ab} \text{ and} \\ &\{\hat{a}_h^a, \hat{a}_{h'}^{\dagger b}\} = \delta_{hh'}\delta^{ab} \ . \end{aligned} \tag{2.5}$$

An arbitrary color-singlet generalized state can be generated from the reference state defined above in the following fashion:

$$|C, B\rangle = \mathcal{N} \exp\left(\sum_{ph} C_{ph} \sum_{a=1}^{N_c} \hat{a}_p^{\dagger a}\hat{a}_h^a\right)|\text{ref}, B\rangle \ , \tag{2.6}$$

where the hole index is labelled h and runs from 1 to B and the particle index is labelled p and runs from $B+1$ to $B+n_p$, where n_p is the number of particle states. Here C is an $n_p \times B$ matrix that is complex valued and $\mathcal{N}$ is the normalization factor that is determined quite straightforwardly. Generally, n_p for a finite volume V is a countably infinite number analogous to momentum modes in a finite box with periodic boundary conditions. For the remainder of the discussion, however,

an ultraviolet cutoff is introduced such that n_p is finite. As long as n_p is sufficiently large, all physical observables will be independent of n_p.

Based on the form of the generalized states, it may not be clear whether these states are the set of all possible color-singlet, Slater determinant states with a baryon charge B. However, by using the anti-commutation relations of Eq. 2.5, these states can be written in a more transparent form such that the Slater determinant nature of these states becomes quite obvious.

$$|C, B\rangle = \mathcal{N} \prod_{h=1}^{B} \prod_{a=1}^{N_c} \left(\hat{a}_h^{\dagger a} + \sum_{ph} C_{ph} \hat{a}_p^{\dagger a} \right) |\text{vac}\rangle \ , \tag{2.7}$$

where $\bar{\mathcal{N}}$ is the normalization factor, which in general may be different from the normalization factor $\mathcal{N}$ that was previously used in Eq. 2.6 but only by a factor of -1 (due to the fermionic nature of the creation/annihilation operators). Note that from Eq. 2.7, it is clear that the generalized coherent states are indeed Slater determinants since for each hole operator of the form: $\left(\hat{a}_h^{\dagger a} + \sum_{ph} C_{ph} \hat{a}_p^{\dagger a} \right)$, the color index a appears once and only once for each of the N_c colors. Here, each of these operators creates a quark state of the following form

$$|q_h^a\rangle + \sum_{ph} C_{ph} |q_p^a\rangle \ , \tag{2.8}$$

where $|q_h^a\rangle$ represents a quark of color a in a hole state h and $|q_h^a\rangle$ represents a quark of color a in a particle state. Note however that the particle state is summed over and the overall state has a free hole index. In other words, the entire state is a hole state.

Having shown that the generalized coherent states are indeed Slater determinants, it remains to be shown that they are indeed the set of all possible baryonic,

color-singlet Slater determinant states. The most general color-singlet Slater determinant has the following form:

$$|S,T,B\rangle = \mathcal{N}' \prod_{h=1}^{B} \prod_{a=1}^{N_c} \left(\sum_{h'} S_{h'h} \hat{a}_{h'}^{\dagger a} + \sum_{p'} T_{p'h} \hat{a}_{p'}^{\dagger a} \right) |\text{vac}\rangle \ , \tag{2.9}$$

where S and T are complex valued matrices of dimension $n_h \times n_h$ and $n_p \times n_h$ respectively. As long as $T \neq 0$, these states remain non-orthogonal to the reference state, i.e. $\langle \text{ref}|S,\ T,\ C\rangle \neq 0$. Due to non-orthogonality to the reference state and the fact that the reference state comprises of hole states but no particle states, the $\det(S) \neq 0$, which means that S is an invertible matrix. If S is invertible then the states above can be transformed into the coherent states of Eq. 2.7 with the identification that $C = TS^{-1}$.

2.4.1 Identity Operator

There are further properties of the generalized coherent states that are required in order to prove the validity of the mean-field approximation. The first of these properties that will proven here is the existence of an identity operator in integral form as written below:

$$\begin{aligned} \hat{1}_{\text{cs},B} &= \int d\mu(C,B) |\text{C},B\rangle\langle\text{C},B| \text{ with} \\ d\mu(C,B) &\equiv J(C,B;N_c,n_p) \prod_{p,h} dC_{ph} dC_{ph}^* \ . \end{aligned} \tag{2.10}$$

$\hat{1}_{\text{cs},B}$ is the identity operator constructed out of color-singlet states with baryon charge B. The state $|C,\ B\rangle$ is a normalized state that is also a color-singlet with baryon charge B and $d\mu(C,\ B)$ is the integration measure, which is required due

to the overcomplete nature of the generalized coherent states basis. The weight function $J(C,\ B;\ N_c,\ n_p)$ appropriately weights each coherent state and is a function of the complex valued matrix, C, the baryon charge, B , the number of colors, N_c and the number of particle states, n_p.

In order to prove the identity operator, it is helpful to start with a space of states having baryon charge B but without the requirement that they be restricted to color-singlet states. These states will be denoted $|D,\ B\rangle$ while the color singlet coherent states will be denoted $|C,\ B\rangle$. Also, an arbitrary color-singlet will be denote $|\psi\rangle_{\rm cs}$ for the rest of this section.

The most general form of $|D,\ B\rangle$, a state with baryon charge B is as follows:

$$|D,B\rangle = \mathcal{N}_D \exp\left(\sum_{pa,hb} D_{pa,hb}\hat{a}_p^{\dagger a}\hat{a}_h^b\right)|\text{ref},\ B\rangle, \tag{2.11}$$

where $\mathcal{N}_D$ is a normalization state and the reference state $|\text{ref},\ B\rangle$ is a color-singlet state. But note that it is possible to generate non-color-singlet states starting with this reference state since the operator in the exponent is not a color-singlet. The identity operator in this larger space is well-known [36] and has the following form:

$$\begin{aligned}
\hat{1}_B &= \int d\mu(D,B)|\mathrm{D},B\rangle\langle\mathrm{D},B| \text{ with} \\
d\mu(D,B) &\equiv J(D,B;N_c,n_p)\prod_{pa,hb} dD_{pa,hb}dD^*_{pa,hb} \text{ and} \\
J(D,B;N_c,n_p) &\equiv \frac{\mathcal{N}_{\rm ncs}(B,n_p,N_c)}{\det(1+D^\dagger D)^{N_c(B+n_p)}}\ .
\end{aligned} \tag{2.12}$$

Here, the determinant is taken with respect to a combined particle-hole and color space, with $\mathcal{N}_{\rm ncs}$ being a numerical factor that depends on B, n_p and N_c. Also, $J(D,\ B;\ N_c,\ n_p)$ is the weight function for this enlarged space, which by the virtue of its overcompleteness requires this function to weigh each state appropriately.

In order to proceed, first a projection operator ($\hat{P}$) that projects any given state into only its color-singlet components only is considered. It has two important properties:

i. $\hat{P}|\psi\rangle_{\rm cs} = |\psi\rangle_{\rm cs}$, where $|\psi\rangle_{\rm cs}$ is a color-singlet state.

ii. $\hat{P}\hat{C}_2\hat{P} = 0$, with $\hat{C}_2$ being the quadratic $SU(N_c)$ Casimir operator. Having defined this projection operator, this operator can be applied on the identity operator of Eq 2.12 in the following way:

$$\hat{1}_{{\rm cs},B} = \hat{P}\hat{1}_B\hat{P} = \int d\mu(D,B)\hat{P}|{\rm D},B\rangle\langle{\rm D},B|\hat{P}\ . \tag{2.13}$$

Before proceeding to simplify the above projection, the action of the projection operator $\hat{P}$ on the state $|D,\ B\rangle$ can be written in the following manner:

$$\begin{aligned}\hat{P}|{\rm D},B\rangle &= \hat{P}\exp\left(\sum_{pa,hb} D_{pa,hb}\hat{a}_p^{\dagger a}\hat{a}_h^b\right)\hat{P}|{\rm ref},B\rangle \\ &= \sum_{n=0}^{\infty}\frac{1}{n!}\mathcal{N}_D\hat{P}\left(\sum_{pa,hb} D_{pa,hb}\hat{a}_p^{\dagger a}\hat{a}_h^b\right)^n\hat{P}|{\rm ref},B\rangle\ .\end{aligned} \tag{2.14}$$

In the second form above, the exponentiated operator of the first term has been Taylor expanded and written as an infinite series. The projection operator, selects only terms in this expansion that are the color-singlet components. The first term ($n = 0$) is trivially a color-singlet since the reference state is a color singlet. The second term ($n = 1$) is a one-particle one-hole term and can be a color-singlet only if the action of $\hat{P}$ is zero on all D except for ones that assume the following form:

$$D_{pa,hb} = \delta_{ab}C_{ph}\ , \tag{2.15}$$

where C is a color-independent matrix. It only possesses particle-hole indices. This imposes a strong constraint on the projection of the identity operator $\hat{1}_B$, which now

becomes:

$$\begin{aligned}\hat{1}_{\mathrm{cs,B}} &= \int \prod_{pa,hb} dD_{pa,hb} dD^*_{pa,hb} J(D,B;N_c,n_p) \hat{P} |\mathrm{D},B\rangle\langle \mathrm{D},B| \hat{P} \\ &= \int \prod_{ph} dC_{ph} dC^*_{ph} \int d\mu(\mathrm{D},B) \prod_{p'h'} \delta\left(C_{p'h'} - \frac{1}{N_c} \sum_{ab} D_{p'a,h'b}\delta_{ab} \right) \\ &\delta\left(C^*_{p'h'} - \frac{1}{N_c} \sum_{ab} D^*_{p'a,h'b}\delta_{ab} \right) |\mathrm{C},B\rangle\langle \mathrm{C},B| \ ,\end{aligned} \tag{2.16}$$

where the constraints from Eq. 2.15 have been imposed by introducing integrals over delta functions with respect to the real and complex components of matrix C. Finally, the following identification for the Jacobian in the identity operator of Eq. 2.10 can be made.

$$\begin{aligned}J(C,B;N_c,n_p) = \int d\mu(\mathrm{D},B) \prod_{p'h'} &\delta\left(C_{p'h'} - \frac{1}{N_c} \sum_{ab} D_{p'a,h'b}\delta_{ab} \right) \\ &\delta\left(C^*_{p'h'} - \frac{1}{N_c} \sum_{ab} D^*_{p'a,h'b}\delta_{ab} \right) \ .\end{aligned} \tag{2.17}$$

2.4.2 Overlap Amplitude

Besides the existence of the unity operator, another property of the generalized coherent states is the overlap of two arbitrary coherent states. This overlap is quite straightforward to determine [34] using standard determinant relations for two fermionic states. Here only the result will be quoted. It is as follows:

$$\langle \mathrm{C},B|\mathrm{C}'B'\rangle = \delta_{BB'} \frac{\det(1+C^\dagger C')^{BN_c}}{\det(1+C^\dagger C)^{\frac{BN_c}{2}} \det(1+C'^\dagger C')^{\frac{BN_c}{2}}} \ . \tag{2.18}$$

Note that the determinant vanishes unless both the states have the same baryonic charge, which is to be expected. Also, note that the determinant is only with respect to particle-hole space since C is independent of color. Finally, the normalization of the states is such that the overlap of two identical coherent states is one.

Next, it is useful to to introduce a variable change, which will prove useful in the next section.

$$\begin{aligned} \overline{C} &= \frac{1}{2}(C + C') \\ \Delta C &= C - C' \ . \end{aligned} \tag{2.19}$$

Then it is possible to rewrite the overlap function in term of the new variables, which are as follows:

$$\begin{aligned} \langle \mathrm{C}, B | \mathrm{C}' B' \rangle &= \langle \overline{C} + \Delta C/2, B | \overline{C} - \Delta C/2, B \rangle \\ &= \delta_{BB'} f\left(\overline{C},\ \Delta C\right)^{N_c} \ . \end{aligned} \tag{2.20}$$

The function $f(\overline{C},\ \Delta C)$ is as follows:

$$\begin{aligned} f(\overline{C}, \Delta C) &= \frac{\det\left(E_{-+-}\right)}{\det(E_{+++})^{\frac{1}{2}} \det(E_{--+})^{\frac{1}{2}}} \\ E_{\pm\pm\pm} &= 1 + \overline{C}^{\dagger}\overline{C} \pm \frac{\overline{C}^{\dagger}\Delta C}{2} \pm \frac{\Delta C^{\dagger}\overline{C}}{2} \pm \frac{\Delta C^{\dagger}\Delta C}{4} \ . \end{aligned} \tag{2.21}$$

From the form of f it is easy to see that for $\Delta C = 0$, $f = 1$ and that $|f(\overline{C},\ \Delta C)| < 1$ if $\Delta C \neq 0$). This indicates that the overlap function f falls exponentially with N_c as ΔC deviates away from zero. This fact is central to the validity of the mean-field approximation at large N_c.

2.4.2.1 Projection onto generalized coherent states

Now that the explicit form of the identity operator and the overlap of two generalized coherent states have been established, it is possible to exploit the over-completeness of the generalized coherent states to write an arbitrary state $|\psi\rangle$, which may or may not be a color-singlet in terms of the color singlet coherent states. In

order to do that the state $|\psi\rangle$ is hit by an operator $\hat{1}$ and the result is follows:

$$|\psi\rangle = \hat{1}|\psi\rangle = \int d\mu(C,B) w_\psi^0(C)|C,B\rangle \ , \tag{2.22}$$

where $w_\psi^0(C)$ is a weight function that is defined as follows:

$$w_\psi^{(0)}(C) \equiv \langle C,B|\psi\rangle \ , \tag{2.23}$$

and this relation follows directly from the definition of the identity operator in Eq. 2.10. The function $w_\psi^{(0)}(C)$ will be called the *primary weight operator*.

However, due to the overcompleteness of the states, the weight function is not unique. In order to see this the unit operator can be applied twice on the state $|\psi\rangle$. The resulting decomposition is

$$\begin{aligned} |\psi\rangle &= \hat{1}\left(\hat{1}|\psi\rangle\right) \\ &= \int d\mu(C) \left(\int d\mu(C') \langle C,\ B|C',\ B\rangle w_\psi^0(C') \right) |C,\ B\rangle \ . \end{aligned} \tag{2.24}$$

In this decomposition, the weight function is different from the primary weight function. It is

$$w_\psi^{(1)}(C) = \left(\int d\mu(C') \langle C,\ B|C',\ B\rangle w_\psi^0(C') \right) \ , \tag{2.25}$$

and can be written in terms of the overlap of the coherent states $|C',\ B\rangle$ and $|C,\ B\rangle$. In fact for any given weight function, w_ψ^j, it is possible to write a new weight function, w_ψ^{j+1}, by applying the identity operator on the resulting decomposition. The form of w_ψ^{j+1} in terms of w_ψ^j is as follows:

$$w_\psi^{(j+1)}(C) = \int d\mu(C',B) \frac{w_\psi^{(j)}(C')\ \det(1+C'^\dagger C)^{BN_c}}{\det(1+C^\dagger C)^{\frac{BN_c}{2}} \det(1+C'^\dagger C')^{\frac{BN_c}{2}}} \ . \tag{2.26}$$

Using this result, the decomposition in can be written entirely in terms of w_ψ^0.

2.5 The Validity of the Mean-Field Approximation

In this section the validity of Witten's mean-field approximation using the generalized baryonic coherent states basis will be established using the results of the previous sections. More specifically, it is proven that a mean-field state (i.e. a generalized coherent state that minimizes the energy in the space of the variational space of generalized coherent states) does so in such a way that the corrections arising from the fact that the state is not the exact ground state is subleading in the N_c power counting. Mathematically, this can be expressed as:

$$\frac{\langle\psi_{\rm gs}|\hat{H}|\psi_{\rm gs}\rangle - \langle C_{\rm mf}|\hat{H}|C_{\rm mf}\rangle}{\langle\psi_{\rm gs}|\hat{H}|\psi_{\rm gs}\rangle} \sim \mathcal{O}(N_c^0) \ . \tag{2.27}$$

while $\langle\psi_{\rm gs}|\hat{H}|\psi_{\rm gs}\rangle \sim \mathcal{O}(N_c^0)$.

2.5.1 Useful Mathematical Relations

In order to demonstrate Eq. 2.27, it is important to establish a set of important relations, which will prove useful. The first of these relations follows from the normalization condition of the many-body state, $|\psi\rangle$ and its decomposition into the coherent states basis similar to Eq. 2.22, but written with an arbitrary weight function instead of the primary one. Using the fact that $\langle\psi|\psi\rangle = 1$, the first useful identity in terms of $w_\psi^{(j)}$ is:

$$\int d\mu(C,B) d\mu(C',B) w_\psi^j(C) w_\psi^j(C') \langle C',B|C,B\rangle = 1 \ . \tag{2.28}$$

The second mathematical relation is the matrix element of the Hamiltonian with respect to the state of generalized coherent states. These matrix elements can

be easily constructed using the anti-commutation properties of the particle-hole operators combined with the definition of the coherent states. The resulting matrix element (assuming that $|C\rangle$ and $|C'\rangle$ are both normalized) is as follows:

$$\langle C|\hat{H}|C'\rangle = N_c h(C,C')\langle C|C'\rangle \ , \tag{2.29}$$

where $h(C,C')$ is an $\mathcal{O}(N_c^0)$ function of the complex-valued matrix elements of C and C'. More specifically $h(C,C')$ has the following form in terms of the new variable ΔC and $\overline{C}$.

$$h(\overline{C},\Delta C) = h_0(\overline{C},\Delta C) + \frac{1}{N_c}h_1(\overline{C},\Delta C) \ , \tag{2.30}$$

with $h_0(\overline{C},\Delta C)$ and $h_1(\overline{C},\Delta C)$ both being $\mathcal{O}(N_c^0)$ functions. The exact form of the functions are quite cumbersome and therefore presented only in the last section of this chapter with the key point being that the functions h_0 and h_1 are smoothly behaved even in the $N_c \to \infty$ limit.

2.5.2 Ground State

Next, to proceed, assume that the ground state of the baryonic system (either a single baryon or a baryon crystal) is $|\psi_{\rm gs}\rangle$. Then the energy of this state can be written in terms of the weight function $w_{\rm gs}^{(j)}$ and the jacobian $J(C,B)$ using the identity decomposition that was derived previously. The resulting energy is in integral form and looks as follows:

$$\langle\psi_{\rm gs}|\hat{H}|\psi_{\rm gs}\rangle = \int [dC][dC'] \left(J(C,B)w_{\psi_{\rm gs}}(C)\right)^* \left(J(C',B)w_{\psi_{\rm gs}}(C')\right) \langle C|\hat{H}|C'\rangle \ , \tag{2.31}$$

where the following notation for the integration variables (which are the complex-valued elements of the matrix C and C') has been used.

$$\begin{aligned}[dC] &\equiv \prod_{php'h'} dC_{ph} dC^*_{ph} \\ [dC'] &\equiv \prod_{php'h'} dC'_{ph} dC'^*_{ph} \ .\end{aligned} \tag{2.32}$$

The product in the equation above is over all particle-hole indices. Furthermore, it is useful to denote the overlap of two coherent states using the following notation:

$$\langle C|C'\rangle \equiv f(\overline{C},\ \Delta C)^{N_c} \ , \tag{2.33}$$

with $f(\overline{C},\ \Delta C)$ being an $\mathcal{O}(N_c^0)$ function and is equal to 1 if $\Delta C = 0$ i.e. for the diagonal elements in the coherent states basis.

It is preferable to write the integral in terms of the variables $\overline{C}$ and ΔC such that it looks as follows:

$$\langle \psi_{\rm gs}|\hat{H}|\psi_{\rm gs}\rangle = N_c \int \prod_{p,h,p',h'} d\overline{C}_{ph} d\overline{C}^*_{ph} d\Delta C_{p'h'} d\Delta C^*_{p'h'}\ G_{\psi_{\rm gs}}(\overline{C},\Delta C) h(\overline{C},\Delta C) \ , \tag{2.34}$$

where the function $G_{\psi_{\rm gs}}$ is defined as:

$$\begin{aligned} G_{\psi_{\rm gs}}(\overline{C},\Delta C) = &\left(J(\overline{C}+\Delta C/2,B) w_{\psi_{\rm gs}}(\overline{C}+\Delta C/2)\right)^* \\ &\left(J(\overline{C}-\Delta C/2,B) w_{\psi_{\rm gs}}(\overline{C}-\Delta C/2)\right) f(\overline{C},\Delta C)^{N_c} \ , \end{aligned} \tag{2.35}$$

and $h(\overline{C},\ \Delta C)$ is defined as:

$$h(\overline{C},\Delta C) \equiv \frac{\langle \overline{C}, +\Delta C/2|\hat{H}|\overline{C}-\Delta C/2\rangle}{N_c \langle \overline{C}+\Delta C/2|\overline{C}-\Delta C/2\rangle} \ . \tag{2.36}$$

Note that G is normalized such that the following condition is satisfied.

$$\int \prod_{p,h} d\overline{C}_{ph} d\overline{C}^*_{ph} \int \prod_{p',h'} d\Delta C_{p'h'} d\Delta C^*_{p'h'}\ G_{\psi_{\rm gs}}(\overline{C},\Delta C) = 1 \ . \tag{2.37}$$

This can be seen by replacing the $\hat{H}$ operator in the previous equation with the identity operator $\hat{1}$ such that it simply becomes the normalization condition that was derived in Eq. 2.28.

It is useful to define the following function

$$g_{\psi_{\rm gs}}(\overline{C}) \equiv \int \prod_{p,h} d\Delta C_{ph} d\Delta C^*_{ph}\, G_{\psi_{\rm gs}}(\overline{C}, \Delta C) \ . \tag{2.38}$$

Because of Eq. 2.37, $g_{\psi_{\rm gs}}(\bar{C})$ is normalized in the sense that $\int \prod_{p,h} d\bar{C}_{p,h} d\bar{C} \ *_{p,h}$ $g(\bar{C}) = 1$. Finally the function, $G_{\psi_{\rm gs}}(\overline{C}, \Delta C)$, is also useful to define. It has the form:

$$G_{\psi_{\rm gs}}(\overline{C}, \Delta C) = g_{\psi_{\rm gs}}(\overline{C}) \prod_{ph} \delta(\Delta C_{ph}) \delta(\Delta C^*_{ph}) + \Delta G_{\psi_{\rm gs}}(\overline{C}, \Delta C) \ . \tag{2.39}$$

The primary motivation for doing this is because in the large N_c limit the function $G_{\psi_{\rm gs}}$ is sharply peaked due to the fact that $f(\overline{C}, \Delta C)^{N_c}$ is a sharply peaked function. Therefore, $G_{\psi_{\rm gs}}$ can be written as a (product of) delta function in ΔC with exponential corrections.

Due to the normalizability of both G and g, note that $\Delta G_{\psi_{\rm gs}}$ integrates to zero. In other words,

$$\int \prod_{ph} d\overline{C}_{ph} \int \prod_{p'h'} \Delta C_{p'h'} \Delta G_{\psi_{\rm gs}} = 0 \ . \tag{2.40}$$

Finally, the energy of the ground state can be written as follows:

$$\langle \psi_{\rm gs} | \hat{H} | \psi_{\rm gs} \rangle = E^{(1)}_{\psi_{\rm gs}} + E^{(2)}_{\psi_{\rm gs}} \tag{2.41}$$

with $E^{(1)}_{\psi_{\rm gs}}$ defined as follows:

$$\frac{E^{(1)}_{\psi_{\rm gs}}}{N_c} = \int \prod_{p,h} d\overline{C}_{ph} d\overline{C}^*_{ph}\, g_{\psi_{\rm gs}}(\overline{C}) h(\overline{C}, 0) \tag{2.42}$$

and $E^{(2)}_{\psi_{\rm gs}}$ defined as follows:

$$\frac{E^{(2)}_{\psi_{\rm gs}}}{N_c} = \int \prod_{p,h,p',h'} d\overline{C}_{ph} d\overline{C}^*_{ph} d\Delta C_{p'h'} d\Delta C^*_{p'h'} \Delta G_{\psi_{\rm gs}}(\overline{C}, \Delta C) h(\overline{C}, \Delta C) \ . \tag{2.43}$$

Note that the two terms above both contribute to the ground state. However, neither is uniquely defined due to the fact that an overcomplete coherent states basis is being used. The weight function $w^{(j)}_{\psi_{\rm gs}}$ is not uniquely defined and therefore $E^{(1)}_{\psi_{\rm gs}}$ and $E^{(2)}_{\psi_{\rm gs}}$ which are integrals over the product of the weight function and the Jacobian is also not uniquely defined. However, the total ground state energy by definition is unique. Therefore, any change in $E^{(1)}_{\psi_{\rm gs}}$ due to the change in weight function will be compensated exactly by changes in $E^{(2)}_{\psi_{\rm gs}}$.

Note that from the definition of $E^{(1)}_{\psi_{\rm gs}}$, it depends only on the integral over elements of the matrix $\overline{C}$ over a function consisting of $h(\overline{C}, 0)$, where $\Delta C = 0$ such that $h(\overline{C}, 0) = h(C)$. The function corresponds to the diagonal elements of the Hamiltonian operator in the coherent states basis. This function is minimized by an appropriate choice of coherent state, which will be called the mean-field state $|C_{\rm mf}\rangle$. In other words, the mean field state $|C_{\rm mf}\rangle$ is defined to be the state that minimizes the following quantity:

$$\frac{\langle C_{\rm mf}|\hat{H}|C_{\rm mf}\rangle}{\langle C_{\rm mf}|C_{\rm mf}\rangle} \equiv h(C_{\rm mf}, C_{\rm mf}) \ . \tag{2.44}$$

However, this quantity is always smaller than $E^{(1)}_{\psi_{\rm gs}}$. Note that $E^{(1)}_{\psi_{\rm gs}}$ is an integral over the function $g_{\psi_{\rm gs}}$, which owing to Eq 2.38 is normalizable. If it is a delta function then,

$$E^{(1)}_{\psi_{\rm gs}} = \langle C_{\rm mf}|\hat{H}|C_{\rm mf}\rangle \ . \tag{2.45}$$

However, for a general function $g_{\psi_{\rm gs}}$, it satisfies the following inequality:

$$E^{(1)}_{\psi_{\rm gs}} \geq \langle C_{\rm mf}|\hat{H}|C_{\rm mf}\rangle \ . \tag{2.46}$$

Furthermore the contribution coming from $E^{(2)}_{\psi_{\rm gs}}$ is of $\mathcal{O}(N_c^0)$. This can be seen from the definition of the ground state energy in Eq. 2.34 and the fact that at large N_c, $G_{\psi_{\rm gs}}$ is expected to be become exponentially narrow as a function of ΔC; therefore this function can be approximated through a Gaussian with a characteristic width of $\mathcal{O}\left(\frac{1}{\sqrt{N_c}}\right)$ with respect to integrals over the elements of the complex-valued matrix ΔC i.e. ΔC_{ph} and $\Delta C'_{ph}$. In doing so, the ground state energy assumes the following form:

$$\langle \psi_{\rm gs}|\hat{H}|\psi_{\rm gs}\rangle = \langle C_{\rm mf}|\hat{H}|C_{\rm mf}\rangle + \mathcal{O}(N_c^0) \tag{2.47}$$

From the fact that the state $|C_{\rm mf}\rangle$ is not an exact state but a variational state, it is already known that [1]:

$$\langle \psi_{\rm gs}|\hat{H}|\psi_{\rm gs}\rangle \leq \langle C_{\rm mf}|\hat{H}|C_{\rm mf}\rangle \ . \tag{2.48}$$

Therefore, the term of $\mathcal{O}(N_c^0)$ from Eq. 2.47 must be negative. In other words, the following condition must be satisfied:

$$\langle \psi_{\rm gs}|\hat{H}|\psi_{\rm gs}\rangle \geq \langle C_{\rm mf}|\hat{H}|C_{\rm mf}\rangle + \mathcal{O}(N_c^0) \ . \tag{2.49}$$

[1] The standard quantum mechanical argument that in a variational approach the trial state always gives an energy larger than the exact state is as follows. Assume that $|E_n\rangle$ are the energy eigenstates of a Hamiltonian $\hat{H}$ with $n = 0$ representing the ground state. Then any normalized, trial state $|\psi_{\rm trial}\rangle$ can be written as a linear combination of these energy eigenstates such that the energy is:

$$\langle \psi_{\rm trial}|\hat{H}|\psi_{\rm trial}\rangle = \textstyle\sum_{n=0}^{\infty} |c_n|^2 \langle E_n|\hat{H}|E_n\rangle \leq \sum_{n=0}^{\infty} |c_0|^2 \langle E_0|\hat{H}|E_0\rangle = E_0.$$

Therefore, a bound has been proven. It restricts the relationship between $\langle\psi_{\rm gs}|\hat{H}|\psi_{\rm gs}\rangle$ and $\langle C_{\rm mf}|\hat{H}|C_{\rm mf}\rangle$. The bound is as follows:

$$0 \leq \frac{\langle\psi_{\rm gs}|\hat{H}|\psi_{\rm gs}\rangle - \langle C_{\rm mf}|\hat{H}|C_{\rm mf}\rangle}{\langle\psi_{\rm gs}|\hat{H}|\psi_{\rm gs}\rangle} \leq \mathcal{O}(N_c^0). \tag{2.50}$$

In other words, it has been shown that the energy can be well-approximated by a mean-field state $|C_{\rm mf}\rangle$, which was chosen from a variational space of generalized coherent states. Keep in mind that the energy of a baryon diverges as N_c, a precise way to state the claim above is that the relative difference in energy between the exact ground state and the mean-field state is of subleading order i.e. $\mathcal{O}(N_c^0)$.

The above derivation relied on the fact that the function $G_{\psi_{\rm gs}}(\overline{C}, \Delta C)$ is well approximated by a Gaussian with respect to one of the variables, ΔC with a characteristic with of $\mathcal{O}(N_c^{-\frac{1}{2}})$. This followed from the fact that the definition of $G_{\psi_{\rm gs}}(\overline{C}, \Delta C)$ in Eq. 2.39 contains the narrow function $f(\overline{C}, \Delta C)^{N_c}$. But it is important to make sure that the remaining factors including the Jacobian $J(C, B)$ and the weight function w_ψ^j are taken into account. There are two possibilities.

a. If these functions are wider (in ΔC) than the function $f(\overline{C}, \Delta C)^{N_c}$, our argument holds.

b. However, a second possibility is that these functions are actually narrower. In this situation, the corrections are smaller in order than the $\mathcal{O}(N_c^0)$ that was assumed in case a. However, in this case the ground state energy is less bound since it is known that the correction piece is negative.

Therefore, given these possibilities, the bound of Eq. 2.50 holds, the lower bound is imposed by the fact that a variational method is being used and the upper bound

by the worst case scenario, which is that from case a.

2.6 Hidden Color States

In this final section, implications of the bound that was constructed in Eq. 2.50 for *hidden color states* is considered. Note that in the early days of quark modeling of nuclear forces, there was much speculation about hidden color states [31–33].

In the language of particle-hole states, this means that hidden color states are many-body states in which each quark with a given baryon index (not baryon charge) may have the same color quantum number. For example, imagine a single baryon within nuclear matter, which occupies some finite volume. Quarks with the same spatial state are defined to be the constituents of a particular baryon. A state that consists of quarks in the same spatial state (i.e. belong to a baryon) and the same color state are considered hidden color states. Conversely, in *non-hidden color states*, quarks with the same baryon index may possess a particular color of the N_c possible colors once but only once. Any repetition implies that it is a hidden color state.

The baryonic generalized coherent states defined in Eq. 2.6 are by construction non-hidden color states. They can be cast in the form of Slater determinants as presented in Eq. 2.7. In each of these states a quark is in the following "hole" state:

$$|q_h^a\rangle + \sum_{ph} C_{ph}|q_p^a\rangle \ , \tag{2.51}$$

where the "hole" index h effectively refers to the baryon label (which could be a

momentum or spatial state). Furthermore, the particular state above consists of quarks in some color a and from the form of the generalized coherent states in Eq. 2.7, it is clear that for each "hole" state, each color index $a = 1$ to N_c appears only once, which is the condition for a non-hidden color state.

The result of Eq. 2.50 suggests that a particular generalized coherent state (one that minimizes the energy in the space of coherent states) largely determines the energy up to relative order of N_c^0, which is an order smaller than the size of the baryon masses, which are of $\mathcal{O}(N_c)$. The corrections to this arise due to the fact that the mean-field state is not the exact state. Nothing precludes hidden color states from being present in the ground state. In fact, it is possible to construct hidden color states from linear combinations of baryonic coherent states. However, since the mean-field state $|C_{\rm mf}\rangle$ is a non-hidden color state, a hidden color state can only contribute to the correction piece, which if of sub-leading order. This proves that hidden color states play a sub-dominant role in the combined heavy quark mass and large N_c limits.

2.7 APPENDIX: h_0 and h_1

For completeness, here the explicit forms of h_0 and h_1 are presented. They are defined in Eqs. (2.29) and (2.30). h_0 has the following form:

$$
\begin{aligned}
& h_0(\overline{C}, \Delta C) \\
& = \sum_{\alpha\beta hh'} (M_Q \delta_{\alpha\beta} + t_{\alpha\beta}) \\
& \left(1 + \overline{C} - \frac{\Delta C}{2}\right)_{\alpha h} \left(1 + \overline{C}^\dagger \overline{C} - \frac{\overline{C}^\dagger \Delta C}{2} + \frac{\Delta C^\dagger \overline{C}}{2} - \frac{\Delta C^\dagger \Delta C}{4}\right)^{-1}_{hh'} \left(1 + \overline{C}^\dagger + \frac{\Delta C^\dagger}{2}\right)_{h'\beta} \\
& + \sum_{\alpha\beta\gamma\delta} v_{\alpha\beta\gamma\delta} \\
& \left(1 - \left(1 + \overline{C} - \frac{\Delta C}{2}\right) \left(1 + \overline{C}^\dagger \overline{C} - \frac{\overline{C}^\dagger \Delta C}{2} + \frac{\Delta C^\dagger \overline{C}}{2} - \frac{\Delta C^\dagger \Delta C}{4}\right)^{-1} \left(1 + \overline{C}^\dagger + \frac{\Delta C^\dagger}{2}\right)\right)_{\alpha\delta} \\
& \left(1 - \left(1 + \overline{C} - \frac{\Delta C}{2}\right) \left(1 + \overline{C}^\dagger \overline{C} - \frac{\overline{C}^\dagger \Delta C}{2} + \frac{\Delta C^\dagger \overline{C}}{2} - \frac{\Delta C^\dagger \Delta C}{4}\right)^{-1} \left(1 + \overline{C}^\dagger + \frac{\Delta C^\dagger}{2}\right)\right)_{\beta\gamma} \\
& + \sum_{\alpha\beta\gamma\delta} v_{\alpha\beta\gamma\delta} \\
& \left(\left(1 + \overline{C} - \frac{\Delta C}{2}\right) \left(1 + \overline{C}^\dagger \overline{C} - \frac{\overline{C}^\dagger \Delta C}{2} + \frac{\Delta C^\dagger \overline{C}}{2} - \frac{\Delta C^\dagger \Delta C}{4}\right)^{-1} \left(1 + \overline{C}^\dagger + \frac{\Delta C^\dagger}{2}\right)\right)_{\alpha\delta} 1_{\beta\gamma} \\
& + \sum_{\alpha\beta\gamma\delta} v_{\alpha\beta\gamma\delta} \\
& 1_{\alpha\delta} \left(\left(1 + \overline{C} - \frac{\Delta C}{2}\right) \left(1 + \overline{C}^\dagger \overline{C} - \frac{\overline{C}^\dagger \Delta C}{2} + \frac{\Delta C^\dagger \overline{C}}{2} - \frac{\Delta C^\dagger \Delta C}{4}\right)^{-1} \left(1 + \overline{C}^\dagger + \frac{\Delta C^\dagger}{2}\right)\right)_{\beta\gamma} \\
& - 1_{\alpha\delta} 1_{\beta\gamma}
\end{aligned}
\tag{2.52}
$$

h_1 has the following form:

$$
\begin{aligned}
& h_1(\overline{C}, \Delta C) \\
= & -\sum_{\alpha\beta\gamma\delta} v_{\alpha\beta\gamma\delta} \\
& \left(1 - \left(1 + \overline{C} - \frac{\Delta C}{2}\right)\left(1 + \overline{C}^\dagger\overline{C} - \frac{\overline{C}^\dagger\Delta C}{2} + \frac{\Delta C^\dagger\overline{C}}{2} - \frac{\Delta C^\dagger\Delta C}{4}\right)^{-1}\left(1 + \overline{C}^\dagger + \frac{\Delta C^\dagger}{2}\right)\right)_{\alpha\gamma} \\
& \left(1 - \left(1 + \overline{C} - \frac{\Delta C}{2}\right)\left(1 + \overline{C}^\dagger\overline{C} - \frac{\overline{C}^\dagger\Delta C}{2} + \frac{\Delta C^\dagger\overline{C}}{2} - \frac{\Delta C^\dagger\Delta C}{4}\right)^{-1}\left(1 + \overline{C}^\dagger + \frac{\Delta C^\dagger}{2}\right)\right)_{\beta\delta} \\
& -\sum_{\alpha\beta\gamma\delta} v_{\alpha\beta\gamma\delta} \\
& \left(\left(1 + \overline{C} - \frac{\Delta C}{2}\right)\left(1 + \overline{C}^\dagger\overline{C} - \frac{\overline{C}^\dagger\Delta C}{2} + \frac{\Delta C^\dagger\overline{C}}{2} - \frac{\Delta C^\dagger\Delta C}{4}\right)^{-1}\left(1 + \overline{C}^\dagger + \frac{\Delta C^\dagger}{2}\right)\right)_{\alpha\gamma} 1_{\beta\delta} \\
& -\sum_{\alpha\beta\gamma\delta} v_{\alpha\beta\gamma\delta} \\
& 1_{\alpha\gamma}\left(\left(1 + \overline{C} - \frac{\Delta C}{2}\right)\left(1 + \overline{C}^\dagger\overline{C} - \frac{\overline{C}^\dagger\Delta C}{2} + \frac{\Delta C^\dagger\overline{C}}{2} - \frac{\Delta C^\dagger\Delta C}{4}\right)^{-1}\left(1 + \overline{C}^\dagger + \frac{\Delta C^\dagger}{2}\right)\right)_{\beta\delta} \\
& + 1_{\alpha\gamma}1_{\beta\delta} \ .
\end{aligned}
\tag{2.53}
$$

In both h_1 and h_0, α, β, γ and δ represent either particle or hole indices. Furthermore, note that $\overline{C}_{\alpha h}$ and $\Delta C_{\alpha h}$ are zero if α is a hole index.

Chapter 3: Baryons and Low-Density Baryonic Matter in 1+1 Dimensional Large N_c QCD with Heavy Quarks

3.1 Introduction

In this chapter, the heavy quark baryon problem is considered in one-spatial dimension [37]. The mean-field approximation remains trivially valid in one-spatial dimension at large N_c with the added virtue that the fully-relativistic problem is simple enough to solve. [17, 18]. This simplicity allows for a cross-check of the mean-field approximation that was proved in the previous chapter.

The primary reason for the simplicity of large N_c QCD in 1+1 dimension [21, 22, 38] is that in one-spatial dimension gluons do not propagate. This is due to the absence of magnetic fields. Therefore, gluonic effects manifest themselves as a linear color-Coulomb potential between any two colored charge densities. A further simplification occurs in that all gluon-gluon couplings can be eliminated by appropriate choice of gauge (for example, Weyl or axial). Furthermore, it was shown in a classic paper by 't Hooft [22] that in the light cone gauge, large N_c QCD can be solved for the meson spectrum in spite of the fact that an infinite number of self-energy and ladder diagrams have to be summed. A Bethe-Salpeter equation for

bound mesons was constructed to solve for the mass spectrum of the mesons. It was found that there exists a linear "Regge trajectory" for asymptotically large masses with no continuum. Furthermore, no states with free quarks were discovered in the spectrum.

3.1.1 The Large N_c Baryon Problem in 1+1 dimension

While the large N_c meson problem in 1+1 dimension was solved immediately after the discovery of the 't Hooft limit of QCD [22,38], the fully relativistic baryonic problem proved more challenging and has only been solved fully recently [17,18] for arbitrary quark masses and baryon densities. Earlier attempts to solve the problem were restricted to either only the chiral limit [39] or to the single baryon problem [40]. Ref. [39] solves the finite baryon density problem near the chiral limit using an ansatz that is translationally invariant for zero quark masses when the baryons are expected to be completely delocalized because both quarks and gluons are moving at the speed of light and hence the gluons cannot catch up with the quarks and thus cannot bind them into localized baryons. It is found that as the the chiral limit is approached single baryons become Sine-Gordon solitons and baryon crystals are characterized by a spatially varying chiral angle suggesting a "chiral spiral" structure [47–49]. Ref. [40] on the other hand only solves the single baryon problem but for arbitrary baryon masses. The approach (which will be called LNS approach) here involves constructing an infinite volume Hamiltonian with linear color-Coulomb interactions as in Ref. [22], constructing many body states with the quantum number

of a baryon and minimizing the mean-field energy functional. This minimization is performed using a latticized version of the mean-field energy functional with the correct limit of a linear Coulomb potential in the infinite box size and continuum limits. The paper assumes that performing the energy minimization in a finite box is not problematic given that the size of the baryon in the box is small enough such that edge effects are effectively negligible. Finally, Ref. [41] argues controversially that the problem of finite baryon density can be reduced to a single-site problem via Eguchi-Kawai reduction [42] suggesting that 1+1 large N_c QCD is completely independent of baryon chemical potential, which seems unphysical. The work in this chapter rules out the scenario of Ref. [41].

The Bringoltz approach of Ref. [17, 18] is different from other approaches of Refs. [40], [39] and [41] for a number of reasons. In this dicussion, the focus will be only on the differences of the Bringoltz approach to that of the LNS approach of Ref. [40]. Ref. [17,18] argues that in a finite box with periodic boundary conditions color charge densities interact via a color-Coulomb potential of the form $|x-y+QL|$, where Q is an integer and L is the size of the box. This differs from the LNS approach [40] in that it assumes that color Coulomb interactions are limited to the $Q = 0$ sector and that the windings associated with non-zero Q can be neglected for boxes whose sizes are bigger than the width of the baryon. While this seems quite plausible, it is wrong as shown in Ref. [17, 18], where the winding Q seem to be important even for boxes of size much larger than the baryon width.

Since there exists a completely independent way of studying the baryon problem using a mean-field approach, it is possible to check whether baryon masses in

the mean-field approximation agree with the approach of Ref. [17, 18] or Ref. [40] and find out whether finite volume effects are significant. While the mean-field approach itself is valid for arbitrary quark masses, the formalism of the previous chapter applies only to the non-relativistic Hamiltonian in the heavy quark mass limit. In this chaper, a variational approach is used to calculate the mass of a baryon for large quark masses and compared against numerical results to those based on the Bringoltz approach. It is shown that numerically our mean-field result agrees at a very high accuracy to the results based on the Hamiltonian of Ref. [17, 18], where the color-Coulomb interaction involves an infinite number of windings around the box.

In this chapter, a further issue is investigated numerically. This pertains to the *hidden colors states* that was shown to play a sub-leading role in the previous chapter. Previously, a low-density baryon crystal was studied in Ref. [28] using a mean-field approach similar to the one that will be considered in this chapter. In studying the problem, the paper made an *ad hoc* assumption regarding the color structure of the baryon crystal ground state. It assumed that each baryon in a low-density baryon crystal assumes a color singlet state even though at the time there was no compelling reason precluding a more complicated color structure, in which each baryon may not be in a color singlet state even though the crystal ground state must be a color-singlet. Subsequently, the formal approach discussed in the previous chapter was developed and indicated that hidden color is suppressed. However, it is useful to explicitly verify the no hidden color assumption numerically. While there are no independent ways of checking the validity of this assumption in 3+1

dimension, a similar assumption regarding no hidden color structure in the mean-field wave function in 1+1 dimension can be checked using the results based on the Bringoltz approach. It is found that in the low-density regime, our mean-field crystal interaction energies agree extremely well with the result based on the Hamiltonian of Ref. [17, 18].

This chapter is organized as follows: in the next section, the wave function for the baryon ground state is calculated variationally in the mean-field approach but only in the heavy quark mass limit. Next, a brief description of the approach that was taken up in Ref. [17, 18] is provided; here the origin of the windings in the box is explained and results with the single baryon masses for large quark masses in the mean-field approach are compared with the results derived based on the Bringoltz approach and the approach of Ref. [40]. In the following section, the interaction energy of nuclear matter per unit cell for parametrically low baryon densities is calculated and compared against numerical results based on the Bringoltz approach. Then, a brief discussion of our findings is provided and finally in the appendix, details of the variational calculation is provided.

3.2 Baryons in the Combined Large N_c and Large m_q Limits

3.2.1 The Energy Functional in the Mean Field Approximation

In this section, the mean-field energy functional for baryons is calculated in 1+1 dimension. A similar calculation for baryons in 3+1 dimensions was done in Ref. [28] using numerous simplifying assumptions that were argued by Witten in

Ref. [15]. Most of the simplication comes from the fact that in the mean-field approach the problem can be formulated in terms of N_c quarks moving in an average potential created by the remaining quarks. This was proved rigorously in the previous chapter. It was shown that in the heavy quark mass limit, the interactions are dominated by coherent one-gluon exchanges between any pair of N_c quarks. Multiple gluons interactions are suppressed at least at a relative order of $\frac{1}{N_c}$. Furthermore, quarks loops are suppressed at relative order of at least $\frac{1}{N_c}\frac{\Lambda_{QCD}}{m_q}$ as a result of the large N_c and non-relativistic limits.

The mean-field argument simplifies further in one spatial dimension. Here, the quarks are spinless fermions and gluon-gluon couplings can be eliminated by appropriate choice of gauge (e.g. the axial gauge as in Refs. [22] and [40]). The leading order contribution to the energy comes from a coherent one-gluon exchange between pairs of N_c quarks. Here the mean-field energy functional in 1+1 dimension is derived; the results are identical to that in 3+1 dimensions [28]. However, as mentioned in the Chapter 2, the color Coulomb potential in the context of one spatial dimension is linear. Here, the strength of the coupling is chosen to be $\frac{g^2}{4}$. This convention has been adopted from Refs. [22], [17,18] and [40]. Also note that the argument made in the previous chapter was completely independent of the potential as long as the potential is smoothly behave in N_c. In our case, the potential itself is $\mathcal{O}(N_c^0)$.

The energy of the baryon at leading order in $\frac{1}{N_c}$ and $\frac{\sqrt{\lambda}}{m_q}$ is

$$\begin{aligned}\langle\psi|H|\psi\rangle &= M_{baryon} \\ &= N_c\left(m_q + \int dx \frac{|\partial_x\psi(x)|^2}{2m_q} + \frac{\lambda}{4}\int dx dx' \frac{|\psi(x)|^2|\psi(x')|^2}{2}|x-x'|\right) \ ,\end{aligned} \tag{3.1}$$

where m_q is the quark mass, $\psi(x)$ is the normalized baryon wave function and $\lambda \equiv g^2 N_c$. Minimizing the energy functional with respect to the wave function while imposing the normalization leads to a Schrödinger equation for the ground state baryon, the following equation is obtained

$$\left(-\frac{\partial_x^2}{2m_q} + \frac{\lambda}{4}\int dx' |\psi_{min}(x')|^2|x-x'|\right)\psi_{min}(x) = \epsilon\ \psi_{min}(x) \ , \tag{3.2}$$

where ϵ is the Lagrange multiplier that keeps the wave function normalized.

3.2.2 The Variational Calculation

The ground state baryon wave function $\psi_{min}(x)$ is chosen using a variational approach. From here on, $\psi(x)$ will be taken to mean the ground state wave function $\psi_{min}(x)$. In order to proceed, it is useful to define a scaling variable R and a scaled wave function $f(y)$ where y is a dimensionless variable defined as $y \equiv \frac{x}{R}$. Then, the baryon wave function is:

$$\psi(x) = \frac{1}{\sqrt{R}} f\left(y\right) \ . \tag{3.3}$$

The normalization of the wave function $\psi(x)$ is independent of the scaling variable R as long as $f(y)$ is normalized, i.e. $\int dy |f(y)|^2 = 1$.

Next the functionals for the kinetic and potential energies, $\mathcal{T}$ and $\mathcal{V}$, are defined:

$$\mathcal{T}[f(y)] \equiv \int dy \frac{|\partial_y f(y)|^2}{2}$$
$$\mathcal{V}[f(y)] \equiv \int dy dy' \frac{|f(y)|^2 |f(y')|^2}{2} |y - y'| \ . \tag{3.4}$$

3.2.2.1 Minimization of the Energy

Rewriting the energy functional in terms of the new variables R, $\mathcal{T}[f]$ and $\mathcal{V}[f]$, the mass of the baryon has the following form:

$$\langle \psi | H | \psi \rangle \equiv M_{baryon} = N_c \left(m_q + \frac{\mathcal{T}[f(y)]}{R^2 m_q} + \frac{\lambda}{4} R \mathcal{V}[f(y)] \right) \ . \tag{3.5}$$

For simplicity, a normalized functional form for $f(y)$ is chosen to be a polynomial times a Gaussian:

$$f(y) = \frac{1}{\sqrt{\int dy (e^{\frac{-y^2}{2}} \sum_{i=0}^{n} a_i y^{2i})^2}} e^{\frac{-y^2}{2}} \sum_{i=0}^{n} a_i y^{2i} \ , \tag{3.6}$$

where n indicates the number of terms kept. Only even powers of y appear in the wave function because the ground state is expected to be symmetric. It is found that that using $n = 9$ gives energy with a very high accuracy. In order to proceed, an energy functional, which is a function of R and a_i is defined. Then, the next step is to minimize the functional with respect to each of these variables, i.e. $\partial_h \langle \psi | H | \psi \rangle = 0$ for $h \epsilon \{R, a_i\}$.

Minimizing with respect to R gives

$$R = \left(\frac{8\mathcal{T}[f(y)]}{\lambda m_q \mathcal{V}[f(y)]} \right)^{\frac{1}{3}} \ , \tag{3.7}$$

which yields:

$$\langle\psi|H|\psi\rangle = N_c\left(m_q + \frac{3}{4}\mathcal{T}^{\frac{1}{3}}[f(y)]\mathcal{V}^{\frac{2}{3}}[f(y)]m_q^{-\frac{1}{3}}\lambda^{2/3}\right) \ . \tag{3.8}$$

Next, $\langle\psi|H|\psi\rangle$ is minimized with respect to each a_i for i = 1 to 9 with a_0 chosen to be 1. Including R, there are a total of 10 parameters in the variational calculation. Since, the energy is determined very accurately with the choice of 10 variational parameters, the truncation of the variational parameters at $n = 9$ is well-justified.

The binding energy of the of the baryon is the second term in Eq. (3.12) and is characterized by the quantity $\mathcal{T}^{\frac{1}{3}}\mathcal{V}^{\frac{2}{3}}$ and converges rapidly with increasing number of parameters i.e. a_i. This is sufficient to determine the ground state energy in Eq. (3.12) and R in Eq. (3.7). The wave function is determined by the a_i, which are

$$\begin{aligned}
&a_1 \approx -0.0450660,\ a_2 \approx 0.0202162,\\
&a_3 \approx -0.0021246,\ a_4 \approx 0.0001965,\\
&a_5 \approx -6.6218907\times10^{-6},\ a_6 \approx -4.4275328\times10^{-8},\\
&a_7 \approx 7.8179284\times10^{-9},\ a_8 \approx 4.2375112\times10^{-11},\\
&a_9 \approx -4.6069215\times10^{-12}\ ,
\end{aligned} \tag{3.9}$$

such that the normalized wave function is

$$\begin{aligned}
\bar{\psi}_{min}(\bar{x}) \approx e^{-0.428871\bar{x}^2}&(0.730266 - 0.282285\bar{x}^2 + 0.0108616\bar{x}^4\\
&- 0.000979116\bar{x}^6 + 0.0000776806\bar{x}^8 - 2.24516\times10^{-6}\bar{x}^{10}\\
&- 1.28761\times10^{-8}\bar{x}^{12} + 1.95016\times10^{-9}\bar{x}^{14} + 9.06663\times10^{-12}\bar{x}^{16})\ .
\end{aligned} \tag{3.10}$$

where the following definitions have been used:

$$\begin{aligned} \bar{x} &= \left(\frac{\lambda}{4} m_q\right)^{\frac{1}{3}} x \\ \bar{\psi}_{asy}(\bar{x}) &= \left(\frac{\lambda}{4} m_q\right)^{-\frac{1}{6}} \psi_{asy}(x) \ . \end{aligned} \tag{3.11}$$

Ultimately, the result of this variational calculation (valid for heavy quarks) is compared to a result based on a more general approach based on the Hamiltonian constructed in Ref. [17, 18]. Hence, it is sensible to present the results in units of λ i.e. $g^2 N_c$, which is the only scale involved in large N_c QCD. Hence masses will be written in the units of $\sqrt{\lambda}$ and lengths in the units of $\frac{1}{\sqrt{\lambda}}$.

The ground state energy per color in units of $\sqrt{\lambda}$ obtained using a variational result that converged well is:

$$\frac{\langle\psi|H|\psi\rangle}{N_c\sqrt{\lambda}} \approx \frac{m_q}{\sqrt{\lambda}} + 0.25574 \left(\frac{m_q}{\sqrt{\lambda}}\right)^{-\frac{1}{3}} \ , \tag{3.12}$$

the parameter R is given by:

$$R = \left(\frac{8\mathcal{T}[f(y)]}{\lambda m_q \mathcal{V}[f(y)]}\right)^{\frac{1}{3}} \approx 1.079746 \left(\frac{\lambda}{4} m_q\right)^{-\frac{1}{3}} \ , \tag{3.13}$$

the dimensionless Lagrange multiplier is

$$\bar{\epsilon} \equiv \left(\frac{\lambda}{4}\right)^{-\frac{2}{3}} m_q^{\frac{1}{3}} \epsilon \approx 1.07 \ . \tag{3.14}$$

3.2.3 Asymptotic Behavior of the Wave function

While the Gaussian form of the trial wave function that was chosen for the variational calculation is very convenient to use and provides for an extremely accurate calculation for the energy for a large portion of the baryon wave function, it

however fails to correctly capture the behavior of the wave function at asymptotically large distances. At large x, the drop off of the true wave function is slower than a Gaussian [28]. Since one of the goals of this chapter is to study low-density baryon crystals, capturing the correct behavior at asymptotic distances is crucial for the study of low-density nuclear matter, where the physics is sensitive to the description of the baryon wave function tails.

In order to proceed, it is useful to analyze Eq. (3.2) in the limit where $|x| \gg |x'|$. In doing so, a Schrödinger equation that captures the asymptotic behaviour of the baryon wave function is obtained:

$$\left(-\frac{\partial_x^2}{2m_q} + \frac{\lambda}{4}|x|\right)\psi_{asy}(x) = \epsilon\psi_{asy}(x) \ . \tag{3.15}$$

The general solution is a linear combination of the Airy functions. Taking only the normalizable solution, it is found in units where

$$\begin{aligned} \bar{x} &= \left(\frac{\lambda}{4}m_q\right)^{\frac{1}{3}} x \\ \bar{\psi}_{asy}(\bar{x}) &= \left(\frac{\lambda}{4}m_q\right)^{-\frac{1}{6}} \psi_{asy}(x) \\ \bar{\epsilon} &\equiv \left(\frac{\lambda}{4}\right)^{-\frac{2}{3}} m_q^{\frac{1}{3}}\epsilon \end{aligned} \tag{3.16}$$

that

$$\bar{\psi}_{asy}(\bar{x}) = aAi(2^{\frac{1}{3}}(|\bar{x}| - \bar{\epsilon})) \ , \tag{3.17}$$

where a is an appropriate constant that determines both the matching and the normalization.

Finally, by matching the two pieces in a region where the ratio of the two functions is approximately constant, the normalization for the asymptotic wave

function is determined. Such a stable region was found in the vicinity of $\bar{x} = 3$ and the asymptotic wave function takes the form:

$$\bar{\psi}_{asy}(\bar{x}) = k\frac{e^{-\frac{2}{3}}[2^{\frac{1}{3}}(|\bar{x}| - \bar{\epsilon})]^{\frac{3}{2}}}{2\sqrt{\pi}[2^{\frac{1}{3}}(|\bar{x}| - \bar{\epsilon})]^{1/4}} \text{ with } k \approx 1.21 \text{ and } \bar{\epsilon} \approx 1.07 \ . \tag{3.18}$$

3.3 Comparison of single baryon with more general approaches

In this section, the single baryon masses calculated in the mean-field approach in the previous section is compared with baryon masses calculated using the Hamiltonian of Refs. [17, 18] and [40]. The approaches of Refs. [17, 18] and [40] both calculate baryon masses for arbitrary baryon masses and hence are more general than our mean-field approach. The primary difference between the two are associated with the nature of the Coulomb interaction between color charges. In Ref. [17, 18], the interaction is of the form $|x - y + QL|$, where L is the size of the box and Q represents the number of windings around the box. The sign of Q determines the direction around which the winding occurs, either clockwise or anti-clockwise. However, Ref. [40] only considers color Coulomb intearction of the form $|x - y|$. While the original approach of Ref. [40] is somewhat different from that of Ref. [17, 18], the numerical results for single masses can be calculated within the context of the Hamiltonian of Ref. [17, 18] by limiting the calculation to the $Q = 0$ sector of the Hamiltonian.

3.3.1 Description of the Bringoltz Approach

Here a brief description of the methods that was used in Ref. [17,18] to derive a classical Hamiltonian for the baryon sector of 1+1 large N_c QCD is provided. The starting point of the approach involves the quantum Hamiltonian of large N_c QCD, which was originally studied in Ref. [43]. It is well known that in the Hamiltonian approach of either QCD or QED Gauss' law appears as a constraint rather than equations of motion as it does in the Lagrangian approach of QCD or QED. In the Hamiltonian approach to QCD, all the physical information is encoded in a sector of the QCD Hilbert which satisfies the Gauss' law constraint. As such it is sensible to project out only these physical states. In order to achieve this, Ref. [43] finds appropriate unitary transformations to rotate the Hamiltonian such that it is specified completely in terms of unconstrained variables. This is done in the Weyl gauge such that the only gauge degrees of freedom that appear in theory are in the form of spatial Polyakov loops. Additionally, a color rotation is performed such that the Polyakov loop operators become diagonal.

However, this still leaves the Gauss' law constraint that must be imposed on the Hamiltonian. In the axial gauge, there are either local or global Gauss' law constraints [17,18]. The local ones can be solved easily and in the Hamiltonian approach these gauge fields manifest themselves as electric field operators, which can be explicitly written terms of fermion charges. However, there are $N_c - 1$ remaining gluonic modes of the gauge field, which are associated with the global Gauss' law constraint that cannot be gauged away from theory and manifest themselves as

dynamical degrees of freedom in theory.

Having constructed the quantum Hamiltonian of 1+1 large N_c QCD, Ref. [17, 18] proceeds to diagonalize the Hamiltonian using a coherent states formalism. A thorough technical discussion of this approach is presented in Ref. [44]. Here, a summary of only the most important elements of the coherent states formalism is provided. The approach relies on the fact that at large N_c, quantum fluctuations vanish and therefore any large N_c theory behaves classically. To project out a classical phase space from a quantum theory, one proceeds by constructing an over-complete set of gauge invariant states relativistic, baryonic coherent states whose diagonal projections in the large N_c limit correspond to a classical Hamiltonian whose dynamics now exist in a classical phase space instead the original quantum Hilbert space.

The classical Hamiltonian for finite density QCD at large N_c in one spatial dimension derived in Ref. [17, 18] for a box of length L is as follows:

$$\frac{\mathcal{H}}{N_c} = \lim_{M\to\infty} -\frac{i}{2}\int_0^L dxdy \frac{1}{M}\sum_{j=1}^{M}\Bigg[\left\{\mathrm{tr}\sigma_3\partial_x\rho^j(x,y) + c.c. + m\ \mathrm{tr}\sigma_1\rho^j(x,y)\right\}\delta(x-y) \\ -\frac{\lambda}{8}\frac{1}{M}\sum_{j'=1}^{M}\mathrm{tr}\{\rho^j(x,y)\rho^{j'}(y,x)\}\frac{L+(x-y)(e^{-\frac{2\pi i(j-j')}{M}}-1)}{2\sin^2(\frac{\pi(j-j')}{M}+i\epsilon)}\Bigg], \tag{3.19}$$

where the trace is only over Dirac indices. The Hamiltonian is given in terms of density matrices $\rho^j(x,y)$ but can also be represented in terms of the conjugate space density matrix $P^Q(x,y)$ as follows:

$$\rho^j(x,y) = \sum_{Q\epsilon Z} P^Q(x,y)e^{-\frac{2\pi ijQ}{M}} \tag{3.20}$$

The index Q here represents integers and $P^Q(x,y)$ is defined as:

$$P^Q(x,y) = \langle \langle C[A]|\psi^\dagger(y)U^\dagger(y,x+QL)\psi(x)|C[A]\rangle \rangle_A \ . \tag{3.21}$$

$\langle \mathcal{O} \rangle_A$ in Eq. (3.21) represents the average over all possible gauge field configurations of a gauge-invariant quantity $\mathcal{O}$.

$$\langle \mathcal{O} \rangle_A = \int d[A]\mathcal{O} \ , \tag{3.22}$$

The integral measure associated with the gauge field averaging is calculated in [45]. It is found that in the pure gauge sector, the wave functions can be written in terms of Polyakov loop eigenvalues $e^{i\phi_a}$ for $a = 1, 2...N_c$. In terms of the variable ϕ_a, the gauge wave functions for odd values of N_c behave analogous to free, non-relativistic fermions of mass $\frac{2}{g^2 L}$ on a circle that is invariant under $\phi_a \to \phi_a + 2\pi$. The eigenstates have energies proportional to the length of the box L and hence get pushed to infinity and become non-dynamical as $L \to \infty$.

U is a path-ordered (denoted $\mathcal{P}$) spatial gauge field operator

$$U(x,y) = \mathcal{P} e^{ig\int_x^y A(x')dx'} \ . \tag{3.23}$$

and $|C[A]\rangle$ represents appropriately normalized coherent states

$$|C[A]\rangle = e^{\int dxdy C(x,y)g(x,y)}|0\rangle \ . \tag{3.24}$$

Note that $|C[A]\rangle$ has implicit dependence on the gauge fields that survive the gauge fixing prcedure (denoted A) via $g(x,y)$, the gauge-invariant generators of the fermionic coherent group [17, 18]

$$g(x,y) = \psi^\dagger(x)U(x,y)\psi(y) \ , \tag{3.25}$$

$C(x,y)$ are the corresponding weights to $g(x,y)$ and $|0\rangle$ is a color singlet reference state for the fermions sector of the theory.

The diagonal projection onto coherent states defined in Eq. (3.21) is for a particular gauge configuration; however, P^Q reflects averaging over all possible gauge configurations. In this averaging, the only non-trivial structure that survives are the windings Q around the periodic box.

Note that $\rho^j(y,x)$ has the following properties:

$$\begin{aligned} \rho^j(x,y) &= \rho^j(y,x)^* \\ \int_0^L \rho^j(x,y)\rho^j(y,z)dy &= \rho^j(x,z) \\ \int_0^L dx\ \mathrm{tr}(\rho^j(x,x) - \rho^j_{vac}(x,x)) &= B\ . \end{aligned} \tag{3.26}$$

Here $\rho^j_{vac}(x,x)$ is the density matrix associated with the baryon Dirac sea and gives a contribution to the integral that is formally divergent in the absence of regularization. B is the baryon number in the box.

The baryon Hamiltonian of Eq. (3.19) can be solved numerically. In order to make the problem numerically tractable, the theory is truncated such that M in Eq. (3.19) is kept finite. This truncation introduces corrections to observables (including the baryon mass) that scale as $\frac{1}{M}$ for large M. In order to obtain the observables in the full theory, the observables are calculated for different values of M and the result in the $M \to \infty$ is obtained by extrapolation.

In order to formulate the problem numerically, the Hamiltonian is also discretized in space and the continuum results are obtained by extrapolation to the continuum limit.. A latticized Hamiltonian using staggered fermions is discussed

in detail in Ref. [17, 18]. Note that the act of latticizing the theory introduces an ultraviolet cutoff and thereby regularizes the theory and renders the density matrix, $\rho^j_{vac}(x,x)$, finite. Here, only the latticized form of the density matrix $\rho^j(x,y)$ (using staggered fermions) is presented. These matrices satisfy the properties in Eq. (3.26) can be written in terms of a finite dimensional basis of orthogonal wave functions $\phi^j_n(x)$ for each j with the indices $n, x = 1, 2...Ls$, where L_s is the number of lattice sites. The discretized density matrix is

$$\rho^j(x,y) = \sum_{n=1}^{B+\frac{L_s}{2}} \phi^j_n(x)\phi^j_n(y)^* \tag{3.27}$$

with the following orthonormality constraints on the wave functions:

$$\begin{aligned} \sum_{x=1}^{L_s} \phi^j_n(x)\phi^j_m(x)^* &= \delta_{nm} \ , \\ \sum_{n=1}^{L_s} \phi^i_n(x)\phi^j_m(x)^* &= \delta_{ij} \ . \end{aligned} \tag{3.28}$$

The sum from $n = 1$ to $\frac{L_s}{2}$ in Eq. (3.27) is the lattice version of the Dirac trace of vacuum density matrix $\rho^p_{vac}(x,x)$ in Eq. (3.26). The integral becomes regularized on the lattice and gives a finite contribution.

The classical Hamiltonian has a number of interesting features. First, the classical Hamiltonian for the baryons exhibits a softer form of volume independence [17, 18, 46]; this means that two systems with two different volumes are large N_c equivalent as long as the baryon densities are equal. Second, color charges interact via a linear Coulomb potential of the form $|x - y + QL|$, where L is the size of the box and Q refers to the number of windings around the box. The sign of Q determines the direction of the windings. The presence of these windings is a result

of the inability to gauge away all the spatial gauge degrees of freedom in a finite box. Specifically, there are $N_c - 1$ spatial gluon windings that remain in the axial gauge even after the imposition of the Gauss' law constraint.

Ref. [40], on the other hand, formulates the baryon Hamiltonian in infinite volume, where the windings represented by Q are absent; the form of the Hamiltonian is exactly the same as that of Eq. (3.19) except that $Q = 0$. However, in constructing the lattice regularized version of the resulting Hartree-Fock equations, Ref. [40] assumes that the correct approach is to use a box large enough such that finite volume effects on the baryon structure is small and with lattice spacing small enough that the baryon density can be easily resolved. For this purpose, Ref. [40] constructs a lattice potential, which has the form $|x - y|$ in the continuum and infinite volume limits, while continuing to ignore the windings. Thus, the resulting latticized theory of Ref. [40] is equivalent to the $M = 1$ truncation of the Hamiltonian in Eq. (3.19) and, for small boxes, may have significant errors. One expects these errors to go to zero as the box size goes to infinity.

3.3.2 Comparison of Single Baryon Mass and Density Profile

In the heavy quark mass limit, it is found that there is remarkable agreement between the variational result and the calculation based on the latticized baryon Hamiltonian of Ref. [17, 18]. In Figs. 3.1 and 3.4, the baryon mass extrapolations (in $\frac{1}{M}$) in boxes of size $L\sqrt{\lambda} = 2\sqrt{2\pi}$ for $\frac{m_q}{\sqrt{\lambda}} = 100$ and $L\sqrt{\lambda} = 1.6\sqrt{2\pi}$ for $\frac{m_q}{\sqrt{\lambda}} = 200$ are plotted. Note that the points plotted are the baryon masses in the continuum

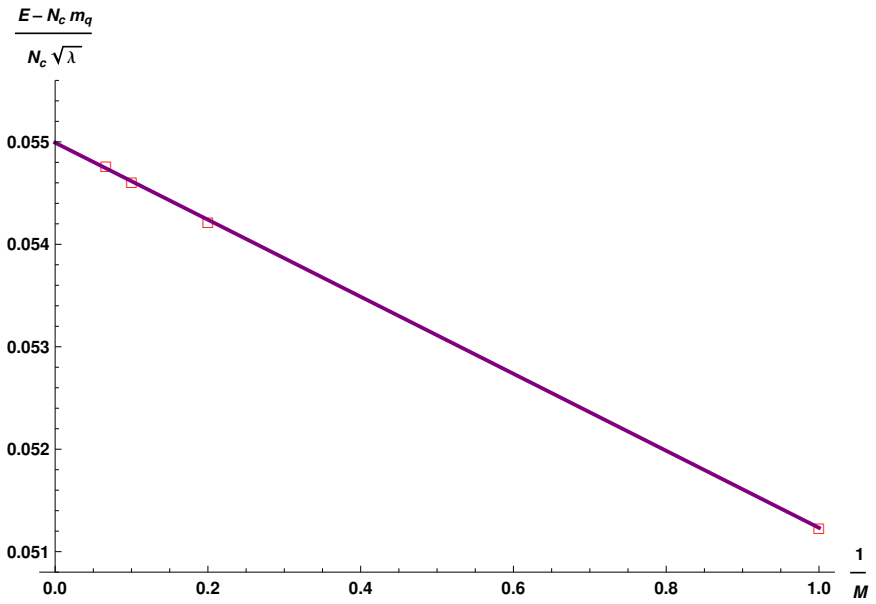

Figure 3.1: Baryon Mass Extrapolation for $\frac{m_q}{\sqrt{\lambda}} = 100$ in a box of size $L\sqrt{\lambda} = 2\sqrt{2\pi}$. Only interaction energies in the continuum are shown.

limit but for different finite values of M. The points for $M = 1, 5, 10, 15$ are have been plotted.

It is found that for quark masses of $\frac{m_q}{\sqrt{\lambda}} = 100$, the baryon mass including numerical uncertainty is $\frac{E}{N_c\sqrt{\lambda}} \approx 100.0550 \pm 0.0001$ and for quark masses of $\frac{m_q}{\sqrt{\lambda}} = 200$, the baryon mass with numerical uncertainty is $\frac{E}{N_c\sqrt{\lambda}} \approx 200.0439 \pm 0.0003$. For convenience, this result is summarized in Table 3.1, where the interaction energy for single baryons (i.e. excluding bare masses) from numerical results plotted in Figs. (3.1) and (3.4), which is denoted E_H. The interaction energy from our variational calculation as stated in Eq. (3.12) is also presented. This quantity is denoted E_v in the Table 3.1. Up to the uncertainties in the mean-field calculation, the masses are 100.055098 and 200.043731 for quark masses $(\frac{m_q}{\sqrt{\lambda}})$ of 100 and 200 respectively. It

is clear that the numerical results based on the Bringoltz approach are consistent with the results from the mean-field approximation.

Table 3.1: Single baryon interaction energy comparison between the variational calculation (E_v) and 't Hooft model with $M \to \infty$ (E_H).

	Baryon Masses−Quark Mass	
$\frac{m_q}{\sqrt{\lambda}}$	E_v	E_H
100	0.055098	0.0550 ± 0.0001
200	0.043731	0.0439 ± 0.0003

Next, baryon density profiles are plotted for the two calculations with the line representing the result of the variational calculation and the dots representing the result of the general finite baryon density Hamiltonian. The densities are plotted for $M = 15$ and with the number of lattice points, $L_s = 170$. The two results agree quite well in spite of the errors associated with discretization of space and truncation in the number of windings.

3.3.2.1 Relevance of the Zero Modes

It is clear from the single baryon energies that including the zero modes gives baryon masses in reasonably-sized boxes that are consistent with Witten's heavy quark results. In Table 3.2, the interaction energy of the $M = 1$ baryon mass (which is labelled by E_h) with the interaction energy from of the baryon mass calculated using Witten's heavy quark mean-field argument are compared. The

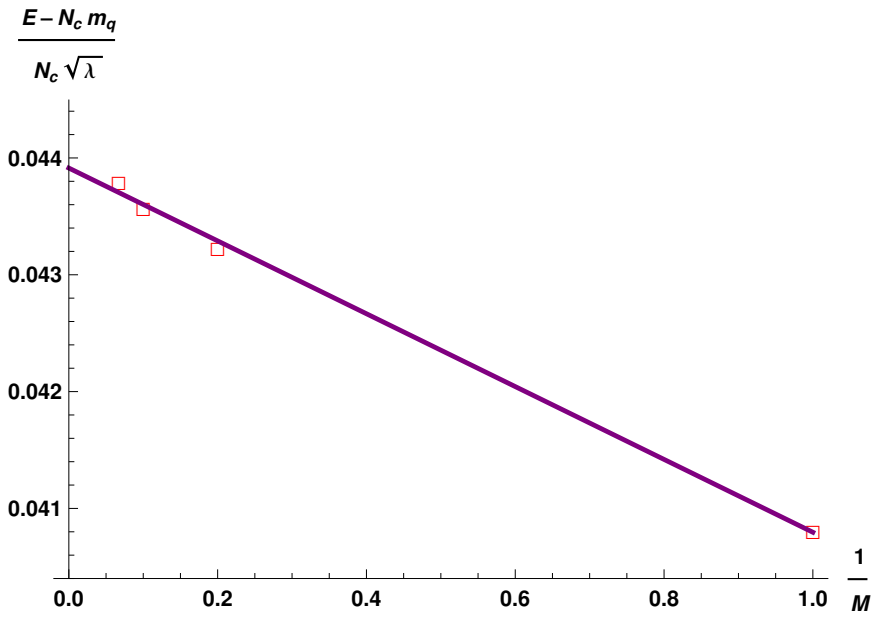

Figure 3.2: Baryon Mass Extrapolation for $\frac{m_q}{\sqrt{\lambda}} = 200$ in a box of size $L\sqrt{\lambda} = 1.6\sqrt{2\pi}$. Only interaction energies in the continuum are shown.

relative difference in interaction energies between the two baryon masses, which is defined as $\frac{E_v - E_h}{\frac{1}{2}(E_v + E_h)}$, is also presented.

The relative difference between the $M = 1$ result (which is consistent with Ref. [40]) and Witten's heavy quark mean-field formulation is significantly larger and inconsistent even though the box sizes used were large enough to comfortably contain the baryon wave function. This is consistent with the claims made in Ref. [17, 18], where it was argued that it is impossible to gauge away zero modes in a finite box and taking account of these degrees of freedom is crucial to not only obtain correct physical observables but also observe another physical effect namely volume independence, which is expected to hold on more general grounds for translationally invariant states assuming Z_N symmetry is intact, which it is in the finite volume

Table 3.2: Single baryon interaction energy comparison between the variational calculation (E_v) and 't Hooft model with $M = 1$ (E_h).

	Baryon Masses−Quark Mass		
$\frac{m_q}{\sqrt{\lambda}}$	E_v	E_h	$\frac{E_v - E_h}{\frac{1}{2}(E_v + E_h)}$
100	0.055098	0.05124 ± 0.00002	0.07
200	0.043731	0.04081 ± 0.00002	0.07

treatement of the 't Hooft model [17, 18, 46]. Naively, one might have expected these finite box size to be relatively small. However, the single baryon sector shows that for infinitely heavy quark masses, our mean-field results are consistent with the claims of Ref. [17, 18].

3.4 Baryonic matter

3.4.1 Introduction to the Multi-baryon Problem

Now that it has been established that the Witten's heavy-quark formulation for single baryons is consistent with results based on Bringoltz's Hamiltonian, baryonic matter is considered. It is believed that at large N_c, baryons form a crystal: the baryons are heavy and so tend to lie in equilibrium in the potential wells created by the other baryons. In this section, the problem of infinite nuclear matter at low enough densities (such that only inter-baryon interactions between nearest neighbors are relevant) is considered.

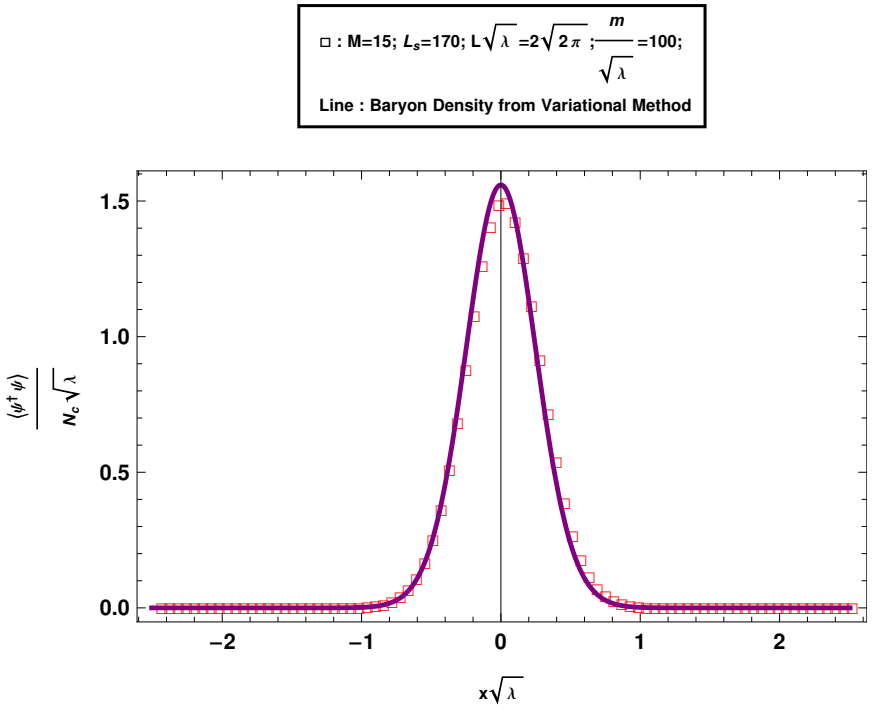

Figure 3.3: Baryon Density for $\frac{m_q}{\sqrt{\lambda}} = 100$ with $M = 15$ and $L_s = 170$ in a box of size $L\sqrt{\lambda} = 2\sqrt{2\pi}$.

Here, in agreement with results of Chapter 2, it is assumed that the many-baryon sector consists of distinct color-singlet clusters of N_c quarks with identical wave functions, as in Witten's discussion of baryon scattering [15]. It was rigorously established in the previous chapter that the hidden color states only contribute at sub-leading order in the large N_c expansion.

First, the mean-field energy functional is constructed for a low-density baryon crystal in a heavy quark and non-relativistic formalism. The energy per unit-cell of the low-density baryon crystal is:

$$\begin{aligned}\frac{\bar{E}}{N_c} &= \frac{1}{2}\int d\bar{x}\,(\partial_{\bar{x}}\bar{\Psi}_i(\bar{x}))^2 + \frac{1}{2}\int d\bar{x}\,d\bar{y}\,|\bar{\Psi}_i(\bar{x})|^2|\bar{\Psi}_i(\bar{y})|^2|\bar{x}-\bar{y}| \\ &+ \frac{1}{2}\int d\bar{x}\,d\bar{y}\,\bar{\Psi}_i(\bar{x})\bar{\Psi}_{i-1}(\bar{y})\bar{\Psi}_{i-1}(\bar{x})\bar{\Psi}_i(\bar{y})|\bar{x}-\bar{y}| \\ &+ \frac{1}{2}\int d\bar{x}\,d\bar{y}\,\bar{\Psi}_i(\bar{x})\bar{\Psi}_{i+1}(\bar{y})\bar{\Psi}_{i+1}(\bar{x})\bar{\Psi}_i(\bar{y})|\bar{x}-\bar{y}|\ ,\end{aligned} \tag{3.29}$$

where $\bar{\Psi}_i(\bar{x})$ is the wave function of the reference baryon in the unit cell, $\bar{\Psi}_{i\pm1}(\bar{x})$ are the wave functions of the nearest-neighbor baryons, the first term is the contribution to intrabaryon kinetic energy, the second term is the contribution to intrabaryon potential energy and the last two terms are the contributions to interbaryon energy. Note that the intrabaryon potential is different from the free space one because of the fact that the baryon wave function is now distorted the nearest neighbor interactions. By assumption, interactions beyond the nearest-neighbor are negligible. Note that both λ and m_q have been scaled out of the energy density using the following

transformations:

$$\begin{aligned}
\bar{x} &= \left(\frac{\lambda}{4} m_q\right)^{\frac{1}{3}} x \\
\bar{\psi} &= \left(\frac{\lambda}{4} m_q\right)^{-\frac{1}{6}} \psi \\
\bar{E} &= \left(\frac{\lambda}{4}\right)^{-\frac{2}{3}} m_q^{\frac{1}{3}} E \ .
\end{aligned} \tag{3.30}$$

The wave function for the baryon crystal is constrained by the Pauli exclusion principle, which precludes two fermions from simultaneously occupying the same position. Mathematically speaking, this demands that the wave function of a reference baryon state $\bar{\Psi}(x)$ be completely orthogonal to the wave function of the neighboring baryon states $\bar{\Psi}(\bar{x}+\bar{d})$ and $\bar{\Psi}(\bar{x}-\bar{d})$.

$$\begin{aligned}
&\bar{\Psi}(\bar{x}) = (1+\kappa)\bar{\psi}_0(\bar{x}) - \alpha\bar{\phi}(\bar{x}-\bar{d}) - \alpha\bar{\phi}(\bar{x}+\bar{d}) \\
&\text{with } \int d\bar{x}\, |\bar{\Psi}(\bar{x})|^2 = 1 \text{ and } \int d\bar{x}\, \bar{\Psi}(\bar{x})\bar{\Psi}(\bar{x}\pm\bar{d})| = 0 \ ,
\end{aligned} \tag{3.31}$$

where $\bar{\phi}$ is some normalized wave function.

Here, it has been assumed that densities are low enough that the reference baryon wave function is dominated by the single baryon wave function $\bar{\psi}(\bar{x})$ except for corrections centered around $\bar{x} = \pm\bar{d}$. The choice of κ and α is determined by the orthogonality constraint of the neighboring baryons and by normalization of the baryon wave function. κ and α are calcualted in terms of $\gamma \equiv \int d\bar{x}\bar{\psi}_0(\bar{x})\bar{\phi}(\bar{x})$, which characterizes the overlap at the same spatial points of the neighboring baryon wave functions and the quantity $\mathcal{A}' \equiv \int d\bar{x}\bar{\psi}_0(\bar{x})\bar{\phi}(\bar{x}+\bar{d})$, which characterizes the orthogonality of the neighboring wave functions:

$$\begin{aligned}
&\alpha = \frac{\mathcal{A}}{2\gamma} \text{ and } \kappa = \frac{\mathcal{A}\mathcal{A}'}{\gamma} - \frac{\mathcal{A}^2}{4\gamma^2} \\
&\text{where } \mathcal{A} \equiv \int d\bar{x}\, \bar{\psi}_0(\bar{x})\bar{\psi}_0(\bar{x}\pm\bar{d}) \ .
\end{aligned} \tag{3.32}$$

The analysis disregards $\mathcal{O}(\mathcal{A}^3)$ effects because $\mathcal{A}$ becomes exponentially small with decreasing density and in the low density regime, the higher order effects are exponentially small. Effectively a simultaneous expansion in terms of $\mathcal{A}$ and $\frac{w}{d}$ is being performed, with w being the characteristic width of a baryon and d is the separation between neighboring baryons.

In order to proceed, it is assumed that $\bar{\phi}(\bar{x}) = \bar{\psi}_0(\bar{x})$, which is the most efficient way to orthogonalize neighboring crystal wave functions. The orthogonality constraint in doing so becomes

$$\int d\bar{x}\bar{\Psi}(\bar{x})\bar{\Psi}(\bar{x}+\bar{d}) = -\mathcal{A}(\bar{d}) + \mathcal{O}(\mathcal{A}^3) \ . \tag{3.33}$$

As can be seen from the explicit form of $\mathcal{A}(\bar{d})$, which will be calculated in the following subsection, for parametrically low densities $\mathcal{A}(\bar{d}) \sim e^{-\bar{d}^{\frac{3}{2}}}$. Hence, it is plausible that in the low density regime, where only nearest neighbor interactions are relevant, the choice of $\bar{\phi}(\bar{x}) = \bar{\psi}_0(\bar{x})$ is indeed the correct one. In the appendix, corrections to single baryon wave function are introduced such that $\bar{\phi}(\bar{x}) = \eta(\bar{\psi}_0(\bar{x}) + \delta\bar{\Delta}(\bar{x}))$ and explicitly find that contributions to energy at $\mathcal{O}(\delta)$ only contributes at $\mathcal{O}(\mathcal{A}^2\bar{d}^0)$ and hence is parametrically small in the low-density limit.

3.4.2 Calculation of the overlap function $\mathcal{A}$

Before calculating the low-density crystal interaction energy (i.e. energy per baryon modulo the isolated baryon mass), it is useful to calculate the overlap function $\mathcal{A}$, which is a very useful quantity that has been defined in Eq. (3.32). Most

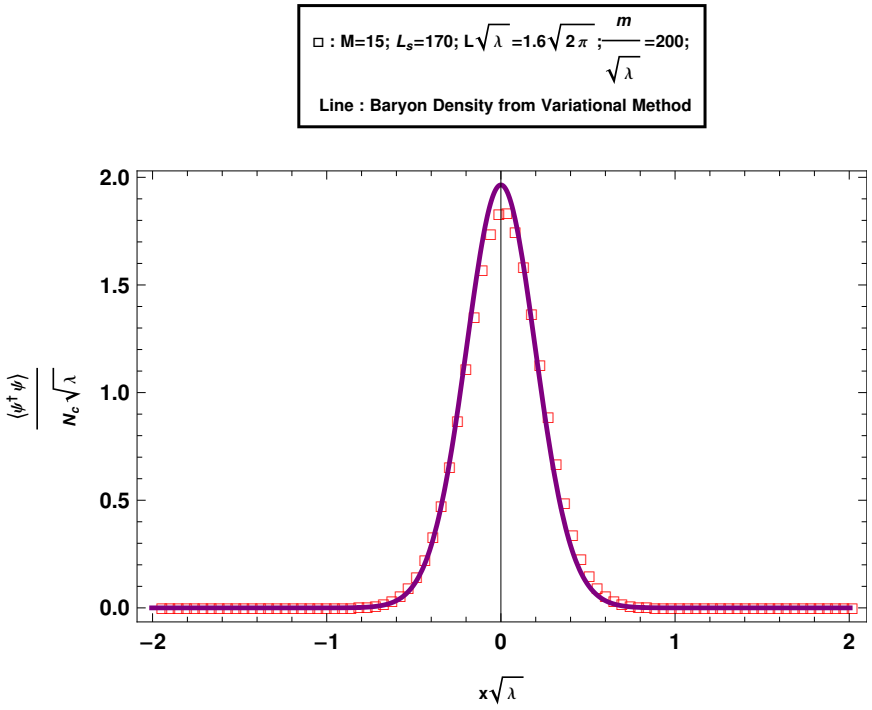

Figure 3.4: Baryon Density for $\frac{m_q}{\sqrt{\lambda}} = 200$ with $M = 15$ and $L_s = 170$ in a box of size $L\sqrt{\lambda} = 1.6\sqrt{2\pi}$.

of the contribution to $\mathcal{A}$ comes from the localized baryon density at $\bar{x} = \frac{\bar{d}}{2}$. In the low density regime, the contributions to $\mathcal{A}$, localized at $\bar{x} = 0$ and $\bar{x} = \bar{d}$ are exponentially suppressed. The contribution to the center comes from the tails of neighboring baryons, which have the form of Airy functions. Using the asymptotic form of Airy functions, the following result is obtained.

$$\mathcal{A} = \int d\bar{x} \, \frac{k^2 e^{-\frac{1}{3}(2\bar{d}-2\bar{\epsilon}-2\bar{x})^{3/2} - \frac{1}{3}(-2\bar{\epsilon}+2\bar{x})^{3/2}}}{2^{5/3}\pi(2\bar{d}-2\bar{\epsilon}-2\bar{x})^{1/4}(-2\bar{\epsilon}+2\bar{x})^{1/4}} \, . \tag{3.34}$$

Here, $k \approx 1.21$ is the strength of the asymptotic wave function of Eq. (3.18).

The function in the exponent has a minima at $\bar{x} = \frac{\bar{d}}{2}$ and hence the baryon density (i.e. the integrand) contributing to $\mathcal{A}$ has a maxima at $\bar{x} = \frac{\bar{d}}{2}$. Using a standard steepest descent method to calculate the integral (which involves series expanding the exponent around the turning point, evaluating the denominator of $\mathcal{A}$ at $\bar{x} = \frac{\bar{d}}{2}$ and performing the integral), the following expression for the overlap function is obtained:

$$\mathcal{A}(\bar{d}) = \frac{k^2 e^{-\frac{2}{3}(\bar{d}-2\bar{\epsilon})^{3/2}}}{2 \; 2^{2/3}(\bar{d}-2\bar{\epsilon})^{1/4}\sqrt{\pi}} \, . \tag{3.35}$$

with a leading order correction term that is proportional to $\frac{e^{-\frac{2}{3}(\bar{d}-2\bar{\epsilon})^{3/2}}}{(\bar{d}-2\bar{\epsilon})^{7/4}}$. The correction is suppressed for parametrically large distances, which is the relevant regime being considered here.

3.4.3 Energy at $\mathcal{O}(\mathcal{A}^2)$

Here, the calculation of the interaction energy per unit cell of a low density baryon crystal is done upto $\mathcal{O}(\mathcal{A}^2)$ and leading order in $\mathcal{O}\left(\frac{w}{d}\right)$ using units of

Eq. (3.30). w is the characteristic width of an isolated baryon and d is the interbaryon separation.

3.4.3.1 Interbaryon Potential Energy

The contribution to the interbaryon energy under the assumption that only nearest neighbor interactions are relevant comes from the following term:

$$\begin{aligned}\frac{\bar{E}^{\text{interbaryon}}_{\text{potential}}}{N_c} &= \frac{1}{2}\int d\bar{x}\, d\bar{y}\, \bar{\Psi}(\bar{x})\bar{\Psi}(\bar{x}+\bar{d})\bar{\Psi}(\bar{y})\bar{\Psi}(\bar{y}+\bar{d})|\bar{x}-\bar{y}| \\ &+ \frac{1}{2}\int d\bar{x}\, d\bar{y}\, \bar{\Psi}(\bar{x})\bar{\Psi}(\bar{x}-\bar{d})\bar{\Psi}(\bar{y})\bar{\Psi}(\bar{y}-\bar{d})|\bar{x}-\bar{y}|\ ,\end{aligned} \tag{3.36}$$

where

$$\begin{aligned}\bar{\Psi}(\bar{x})\bar{\Psi}(\bar{x}\pm\bar{d}) &= (1+\kappa)^2\bar{\psi}_0(\bar{x})\bar{\psi}_0(\bar{x}\pm\bar{d}) - \alpha(1+\kappa)\bar{\psi}_0(\bar{x})\bar{\psi}_0(\bar{x}) \\ &- \alpha(1+\kappa)\bar{\psi}_0(\bar{x}\pm\bar{d})\bar{\psi}_0(\bar{x}\pm\bar{d}) + \alpha^2(\bar{\psi}_0(\bar{x}\pm\bar{d})\bar{\psi}_0(\bar{x}\pm 2\bar{d}) \\ &+ \bar{\psi}_0(\bar{x})\bar{\psi}_0(\bar{x}\pm\bar{d}) + \bar{\psi}_0(\bar{x})\bar{\psi}_0(\bar{x}\mp\bar{d}))\ .\end{aligned} \tag{3.37}$$

The structure of the contributions to the interbaryon energy is of the form $\int d\bar{x}\, d\bar{y}\, \rho(\bar{x})\rho(\bar{y})|\bar{x}-\bar{y}|$, which is similar to that of two identical effective charge densities $\rho(\bar{x})$ interacting via a linear Coumlomb potential analogous to how charge densities would interact in 1+1 dimensional electrostatics.

The effective charge density $\rho(\bar{x}) \equiv \bar{\Psi}(\bar{x})\bar{\Psi}(\bar{x}+\bar{d})$ is presented in Eq. (3.37). It is composed of single baryon charge densities which either scale with $\bar{d}$ or do not. In the low-density regime that is of concern here, any contributions to interbaryon energy that does not scale with baryon separation can be ignored as these contributions are small compared to the contributions from terms that do depend on $\bar{d}$.

Furthermore, since it has been assumed that $\bar{\phi}(\bar{x}) = \bar{\psi}_0(\bar{x})$ minimizes the interaction energy; in this case, from Eq. (3.32), the result is that $\alpha = \mathcal{A}^2$ and $\kappa = \frac{3}{4}\mathcal{A}^2$.

A schematic diagram for the effective charge densities of Eq. (3.37) upto $\mathcal{O}(\mathcal{A}^2)$ is plotted in Fig. 3.5. The effective charge density consists of localized charges at $\bar{x} = 0$, $\frac{\bar{d}}{2}$ and $\bar{d}$. The charge density contributions at $\bar{x} = 0$ and $\bar{d}$ come from charge densities of the form $\bar{\psi}_0(\bar{x})\bar{\psi}_0(\bar{x})$ and $\bar{\psi}_0(\bar{x} \pm \bar{d})\bar{\psi}_0(\bar{x} \pm \bar{d})$ respectively. As such they do not scale with baryon density. However, the charge density in the middle comes from a shifted piece of the form $\bar{\psi}_0(\bar{x})\bar{\psi}_0(\bar{x} \pm \bar{d})$ and hence scales with $\bar{d}$. In order to proceed, it is assumed that in the low density limit, the effective charge densities can be approximated using delta functions (with appropriate integrated charges) except for the corrections arising from the finite width of the charge density at $\bar{x} = \frac{\bar{d}}{2}$. Then, the total interbaryon energy is

$$\frac{\bar{E}^{\text{interbaryon}}_{\text{potential}}}{N_c} = -\frac{\mathcal{A}^2 d}{2} + \frac{\Delta\bar{E}^{\text{correction}}}{N_c} \ , \tag{3.38}$$

where $\frac{\Delta\bar{E}^{\text{correction}}}{N_c}$ is the afore-mentioned finite width correction from the center peak. The size of the correction can be calculated using the approximation to the asymptotic form of the Airy function that was used to calculate the overlap integral $\mathcal{A}$ and the resulting integral can be calculated easily using the method of steepest descent to yield the result:

$$\frac{\Delta\bar{E}^{\text{correction}}}{N_c} = \sqrt{\frac{2}{\pi}}(d - 2\epsilon)^{1/4}\mathcal{A}^2(d) \ . \tag{3.39}$$

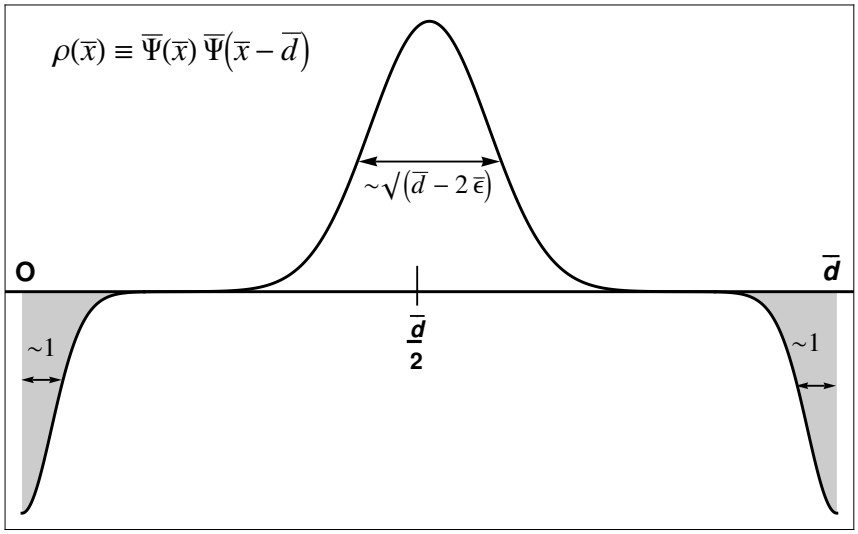

Figure 3.5: Schematic plot of the effective charge density $\Psi(\bar{x})\Psi(\bar{x}-\bar{d})$ associated with the interbaryon energy including the characteristic width of the relevant baryon densities in units of Eq. (3.30). The magnitude of the effective charge in each region is $\mathcal{A}$. The total effective charges are $\mathcal{A}$ in the peak at $\bar{x} = \frac{\bar{d}}{2}$ and $-\frac{\mathcal{A}}{2}$ each in the peaks at $\bar{x} = 0\ , \bar{d}$

3.4.3.2 Intrabaryon Potential Energy

Next the intrabaryon potential energy contribution to the interaction energy per unit cell of the baryon crystal is calculated. This contribution comes from the following term:

$$\frac{\bar{E}^{\text{intrabaryon}}_{\text{potential}}}{N_c} = \frac{1}{2}\int d\bar{x}\, d\bar{y}\, |\bar{\Psi}(\bar{x})|^2 |\bar{\Psi}(\bar{y})|^2 |\bar{x}-\bar{y}| \ , \tag{3.40}$$

where

$$\begin{aligned} |\Psi(\bar{x})|^2 = {} & (1+\kappa)^2 \bar{\psi}_0(\bar{x})^2 + \alpha^2(\bar{\psi}_0(\bar{x}+\bar{d})^2 + \bar{\psi}_0(\bar{x}-\bar{d})^2) \\ & - 2(1+\kappa)\alpha(\bar{\psi}_0(\bar{x})\bar{\psi}_0(\bar{x}+\bar{d}) + \bar{\psi}_0(\bar{x})\bar{\psi}_0(\bar{x}-\bar{d})) \\ & + \alpha^2(\bar{\psi}_0(\bar{x}+\bar{d})\bar{\psi}_0(\bar{x}-\bar{d})) \ . \end{aligned} \tag{3.41}$$

Again, working up to $\mathcal{O}(\mathcal{A}^2)$ in the interaction energy and only at leading order in $\mathcal{O}\left(\frac{w}{d}\right)$, where w is the width of a baryon and d the separation between baryons.

A schematic plot of the charge density of Eq. (3.41) is shown in Fig. 3.6. In the diagram, an order one piece coming from the isolated baryon wave function, which does not contribute to the baryon interaction energy, has been subtracted off. Additionally, only the region of the charge density $0 < \bar{x} < \bar{d}$ has been plotted. The effective charge density associated with the intrabaryon energy is even around $\bar{x} = 0$.

An obvious difference between the effective charge density associated with interbaryon energy and that associated with intrabaryon potential energy is that the intrabaryon one does not have distinctly localized charges unlike the interbaryon

one. However, in spite of this the charge densities in Fig. (3.5) and the order one piece $|\bar{\psi}_0(\bar{x}|^2$ can be approximated as delta functions localized at $\bar{x} = 0$, $\frac{\bar{d}}{2}$ and $\bar{d}$ with the appropriate integrated charges for the charge densities. There may be corrections coming from the fact that the charge density at the center has a width. However, any interactions within the peak at $\bar{x} = 0$ is of $\mathcal{O}(\mathcal{A}d\bar{w})$, where w is the width of the single baryon density. Finally, the contribution from the intrabaryon potential energy is

$$\frac{\bar{E}^{\text{intrabaryon}}_{\text{potential}}}{N_c} = -\frac{\mathcal{A}^2\bar{d}}{2} \ . \tag{3.42}$$

3.4.3.3 Intrabaryon Kinetic Energy

The intrabaryon kinetic energy contribution at leading order in $\frac{w}{d}$ is presented in Eq. (3.43). Note that the first four terms are independent of the interbaryon spacing or $\bar{d}$, whereas the remaining terms are not; in the low-density regime, the contribution from these terms independent of $\bar{d}$ are parametrically small. Furthermore, the $\mathcal{O}(1)$ term is ignored because it is the contribution to the single baryon energy and not the crystal interaction energy. Also, the last term is ignored because it is not nearest neighbor.

$$\begin{aligned}\frac{\bar{E}^{\text{intrabaryon}}_{\text{kinetic}}}{N_c} &= \frac{1}{2}\int d\bar{x}\,(\partial_{\bar{x}}\bar{\Psi}(\bar{x}))^2 \\ &= \frac{1}{2}(1+\kappa)^2\int d\bar{x}\,(\partial_{\bar{x}}\bar{\psi}_0(\bar{x}))^2 + \frac{1}{2}\alpha^2\int d\bar{x}\,(\partial_{\bar{x}}\bar{\psi}_0(\bar{x}+\bar{d}))^2 \\ &+ \frac{1}{2}\alpha^2\int d\bar{x}\,(\partial_{\bar{x}}\bar{\psi}_0(\bar{x}-\bar{d}))^2 - \alpha(1+\kappa)\int d\bar{x}\,(\partial_{\bar{x}}\bar{\psi}_0(\bar{x}))(\partial_{\bar{x}}\bar{\psi}_0(\bar{x}+\bar{d}))- \\ &\alpha(1+\kappa)\int d\bar{x}\,(\partial_{\bar{x}}\bar{\psi}_0(\bar{x}))(\partial_{\bar{x}}\bar{\psi}_0(\bar{x}-\bar{d})) + \alpha^2\int d\bar{x}\,(\partial_{\bar{x}}\bar{\psi}_0(\bar{x}+\bar{d}))(\partial_{\bar{x}}\bar{\psi}_0(\bar{x}-\bar{d}))\end{aligned} \tag{3.43}$$

The remaining terms can be calculated using the asymptotic form of the Airy function and the steepest descent method to evaluate the integral as the integrand is sharply peak about $\bar{x} = \pm\frac{\bar{d}}{2}$. The kinetic energy contribution to the interaction energy is

$$\frac{\bar{E}^{\text{intrabaryon}}_{\text{kinetic}}}{N_c} = \mathcal{A}^2\bar{d}\ . \tag{3.44}$$

3.4.3.4 Total Interaction Energy

Therefore, putting all the interaction energies together, the energy per unit cell of a low-density baryon crystal in the heavy quark mass limit up to $\mathcal{O}(\mathcal{A}^2)$ and to leading order in $\frac{w}{d}$ is:

$$\begin{aligned}\frac{\bar{E}}{N_c} &= \frac{\bar{E}^{\text{interbaryon}}_{\text{potential}}}{N_c} + \frac{\bar{E}^{\text{intrabaryon}}_{\text{potential}}}{N_c} + \frac{\bar{E}^{\text{intrabaryon}}_{\text{kinetic}}}{N_c} \\ &= \sqrt{\frac{2}{\pi}}(\bar{d}-2\bar{\epsilon})^{1/4}\mathcal{A}^2(\bar{d})\ .\end{aligned} \tag{3.45}$$

Since this relation is valid only in the regime $\bar{d} \gg 1$, one might be tempted to do an expansion in powers of $\bar{d}$. However, the expression for $\mathcal{A}$ in Eq. (3.35) converges extremely slowly and will require a large number of terms to accurately reproduce

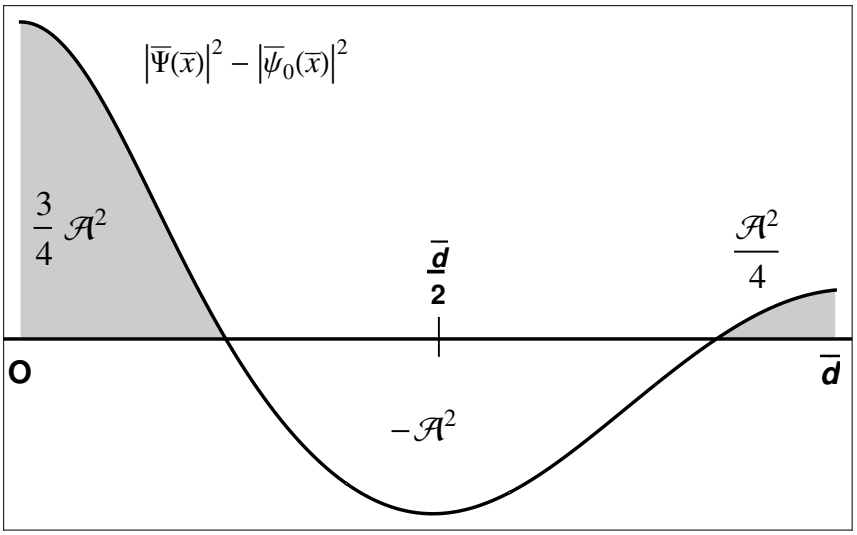

Figure 3.6: Schematic plot of $|\Psi(\bar{x})|^2 - |\bar{\psi}_0(\bar{x})|^2$, the effective charge density minus the single baryon charge density for $0 < \bar{x} < \bar{d}$ including the total baryon charge in each region.

the correct interaction energy. Hence, the interaction energy as it is in Eq. (3.45) is kept. Therefore, the expression remains valid for higher densities than it would otherwise have been.

3.5 Comparison with Bringoltz's Hamiltonian

In this section, a comparison is made between the results of the low-density baryon crystal energy to the numerical results based on Bringholtz's Hamiltonian [17,

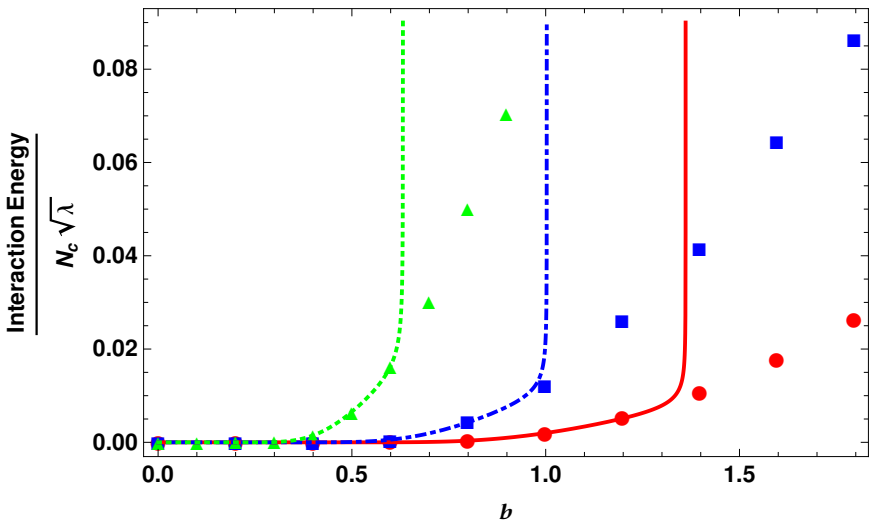

Figure 3.7: Interaction Energy with $\frac{m_q}{\sqrt{\lambda}} = 10, 40, 100$ are represented by triangle (dashed), square (dash-dotted) and circle (solid) respectively. The points are the finite baryon density 't Hooft model results and the lines are the result from the variational calculation.

18]. Below, the plot of the interaction energies for three different quark masses: $\frac{m_q}{\sqrt{\lambda}} = 10, 40, 100$ is made. The plot contains interaction energy (per color) in the y-axis and the baryon density $b = \frac{B}{L\sqrt{\lambda}}$, where B is the baryon number and $L\sqrt{\lambda}$ is the size of the box, in the x-axis. The points represent the results from numerical finite density calculations based on Ref. [17, 18], which is valid at all densities and quark masses; the lines represent the results based on the variational calculation.

The calculation was done for $M = 10$ and $L_s = 130$ at a fixed volume for each of the quark masses. The $\frac{m_q}{\sqrt{\lambda}} = 10$ calculation was done in a box of size $L\sqrt{\lambda} = 4\sqrt{2\pi}$ and the $\frac{m_q}{\sqrt{\lambda}} = 40, 100$ calculations were performed in a box of size $L\sqrt{\lambda} = 2\sqrt{2\pi}$.

Obviously, there are numerical corrections to the interaction energy associated with discretization in space and the fact that M is finite. It will be assumed that for

the large quark masses involved the corrections associated with choosing a finite $M = 10$ and a non-infinite number of lattice sites $L_s = 130$ are relatively small [17, 18]. The discretization correction depends on the number of lattice points that define the wave function of a single baryon. Since, different densities in a box of the same size (for each quark mass) is probed, the error associated with discretization is comparable for different baryon densities.

It is found that the agreement between the low-density variational calculation and the results based on Ref. [17,18] is very good. However, it is remarkable that the agreement extends to densities beyond the extreme low-density regime; note that the regime of validity of the variational result is for parametrically low densities. In deriving Eq. (3.45), rather strong assumptions were made, which one might have thought could break down rapidly as the baryons begin to overlap substantially in space. Apparently, this is not the case. It can also be seen in Fig. (3.5) that the mean-field energy blows up as $\bar{d} \to 2\bar{\epsilon}$. This is expected from the form of $\mathcal{A}$ in Eq. (3.35). However, it is surprising that the variational baryon density result works for masses as low as $\frac{m_q}{\sqrt{\lambda}} = 10$.

3.6 Conclusion

In this chapter, some interesting results relevant to finite density large N_c QCD have been found. The first finding relates to the problem of determining the properties of baryons at arbitrary masses and densities that was solved a few years ago in Ref. [17, 18]. The primary result of this paper is based on the Hamiltonian rep-

resentation of QCD, which was solved in Ref. [43]. From this approach, it becomes quite clear that in a finite box, there are dynamical gauge degrees of freedom, which cannot be completely gauged away. These gauge degrees of freedom manifest themselves in the classical Hamiltonian as color Coulomb interactions with all possible windings around the finite box. One might have expected that for large enough box sizes, these windings are not relevant. However, using an independent mean-field approach based on Witten's argument for infinitely heavy quark masses [15] (which was justified in the previous chapter), it has been shown that even for box sizes that were large enough to fit a baryon wave function comfortably, taking account of these windings is essential to get baryon masses that are consistent with masses calculated using the Hamiltonian of Ref. [17, 18].

The second result of this work is related to the ground state baryon crystal color structure. Obviously physical states have to be a color singlet state; however, the mean-field ground state may possess a color-structure, in which each baryon in the crystal may not be a color-singlet. This assumption was made both in Ref. [15] and in Ref. [28]. In this work, it has been shown by comparison with results based on the Hamiltonian of [17, 18] that this assumption is indeed consistent at least for the low-density regime. The full rigorous proof is presented in the previous chapter and the result is valid both in 3+1 dimensions and 1+1 dimension even though in this chapter the "numerical proof" was limited to parametrically low densities in 1+1 dimension.

3.7 APPENDIX: $\mathcal{O}(\delta)$ contribution to low-density baryon crystal energy

In this section, corrections to $\bar{\phi}(\bar{x})$ are introduced such that $\bar{\phi}(\bar{x}) = \eta(\bar{\psi}_0(\bar{x}) + \delta\bar{\Delta}(\bar{x}))$ and show that the contributions to interaction energies at $\mathcal{O}(\delta)$ is at most of $\mathcal{O}(\mathcal{A}^2\bar{d}^0)$ and therefore is parametrically small compared to the contribution from $\mathcal{O}(\delta^0)$, which has been shown to have a contribution of $\mathcal{O}(\mathcal{A}^2\bar{d}^{\frac{1}{4}})$. In doing the calculation, it is assumed that $\bar{\Delta}(\bar{x})$ is normalized and orthogonal to both $\bar{\psi}(\bar{x})$ and $\bar{\psi}(\bar{x} \pm \bar{d})$. It is always possible to do this because any part of $\bar{\Delta}(\bar{x})$ or $\bar{\Delta}(\bar{x} \pm \bar{d})$ that is not orthogonal to $\bar{\psi}_0(\bar{x})$ can be absorbed into $\bar{\psi}_0(\bar{x})$. Normalization of $\bar{\Delta}$ means that $\eta^2 = \frac{1}{1+\delta^2}$. Furthermore, it is possible identify $\gamma \equiv \eta$ and $\mathcal{A}' = \eta\mathcal{A}$ and using Eq. (3.32), $\kappa = \frac{3}{4}\mathcal{A}^2$.

3.7.1 Intrabaryon Potential Energy

The contribution at $\mathcal{O}(\delta)$ to the intrabaryon potential energy comes from the following eight terms:

$$
\begin{aligned}
\frac{\bar{E}^{\text{intrabaryon}}_{\text{potential}}}{N_c} = -\mathcal{A}\Bigg(&\underline{\int d\bar{x}\, d\bar{y}\, \bar{\psi}_0(\bar{x})^2 \bar{\psi}_0(\bar{y}) \bar{\Delta}(\bar{y}+\bar{d})|\bar{x}-\bar{y}|} \\
&+ \underline{\int d\bar{x}\, d\bar{y}\, \bar{\psi}_0(\bar{x})^2 \bar{\psi}_0(\bar{y}) \bar{\Delta}(\bar{y}-\bar{d})|\bar{x}-\bar{y}|}\Bigg) \\
&+ \frac{\mathcal{A}^2}{2}\Bigg(\int d\bar{x}\, d\bar{y}\, \bar{\psi}_0(\bar{x})^2 \bar{\psi}_0(\bar{y}+\bar{d}) \bar{\Delta}(\bar{y}+\bar{d})|\bar{x}-\bar{y}| \\
&+ \int d\bar{x}\, d\bar{y}\, \bar{\psi}_0(\bar{x})^2 \bar{\psi}_0(\bar{y}-\bar{d}) \bar{\Delta}(\bar{y}-\bar{d})|\bar{x}-\bar{y}|\Bigg) \\
&+ \mathcal{A}^2\Bigg(\int d\bar{x}\, d\bar{y}\, \bar{\psi}_0(\bar{x}) \bar{\psi}_0(\bar{x}-\bar{d}) \bar{\psi}_0(\bar{y}) \bar{\Delta}(\bar{y}+\bar{d})|\bar{x}-\bar{y}| \\
&+ \int d\bar{x}\, d\bar{y}\, \bar{\psi}_0(\bar{x}) \bar{\psi}_0(\bar{x}-\bar{d}) \bar{\psi}_0(\bar{y}) \bar{\Delta}(\bar{y}-\bar{d})|\bar{x}-\bar{y}| \\
&\quad + \int d\bar{x}\, d\bar{y}\, \bar{\psi}_0(\bar{x}) \bar{\psi}_0(\bar{x}+\bar{d}) \bar{\psi}_0(\bar{y}) \bar{\Delta}(\bar{y}+\bar{d})|\bar{x}-\bar{y}| \\
&+ \int d\bar{x}\, d\bar{y}\, \bar{\psi}_0(\bar{x}) \bar{\psi}_0(\bar{x}+\bar{d}) \bar{\psi}_0(\bar{y}) \bar{\Delta}(\bar{y}-\bar{d})|\bar{x}-\bar{y}|\Bigg)
\end{aligned}
\tag{3.46}
$$

The terms that are underlined exactly cancel with kinetic energy contributions at $\mathcal{O}(\delta)$, which are also underlined in Eq. (3.48). The contributions from the remaining terms contribute at most to $\mathcal{O}(\mathcal{A}^2\bar{d}^0)$ under the assumption that inter-baryon separation for the low-density baryon crystal (d) is large compared to the width of an individual baryon (w).

First note that since $\bar{\Delta}(\bar{x})$ is orthogonal to the baryon ground state, it can be written in the basis of excited baryon states. This further implies that $\bar{\Delta}(\bar{x})$ has a width that is necessarily larger than the width of a single baryon wave function $\bar{\psi}_0(\bar{x})$. Therefore, in effective charge densities of the form $\bar{\Delta}(\bar{x})\bar{\psi}_0(\bar{x})$ as in the third and fourth terms, the asymptotic behaviour of the charge density is dominated by the exponential tail of the single baryon wave function. Hence, the width of the effective charge density is comparable to that of the single baryon wave function.

The third and fourth terms contribute at most at $\mathcal{O}(\mathcal{A}^2\bar{d}^0)$. These terms involve a localized effective charge density, $|\bar{\psi}_0(\bar{x})|^2$, of total integrated baryon charge one localized at $\bar{x}=0$ and another charge density, $\bar{\psi}_0(\bar{y}\pm\bar{d})\bar{\Delta}(\bar{y}\pm\bar{d})$, with integrated charge density zero localized at either $\bar{y}=\pm\bar{d}$.

The last four terms do not vanish but contribute at least at $\mathcal{O}(\mathcal{A}^3)$. The effective charge densities that contribute are of the form $\bar{\psi}_0(\bar{x})\bar{\psi}_0(\bar{x}\pm\bar{d})$, which has an integrated baryon charge of magnitude $\mathcal{A}$, or of the form $\bar{\psi}_0(\bar{y})\bar{\Delta}(\bar{y}\pm\bar{d})$, which is dominated by the exponential tail of the single baryon wave function because as mentioned earlier $\bar{\Delta}(\bar{y})$ can be written in the basis of excited baryon wave functions, which are less localized than the single baryon wave function. Therefore, the contribution of last four terms is dominated by extra exponentials as the linear Coulomb potential $|\bar{x}-\bar{y}|$ present in each term cannot overcome the exponential suppression. Hence, the contribution of the last four terms can be ignored up to the order that is being considered here.

3.7.2 Interbaryon Potential Energy

Next, the terms that contribute to the interbaryon potential energy at $\mathcal{O}(\delta)$ is listed:

$$
\begin{aligned}
\frac{E^{\rm interbaryon}_{\rm potential}}{N_c} = -\frac{\mathcal{A}}{2}\Bigg(&\int d\bar{x}\, d\bar{y}\, \bar{\psi}_0(\bar{x})\bar{\psi}_0(\bar{x}+\bar{d})\bar{\psi}_0(\bar{y})\bar{\Delta}(\bar{y})|\bar{x}-\bar{y}| \\
&+ \int d\bar{x}\, d\bar{y}\, \bar{\psi}_0(\bar{x})\bar{\psi}_0(\bar{x}+\bar{d})\bar{\psi}_0(\bar{y}+\bar{d})\bar{\Delta}(\bar{y}+\bar{d})|\bar{x}-\bar{y}| \\
&+ \int d\bar{x}\, d\bar{y}\, \bar{\psi}_0(\bar{x})\bar{\psi}_0(\bar{x}-\bar{d})\bar{\psi}_0(\bar{y})\bar{\Delta}(\bar{y})|\bar{x}-\bar{y}| \\
&+ \int d\bar{x}\, d\bar{y}\, \bar{\psi}_0(\bar{x})\bar{\psi}_0(\bar{x}-\bar{d})\bar{\psi}_0(\bar{y}-\bar{d})\bar{\Delta}(\bar{y}-\bar{d})|\bar{x}-\bar{y}|\Bigg) \\
&+ \frac{\mathcal{A}^2}{4}\Bigg(\int d\bar{x}\, d\bar{y}\, \bar{\psi}_0(\bar{x})^2\bar{\psi}_0(\bar{y}+\bar{d})\bar{\Delta}(\bar{y}+\bar{d})|\bar{x}-\bar{y}| \\
&+ \int d\bar{x}\, d\bar{y}\, \bar{\psi}_0(\bar{x})^2\bar{\psi}_0(\bar{y}-\bar{d})\bar{\Delta}(\bar{y}-\bar{d})|\bar{x}-\bar{y}| \\
&+ \int d\bar{x}\, d\bar{y}\, \bar{\psi}_0(\bar{x}-\bar{d})^2\bar{\psi}_0(\bar{y})\bar{\Delta}(\bar{y})|\bar{x}-\bar{y}| \\
&+ \int d\bar{x}\, d\bar{y}\, \bar{\psi}_0(\bar{x}+\bar{d})^2\bar{\psi}_0(\bar{y})\bar{\Delta}(\bar{y})|\bar{x}-\bar{y}| \\
&+ \int d\bar{x}\, d\bar{y}\, \bar{\psi}_0(\bar{x}+\bar{d})^2\bar{\psi}_0(\bar{y}+\bar{d})\bar{\Delta}(\bar{y}+\bar{d})|\bar{x}-\bar{y}| \\
&+ \int d\bar{x}\, d\bar{y}\, \bar{\psi}_0(\bar{x}-\bar{d})^2\bar{\psi}_0(\bar{y}-\bar{d})\bar{\Delta}(\bar{y}-\bar{d})|\bar{x}-\bar{y}| \\
&+ \int d\bar{x}\, d\bar{y}\, \bar{\psi}_0(\bar{x})\bar{\psi}_0(\bar{x}-\bar{d})\bar{\psi}_0(\bar{y})\bar{\Delta}(\bar{y}-\bar{d})|\bar{x}-\bar{y}| \\
&+ 2\int d\bar{x}\, d\bar{y}\, \bar{\psi}_0(\bar{x})\bar{\psi}_0(\bar{x}-\bar{d})\bar{\psi}_0(\bar{y})\bar{\Delta}(\bar{y}+\bar{d})|\bar{x}-\bar{y}| \\
&+ 2\int d\bar{x}\, d\bar{y}\, \bar{\psi}_0(\bar{x})\bar{\psi}_0(\bar{x}+\bar{d})\bar{\psi}_0(\bar{y})\bar{\Delta}(\bar{y}-\bar{d})|\bar{x}-\bar{y}| \\
&+ \int d\bar{x}\, d\bar{y}\, \bar{\psi}_0(\bar{x})\bar{\psi}_0(\bar{x}+\bar{d})\bar{\psi}_0(\bar{y})\bar{\Delta}(\bar{y}+\bar{d})|\bar{x}-\bar{y}| \\
&+ \int d\bar{x}\, d\bar{y}\, \bar{\psi}_0(\bar{x})\bar{\psi}_0(\bar{x}-\bar{d})\bar{\psi}_0(\bar{y}-\bar{d})\bar{\Delta}(\bar{y}-2\bar{d})|\bar{x}-\bar{y}| \\
&+ \int d\bar{x}\, d\bar{y}\, \bar{\psi}_0(\bar{x})\bar{\psi}_0(\bar{x}+\bar{d})\bar{\psi}_0(\bar{y}+\bar{d})\bar{\Delta}(\bar{y}+2\bar{d})|\bar{x}-\bar{y}| \\
&+ \int d\bar{x}\, d\bar{y}\, \bar{\psi}_0(\bar{x})\bar{\psi}_0(\bar{x}-\bar{d})\bar{\psi}_0(\bar{y}-\bar{d})\bar{\Delta}(\bar{y})|\bar{x}-\bar{y}| \\
&+ 2\int d\bar{x}\, d\bar{y}\, \bar{\psi}_0(\bar{x})\bar{\psi}_0(\bar{x}-\bar{d})\bar{\psi}_0(\bar{y}+\bar{d})\bar{\Delta}(\bar{y})|\bar{x}-\bar{y}|
\end{aligned}
\tag{3.47}
$$

$$+\int d\bar{x}\, d\bar{y}\, \bar{\psi}_0(\bar{x})\bar{\psi}_0(\bar{x}+\bar{d})\bar{\psi}_0(\bar{y}-\bar{d})\bar{\Delta}(\bar{y})|\bar{x}-\bar{y}|$$
$$+2\int d\bar{x}\, d\bar{y}\, \bar{\psi}_0(\bar{x})\bar{\psi}_0(\bar{x}+\bar{d})\bar{\psi}_0(\bar{y}+\bar{d})\bar{\Delta}(\bar{y})|\bar{x}-\bar{y}|$$
$$+2\int d\bar{x}\, d\bar{y}\ \ \bar{\psi}_0(\bar{x})^2\bar{\psi}_0(\bar{y})\bar{\Delta}(\bar{y})|\bar{x}-\bar{y}|\Bigg)$$

It is quite obvious that most of the terms have the same form as the ones that contribute to the intrabaryon potential energy discussed in the previous subsection. The only ones that are different are the terms proportional to $-\frac{\mathcal{A}}{2}$. These terms have effective charge densities of the form $\bar{\psi}_0(\bar{x})\bar{\psi}(\bar{x}\pm\bar{d})$ and $\bar{\psi}_0(\bar{y})\bar{\Delta}(\bar{y})$. The former density has a total effective baryon charge of $\mathcal{A}$ centered around $\bar{x}=\mp\frac{\bar{d}}{2}$ and the latter term has an integrated charge of zero localized at $\bar{x}=0$. Therefore, under the assumption that baryon densities are parametrically small such that the width of a single baryon is much smaller than separation of baryons i.e. $\frac{w}{d}\ll 1$, contribution from these terms are at most $\mathcal{O}(\mathcal{A}^2\bar{d}^0)$.

3.7.3 Intrabaryon Kinetic Energy

$$\frac{E^{\text{kinetic}}_{\text{potential}}}{N_c}=\frac{\mathcal{A}}{2}\left(\int d\bar{x}\,\partial^2_{\bar{x}}\bar{\psi}_0(\bar{x})\bar{\Delta}(\bar{x}+\bar{d})+\int d\bar{x}\,\partial^2_{\bar{x}}\bar{\psi}_0(\bar{x})\bar{\Delta}(\bar{x}-\bar{d})\right) \tag{3.48}$$

Substituting our original Schrödinger equation in Eq. (3.2), and simplifying the

following result is obtained:

$$\frac{E_1^{kinetic}}{N_c} = +\mathcal{A}\Bigg[\underline{\int d\bar{x}\, d\bar{y}\, \bar{\psi}_0(\bar{x})^2 \bar{\psi}_0(\bar{y}) \bar{\Delta}(\bar{y}+\bar{d})|\bar{x}-\bar{y}|} \\ + \underline{\int d\bar{x}\; d\bar{y}\; \bar{\psi}_0(\bar{x})^2) \bar{\psi}_0(\bar{y}) \bar{\Delta}(\bar{y}-\bar{d})|\bar{x}-\bar{y}|} \\ - \bar{\epsilon}\left(\int d\bar{x}\, \bar{\psi}_0(\bar{x}) \bar{\Delta}(\bar{x}+\bar{d}) + \int d\bar{x}\, \bar{\psi}_0(\bar{x}) \bar{\Delta}(\bar{x}-\bar{d})\right)\Bigg]. \tag{3.49}$$

The underlined terms cancel with the corresponding terms in the intrabaryon interaction energy, which have also been underlined in Eq. (3.46). The last two terms disappear because $\bar{\psi}_0(\bar{x})$ and $\bar{\Delta}(\bar{x} \pm \bar{d})$ are orthogonal.

Therefore, the energy per unit cell is

$$\frac{\bar{E}}{N_c} = \frac{\bar{E}_0}{N_c} + \delta^2 \frac{\bar{E}_2}{N_c}, \tag{3.50}$$

where $\frac{\bar{E}_0}{N_c}$ is the leading order contribution, which stated in Eq. (3.45) and $\frac{\bar{E}_2}{N_c}$ is the energy at $\mathcal{O}(\delta^2)$. Contribution at $\mathcal{O}(\delta)$ are parametrically small.

Finally, a simple calculation with δ as the variational parameter shows that the energy per unit cell is minimized at $\mathcal{O}(\mathcal{A}^2 \bar{d}^0)$ when δ equals 0. This shows that the choice of $\bar{\phi}(\bar{x}) = \bar{\psi}_0(\bar{x})$ indeed minimizes the energy of the low-density baryon crystal up to the order to which this calculation was done.

Chapter 4: Saturated Nuclear Matter

4.1 Introduction

The problem of *saturated nuclear matter* in the combined heavy quark and large N_c limits of QCD is considered in this chapter [50]. The problem is analogous to the question of how protons and neutrons self-bind (without any external pressure) to form nuclei in the real world. As mentioned in the first chapter, the real world problem is impossible to study due to the fact that there are no known ways of solving real QCD at finite baryon density using either analytic methods or lattice-based methods. However, in the limit where quark masses are heavy compared to $\Lambda_{\rm QCD}$ and the 't Hooft large N_c limit, the problem is tractable. It is shown in this limit that stable, saturated nuclear matter exists in 3+1 dimensions.

The interactions that lead to saturation are the Pauli exclusion principle, which is a repulsive interaction and is leading order in N_c, and scalar glueball interaction, which is attractive and long-ranged but sub-leading order in N_c. Naively, one may think that the scalar glueball interaction and Pauli repulsion cannot compete with each other since the interactions are relevant at difference orders in the large N_c expansion. However, at parametrically low densities, the size of the leading order interaction (i.e. Pauli repulsion) decreases exponentially with baryon separation.

Therefore, at parametrically low densities, the Pauli interaction can be overcome by a sub-leading attractive interaction i.e. glueball exchange. It is shown in this chapter that the density at which nuclear matter saturates behaves as follows:

$$\rho_{\text{SNM}} \sim \frac{1}{\ln N_c} \ . \tag{4.1}$$

Saturated nuclear matter assumes the structure of either a face-centered cubic or a hexagonal-close packed structure. It is also found that remarkably, the density of saturated nuclear matter is independent of the lightest glueball mass and the coupling between a scalar-glueball and a baryon in the extreme large N_c limit, which will be carefully defined later in the chapter.

However, within the leading order approximations, it is not possible to find the energy of saturated nuclear matter. Each baryon can assume a particular spin-flavor structure. It interacts with other baryons via Pauli repulsion if and only if the baryons also have the same spin-flavor structure. Therefore, a set degenerate baryon crystals form in nuclear matter in the combined heavy quark-large N_c limit that is being considered here. However, these degenerate crystals still interact with each other at sub-leading order via scalar-glueball exchange and possibly other channels too. However, the nature of the interaction is highly non-trivial and as such the interaction energy can be determined for a crystal with baryons in the same spin-flavor structure but not the full nuclear matter problem. However, the energy scale of this interaction is small allowing us to accurately compute the density even though the precise energy is not computed.

4.2 Crystallization of Nuclear Matter through Glueballs

It has already been seen that baryon masses are of $\mathcal{O}(N_c m_q)$, where m_q is the quark mass. For 1+1 dimension, the baryon widths were calculated in the previous chapter and shown to be of $\mathcal{O}\left(\frac{1}{(\lambda m_q)^{\frac{1}{3}}}\right)$. Note that λ is the 't Hooft coupling and has dimension 2. However, in this chapter the relevant case is the one in 3+1 dimension, where baryon widths are of $\mathcal{O}\left(\frac{1}{\tilde{\alpha_s} m_q}\right)$, where $\tilde{\alpha}_s \equiv \frac{g^2 N_c}{4\pi}$ [28]. Nuclear matter forms even at leading order in N_c as long as external pressure is applied. Baryons are fermions and therefore, in the presence of other baryons (with the same quantum state) repel each other via Pauli repulsion, in such a way that the spatial state it assumes is maximally orthogonal to the neighboring baryons. Since the quarks and baryons are heavy, kinetic energies of these baryons are suppressed and therefore cyrstallization is inevitable. However, it is important to point out that crystallization also happens away from the heavy quark mass limit. e.g. Skyrme crystals. [51–55]. In the large N_c limit, the lightest particles are pions - they are pseudoscalar mesons and the channel is attractive and becomes parametrically large with decreasing separation between baryons and therefore saturation is bound to occur.

However, saturation or self-binding does not occur at leading order in the large N_c limit. Baryons repel each other and move infinitely apart unless there is an attractive channel binding the baryons. As mentioned earlier, this attraction occurs through the sub-leading effects in N_c, through the exchange of glueballs, which are the lightest particle in the spectrum of large N_c QCD with heavy quarks. This is

unlike large N_c QCD, where the pions are the lightest particles; however, in the heavy quark mass limit pions have masses of $\mathcal{O}(N_c^0 m_q)$. It will be assumed here that the lightest glueball is a scalar and also that it is not degenerate with vector glueballs, which are the source of repulsive interactions between baryons. Furthermore, it will be assumed that the interaction between baryons via glueball exchange is attractive and also at large distances exponentially large relative to interactions through any other channel.

In real QCD with $N_c = 3$, glueball states are not stable particles. The only theoretical method that is available to show the existence of glueball states is through the use of lattice-based methods [56] but in this context glueball states possess the same quantum numbers as mesons and therefore mix with meson states. As such the question of whether glueball states exist in real QCD is ill-posed.

However, in the heavy quark mass limit, mesons are known to have masses of $\mathcal{O}(m_q)$ and are therefore pushed out to infinity. Therefore, glueball states are well-defined in the large N_c limit as long as quarks are heavy. Furthermore, in the 't Hooft large N_c limit glueballs are stable and have decay widths that are suppressed and of $\mathcal{O}\left(\frac{1}{N_c^2}\right)$. It has also been shown in pure Yang-Mills (where the lightest glueballs are stable) that the lightest glueballs are parity positive scalars [57–59]. The results are derived using QCD inequalities and are completely model-independent. Strictly speaking, however, from a mathematical perspective, there is a possibility that the lightest scalar glueballs are degenerate with other glueballs, for example in the vector channel but under standard assumptions that symmetries are required for the presence of a degeneracy, such a possibility will be ignored here. This result

holds trivially also in the 't Hooft large N_c limit of QCD, further evidence for which comes from lattice calculations of glueball masses for a large number of colors (up to $N_c = 8$). [60, 61]. Therefore, there are extremely strong reasons to believe that the lightest glueballs in the combined large N_c and heavy quark limits will be scalar glueballs and that they are not degenerate with other glueballs.

4.3 The Toy Problem

In this section, the problem of finding the density of saturated nuclear matter in the combined heavy quark and large N_c limits is considered but only with baryons in a single spin-flavor structure. The physical problem involves putting a large number of baryons, assumed to be B, together in a total volume, which is V, at saturation. Another, assumption that will be made is that saturated nuclear matter consists of baryons that are hard spheres with each baryon occupying a spherical volume. Then density of saturated nuclear matter is determined by the following relation:

$$\rho_{\rm SNM} = \frac{B}{V/B} = \frac{1}{\frac{4\pi}{3P}\left(\frac{d_{\rm SNM}}{2}\right)^3} \ , \tag{4.2}$$

where $d_{\rm SNM}$ is the separation of nearest neighbor baryons at saturation and P is the packing factor. This factor is determined by the type of crystalline structure saturated nuclear matter assumes. This issue will be discussed later but first the separation, $d_{\rm SNM}$, between baryons at saturation will be determined by minimizing the energy per baryon.

In order to find this density, the explicit form of energy of nuclear matter has to be considered. First, only the toy problem will be considered since it is conceptually

simpler. The energy of nuclear matter, $E_{\rm NM}^{\rm toy}$, at sub-leading order in N_c, for the toy problem (and subsequently in the full problem) will be stated in terms of not dimensionful length, d. But instead the characteristic length scale in the problem, $\frac{1}{\tilde{\alpha}_s m_q}$, will be used to define the following dimensionless parameter:

$$\tilde{d} = \tilde{\alpha}_s m_q d \ , \tag{4.3}$$

where m_q is the quark mass (note that in the heavy quark mass limit, $\frac{m_q}{\Lambda_{\rm QCD}} \gg 1$) and $\tilde{\alpha}_s = \frac{g^2 N_c}{4\pi}$, is the strong coupling constant, which is of $\mathcal{O}(N_c)$.

The ground state energy (per baryon) in the toy problem consists of the following contributions:

$$\frac{E_{\rm NM}(\tilde{d})}{B} = \frac{E_{\rm Pauli}(\tilde{d})}{B} + \frac{E_{\rm gb}(\tilde{d})}{B} \ . \tag{4.4}$$

The first piece, $\frac{E_{\rm Pauli}}{B}$, encodes the Pauli repulsion between neighboring baryons as long as they possess the same spin-flavor structure. Also, note that this term is of $\mathcal{O}(N_c)$, which is not surprising since Pauli repulsion competes against attractive gluon interactions. These gluon interactions (between two baryons) involve N_c quarks from both states with an $\mathcal{O}(N_c^0)$ color-Coulomb potential but two interaction vertices, which are both of $\mathcal{O}\left(\frac{1}{\sqrt{N_c}}\right)$.

The form of the leading order piece via Pauli repulsion was calculated in Ref. [28]. Here, only the result is stated:

$$\frac{E_{\rm Pauli}}{B} = c_1 N_c m_q \tilde{\alpha}_s^2 \tilde{d}^p \exp\left(-c_2 \tilde{d}\right) \left(1 + \mathcal{O}\left(\frac{\ln \tilde{d}}{\tilde{d}}\right)\right) . \tag{4.5}$$

When this result was derived in Ref. [28], an interaction energy piece of relative order $\mathcal{O}\left(\frac{\ln \tilde{d}}{\tilde{d}}\right)$ was ignored. Also, here $c_1 = 00245881$. It is numerical factor that is

proportional to the potential energy of an isolated baryon. The other two numerical constants are $c_2 = 3.62275$ and $p = 7.0107$ and they depend on the overlap of neighboring baryon wave functions and since the densities are parametrically low, only the tails of the baryon wave functions contribute to c_2 and p.

The second piece in Eq. 4.4 is $E_{\rm gb}$. It is the interaction between two neighboring baryons at subleading order in N_c. This interaction, as discussed previously, occurs through the exchange of scalar glueballs. Since the exchanged particle is a scalar, it can be well-approximated through a Yukawa potential. Of course, this is only an approximation; had the baryon charge densities been delta functions (or point sources in position space), then the Yukawa potential would be exact. However, in this problem, the assumption is that nuclear matter saturates at parametrically low densities. Later it will be seen that this is self-consistently the case. But as long as this is true, the relative corrections due to the fact that baryons are not delta functions but have widths of $\mathcal{O}\left(\frac{1}{\tilde{\alpha}_s m_q}\right)$ are parametrically small, then using a Yukawa-like potential is indeed justified. The size of the relative corrections to the Yukawa potential is of $\mathcal{O}\left(\frac{1}{\tilde{d}}\right)$. Therefore, the explicit form of the potential is as follows:

$$\frac{E_{\rm gb}}{B} = -\tilde{g}_{\rm gb}^2 \frac{\exp\left(-\tilde{m}_{\rm gb}\tilde{d}\right)}{\tilde{d}} \left(1 + \mathcal{O}\left(\frac{1}{\tilde{d}}\right)\right) \ , \tag{4.6}$$

where $\tilde{m}_{\rm gb} \equiv \frac{m_{\rm gb}}{\tilde{\alpha}_s m_q}$ and $\tilde{g}_{\rm gb} \equiv \tilde{\alpha}_s m_q g_{\rm gb}$, with $g_{\rm gb}$ being a dimensionless coupling constant. Furthermore, note that the interaction is of $\mathcal{O}(N_c^0)$, which is down by a factor of N_c relative to the Pauli interaction energy.

It is important to point out that the two constants ($\tilde{m}_{\rm gb}$ and $\tilde{g}_{\rm gb}$) that de-

termine the glueball interaction energy are both unknown but of $\mathcal{O}(N_c^0)$. These can be determined through the use of lattice QCD at large values of N_c through extrapolation to the large N_c limit. For example, the mass of the lightest glueball is determined by the tail of the correlation function:

$$\langle 0|F^2(x)F^2(0)|0\rangle \tag{4.7}$$

at large x. Here, F is the gluon field strength tensor, which was defined in Chapter 1. Glueball masses have already been determined in terms of the fundamental string constant in Ref. [61].

However, the determination of $g_{\rm gb}$, the glueball-baryon coupling is slightly more challenging. In principle, it should be possible to extract the interaction energy between two heavy-quark baryons, which are a fixed distance apart. Since the size of the Pauli repulsion is already known from Eq. (4.5) and the lightest glueball mass is also known from Ref. [61], it should be possible to determine the glueball-baryon coupling.

Now, the energy per baryon in the saturated nuclear matter of the toy problem can be determined by minimizing the energy per baryon with respect to the dimensionless parameter $\tilde{d}$. The resulting equation is as follows:

$$(c_2 - \tilde{m}_{\rm gb})\,\tilde{d} - (p+1)\ln\tilde{d} + \ln\left(\tilde{m}_{\rm gb}\tilde{d}+1\right) - \ln\left(c_2\tilde{d}-p\right) = \ln\left(\frac{N_c c_1 m_q \tilde{\alpha}_s^2}{\tilde{g}_{\rm gb}^2}\right)\ . \tag{4.8}$$

In order to proceed, interaction energies of $\mathcal{O}\left(\frac{\ln\tilde{d}}{\tilde{d}}\right)$ are ignored since in deriving the Pauli interaction energy such terms were ignored. Therefore, the following equation

is obtained:

$$\tilde{d}^{\rm toy}_{\rm SNM}\left(1+\mathcal{O}\left(\frac{\ln\tilde{d}}{\tilde{d}}\right)\right)=\frac{1}{c_2-\tilde{m}_{\rm gb}}\ln\left(\frac{N_c m_q}{\Lambda_{\rm QCD}}\right)+\ln\left(\frac{\Lambda_{\rm QCD}c_1c_2\tilde{\alpha}_{\rm s}^2}{g_{\rm gb}^2 m_{\rm gb}}\right)\ . \tag{4.9}$$

Here, $\tilde{\alpha}_{\rm s}$ decreases logarithmically with increasing quark masses, c_1 and c_2 are constants that were calculated in Ref. [28] and the scalar glueball mass, $m_{\rm gb}$, is also known from Ref. [61]. Furthermore, the result also makes qualitative sense: the separation between neighboring baryons at saturation, $\tilde{d}_{\rm SNM}$, becomes smaller with larger glueball masses. This is expected since the range of interaction becomes smaller with increasing mass. Also, $\tilde{d}_{\rm SNM}$, decreases with increasing strength of coupling between the glueball and baryon ($g_{\rm gb}$). At any given separation, the strength of the interaction increases with the increase in size of coupling.

However, the size of the coupling constant is unknown and it seems that in general it is not possible to determine the separation of baryons. In order to proceed, the following approximation is made:

$$\left|\ln\left(\frac{N_c m_q}{\Lambda_{\rm QCD}}\right)\right|\gg\left|\ln\left(\frac{\Lambda_{\rm QCD}c_1c_2\tilde{\alpha}_{\rm s}^2}{g_{\rm gb}^2 m_{\rm gb}}\right)\right|\ . \tag{4.10}$$

In other words, the regime above is either the extreme large N_c limit of QCD or in the extreme heavy quark mass limit for both. Furthermore, if the quark masses are heavy enough such that $c_2\gg\tilde{m}_{\rm gb}$, the separation between baryons depends on the constant c_2 and logarithmically on the quark mass and the number of colors:

$$\tilde{d}^{\rm toy}_{\rm SNM}\approx\frac{1}{c_2}\ln\left(\frac{N_c m_q}{\Lambda_{\rm QCD}}\right)\ , \tag{4.11}$$

with the relative corrections that have the following orders:

$$\mathcal{O}\left(\frac{\ln\left(\frac{\Lambda_{\rm QCD}c_1c_2\tilde{\alpha}_{\rm s}^2}{g_{\rm gb}^2 m_{\rm gb}}\right)}{\ln\left(\frac{N_c m_q}{\Lambda_{\rm QCD}}\right)}\right)+\mathcal{O}\left(\frac{\tilde{m}_{\rm gb}}{c_2}\right)\ . \tag{4.12}$$

Now that the separation between baryons at saturation has been determined, the only quantity left to determine is the packing factor P. In order to determine the packing factor, it will be assumed that baryons form hard sphere with each sphere assuming a radius that is half the size of the separation between two baryons, i.e. $\frac{d_{\rm SNM}}{2} \equiv \frac{\tilde{d}_{\rm SNM}}{2\tilde{\alpha}_{\rm s} m_q}$.

The packing factor quantifies what fraction of space is occupied by baryons in saturated nuclear matter. The choice of this factor is further determined by what crystalline structure minimizes the total energy of the system. It also happens that this configuration is the densest possible. It was shown by Gauss (in 1831) that the largest possible packing factor for hard spheres has a value of:

$$P_{\rm max} = \frac{\pi}{\sqrt{18}} \ . \tag{4.13}$$

This factor is assumed by either a hexagonal close-packed structure or a face-centered cubic structure. If the packing factor is smaller than this i.e. $P < P_{\rm max}$, then on average baryons will be further apart. In fact from Eqs (4.4,4.5,4.6), it is possible to see that the energy of the baryons will be exponentially larger relative to when baryons assume the largest packing factor. Therefore, the density of saturated nuclear in the toy problem is as follows:

$$\rho^{\rm toy}_{\rm SNM} = \frac{\sqrt{2}\tilde{\alpha}_{\rm s}^2 m_q^3}{\tilde{d}^{\rm toy3}_{\rm SNM}} \approx \sqrt{2}\left(\frac{c_2 \tilde{\alpha}_{\rm s} m_q}{\ln\left(\frac{N_c m_q}{\Lambda_{\rm QCD}}\right)}\right)^3 \ , \tag{4.14}$$

where $c_2 = 3.62275$, m_q is the quark mass and $\tilde{\alpha}_s$ is a coupling constant defined as $\tilde{\alpha}_s \equiv \frac{g^2 N_c}{4\pi}$. Note that in this problem, the spin-flavor degeneracy of the baryons were ignored.

4.4 The Full Problem

In this final section, the full problem of saturated nuclear matter will be considered in the combined heavy quark and large N_c limit. The restriction that all baryons must assume the same spin-flavor structure is relaxed. In the mean-field approximation, the restriction that each state must be anti-symmetric in color and separately symmetric in spin-flavor and in space (for the ground state) means that each baryon must consist only of quarks in the same spin-flavor structure. Since quarks are spin-$\frac{1}{2}$, there are $2N_f$ possible ways of doing this. As mentioned previously, baryons with the same spin-flavor structure interaction via Pauli repulsion and all baryons (regardless of the spin-flavor structure) interaction via scalar glueball exchange. Therefore, nuclear matter in the full problem consists of baryons in the same spin-flavor configuration forming a crystal structure, in which attraction is due to glueball exchange and repulsion due to the Pauli effect. However, there are $2N_f$ copies of these structure that form in the full problem. These copies only interact via glueball exchange, which is an attractive channel and as such it is energetically favourable for them to sit on (or very closely on) top of each other. In this particular case, the energy density of the baryons is given by the following relation:

$$\frac{E_{\rm NM}}{B} = \frac{1}{B}\left(E_{\rm Pauli}(\tilde{d}) + 2N_f E_{\rm gb}(\tilde{d}) + E_{\rm D}\right) \ , \tag{4.15}$$

where $\tilde{d}$ was defined in Eq. (4.3).

The relation above is different from that of the toy problem in two ways. Firstly, there is an additional contribution to the the energy per baryon that arises

due to the attractive glueball exchange between baryons of different spin-flavor configurations that sit on (or nearly on) top of each other. However, this contribution cannot be determined easily. It must be of order unity but the precise form of this term depends not only on the properties of the lightest glueball but also on the details of the short-range interaction, which in principle may include other particles. In fact, it is not even known where exactly the baryon crystals will sit on top of each other. However, regardless of the details of the contribution, the term must be independent of baryon separation, d, as long as the separation between baryons is large. But it does depend on the width of the baryon charge, which is known to be of $\mathcal{O}\left(\frac{1}{\tilde{\alpha}_s m_q}\right)$.

Secondly, the glueball interaction between neighboring baryons of the same spin-flavor structure is also modified. Since there are $2N_f$ copies of baryon crystals that sit on (or nearly on) top of each other, the glueball exchange energy is larger than the toy problem by a factor of $2N_f$. The strength of the attractive channel is enhanced due to the fact that baryons of different spin-flavor structure can interact through glueball exchange.

Now, having defined the energy per baryon in the full problem, finally the density of saturated nuclear matter in the combined heavy quark mass and large N_c limits can be determined. This can be done in spite of the fact that the explicit form of the contribution coming from $\frac{E_D}{B}$ is unknown. However, since this contribution does not depend on d but depends on the width of the baryon charge, which is of $\mathcal{O}\left(\frac{1}{\tilde{\alpha}_s m_q}\right)$, the contribution is parametrically small compared to the contribution coming from the Pauli interaction and scalar glueball exchange between neighboring

baryons. Thus, the contribution can be ignored.

Finally, the density of the full problem can be determined simply using the analogous result in the toy problem with the following replacement:

$$g_{\rm gb}^2 \to 2N_f g_{\rm gb}^2 \ . \tag{4.16}$$

The replacement simply takes account of the fact that the scalar attraction is larger by a factor of $2N_f$ in the full problem. Therefore, using the exact same approximation that were considered in the case of the toy problem, which is also independent of the glueball-baryon coupling, it is found that the density of saturated nuclear matter is as follows:

$$\rho_{\rm SNM} = \sqrt{2}\left(\frac{c_2\tilde{\alpha}_{\rm s}m_q}{\ln\left(\frac{N_c m_q}{\Lambda_{\rm QCD}}\right)}\right)^3\left[1+\mathcal{O}\left(\frac{\ln\left(\frac{\Lambda_{\rm QCD}c_1c_2\tilde{\alpha}_{\rm s}^2}{2N_f g_{\rm gb}^2 m_{\rm gb}}\right)}{\ln\left(\frac{N_c m_q}{\Lambda_{\rm QCD}}\right)}\right)+\mathcal{O}\left(\frac{\tilde{m}_{\rm gb}}{c_2}\right)\right] \ , \tag{4.17}$$

where $c_2 \approx 3.62275$. However, as noted above, it is not possible to compute the energy per baryon of saturated nuclear matter within this approximation scheme. This contribution is dominated by the term $\frac{E_D}{B}$ but the short-range physics that determines this contribution is unknown.

4.5 Summary

In this chapter, the problem of saturated nuclear matter in the combined heavy quark mass and large N_c limits were considered. It was found that nuclear matter in this regime saturates due to competition between interactions at leading and sub-leading order in N_c, namely the Pauli repulsion and scalar glueball attraction respectively. This implies that while the nature of the interactions are analytic, the

density of saturated nuclear matter in not analytic in the N_c expansion. In fact, it was found that it goes logarithmically in N_c. Furthermore, there is an unknown parameter in the problem, which is the glueball-baryon coupling $g_{\rm gb}$. In the extreme large N_c limit or the extreme heavy quark mass limit, it was found that the density is independent of this quantity.

Bibliography

[1] M. A. Stephanov, PoS LAT2006 **024** (2006).

[2] These methods have been discussed previously in Ref. [19].

[3] For a review on the status of lattice QCD, see S.R. Beane, W. Detmold, K. Orginos and M.J. Savage, Prog. Part. Nucl. Phys., **66** (2011).

[4] A. Borici and A. Frommer, "QCD and Numerical Analysis III," (Birkhäuser, 2005)

[5] H.D. Politzer, Phys. Rept. **14**, 129 (1974).

[6] I.M. Barbour, S.E. Morrison, E.G. Klepfish, J. B. Kogut, M.P. Lombardo and UKQCD Collaboration, Nucl. Phys. B **60A** 220 (1998).

[7] I.M. Barbour, S.E. Morrison, E.G. Klepfish, J.B. Kogut and M.P. Lombardo, Nucl. Phys. Proc. Suppl. **60A**, 220 (1998).

[8] S. Hands, Nucl. Phys. Proc. Suppl. **106**, 142 (2002).

[9] H. Leutwyler, Ann. of Phys. **235**, 165 (1994).

[10] M. Alford, K. Rajagopal and F. Wilczek, Nucl. Phys. B. **537**, 443 (1999).

[11] S. Weinberg, Nucl. Phys. B, **363**, 3 (1991); S. Weinberg, Phys. Lett. B **251**, 288 (1990).

[12] E. Epelbaum, H. Krebs, and U-G. Meiner, Nucl. Phys. A **806**, 65 (2008).

[13] E. Epelbaum, W. Glöckle and U-G. Meißner, Nucl. Phys. A **747**, 362 (2005).

[14] P. Adhikari and T.D. Cohen, Phys. Rev. C **88**, 055202 (2013).

[15] E. Witten, Nucl. Phys. B **160**, 57 (1979).

[16] P. Adhikari, T.D. Cohen, A. Jamgochian and N. Kumar, Phys. Rev. C **87** 035205 (2013); arXiv:nucl-th/1212.2167 (2012).

[17] B. Bringoltz, Phys. Rev. D **79**, 105021 (2009).

[18] B. Bringoltz, Phys. Rev. D **79**, 125006 (2009).

[19] P. Adhikari, T.D. Cohen and I. Datta, Phys. Rev. C **89**, 065201 (2014).

[20] F. Wilzcek, Phys. Rev. Lett. **30**, 1343 (1973).

[21] G. 't Hooft, Nucl. Phys. B **72**, 461 (1974).

[22] G. 't Hooft, Nucl. Phys. B **75**, 461 (1974).

[23] For a review of large N_c QCD, see for example, A.V. Manohar, arXiv:hep-ph/9802419 (1997).

[24] For a different limit, where N_c goes to infinity with the ratio $\frac{N_c}{N_f}$ fixed, see G. Veneziano, Nucl. Phys. B **159**, 213 (1979).

[25] Baryons with quarks in the anti-symmetric representation is considered in T. D. Cohen, D. L. Shafer and R. F. Lebed, Phys. Rev. D **81**, 036006 (2010).

[26] The anti-symmetric representation was first considered in E. Corrigan and P. Ramond, Phys. Lett. B **87**, 73 (1993).

[27] For a discussion of relativistic large N_c baryons, see D.B. Kaplan and M.J. Savage, Phys. Lett. B **365**, 244 (1996).

[28] T.D. Cohen, N. Kumar and K. K. Ndousse, Phys. Rev. C **84**, 015204 (2011).

[29] The results presented in this chapter are published in Ref. [14]. Equations and the logical structure of the arguments presented here are similar to the ones in the published version.

[30] J. R. Klauder and E.C.G. Sudarshan *Quantum Optics*, (Benjamin, New York, Amsterdam, 1968).

[31] S. J. Brodsky, C.-R. Ji and G.P. Lepage, Phys. Rev. Lett. **51**, 83 (1983).

[32] D.M. Brink and Fl. Stancu, Phys. Rev. D **49**, 4665 (1994).

[33] M. Harvey, Nucl. Phys. A, **352**, 301 (1981).

[34] Blaizot, J-P, and Ripka, G. *Quantum Theory of Finite Systems*, (MIT Press, Cambridge, London, 1986).

[35] D.J. Thouless, Nucl. Phys. **21** (1960).

[36] J. P. Blaizot and H. Orland, Phys. Rev. C **24**, 1740 (1981).

[37] The results presented in this chapter are published in Ref. [16]. Equations and the logical structure of the arguments presented here are similar to the ones in the published version. Also, large portions of the chapter are borrowed verbatim from my PhD candidacy paper.

[38] I. Bars and M. Green, Phys. Rev. D **17**, 537 (1978).

[39] V. Schon and M. Thies, Phys. Rev. D 62, 096002 (2000); arXiv:hep-th/0003195; arXiv:hep-th/0008175.

[40] L.L. Salcedo, S. Levit and J.W. Negele, Nucl. Phys. B **361**, 585 (1991).

[41] R. Galvez, A. Hietanen and R. Narayanan, Phys. Lett. B 672, 376 (2009).

[42] T. Eguchi and H. Kawai, Phys. Rev. Lett. 48, 1063 (1982).

[43] F. Lenz, H.W.L. Naus and M. Thies, Annals of Physics 233, 317-373 (1994)

[44] L. G. Yaffe, Rev. Mod. Phys. 54, 407-435 (1982).

[45] M.R. Douglas, Nucl. Phys. Proc. Suppl. **41**, 66 (1995).

[46] M. Unsal and L.G. Yaffe, Phys. Rev. D **78**, 065035 (2008).

[47] T. Kojo, T. Hidaka, L. McLerran and R.D. Pisarski, Nucl. Phys. A, **843**, 37 (2010).

[48] G. Basar, G.V. Dunne and D.E. Kharzeev, Phys. Rev. Lett. **104**, 232301 (2010).

[49] E.J. Ferrer, V. de la Incera and A. Sanchez, Acta Physica Polonica B Proceedings Supplement, **5** (2012).

[50] The results presented in this chapter are published in Ref. [19]. Equations and the logical structure of the arguments presented here are similar to the ones in the published version.

[51] I. Klebanov, Nucl. Phys. B, **262**, 133 (1985).

[52] T.S. Walhout, Nucl. Phys. A, **484**, 397 (1988).

[53] A.D. Jackson and J.J.M. Verbaarschot, Nucl. Phys. A, **484**, 419 (1988).

[54] M. Kugler, and S. Shtrikman, Phys. Lett. B, **208**, 491 (1988).

[55] L. Castillejo, P.S.J. Jones, A.D. Jackson, J.J.M. Verbaarschot and A. Jackson, Nucl. Phys. A **501**, 801 (1989).

[56] See for instance the following paper and references therein, E. Gregory, A. Irving, B. Lucini, C. McNeile, A. Rago, C. Richards and Rinaldi, JHEP **10**, (2010).

[57] G. B. West, Phys. Rev. Lett. **77** (1996).

[58] I.J. Muzinich and V.P. Nair, Phys. Rev. Lett. **178** (1986).

[59] For a review, see S. Nussinov and M.A. Lampert, Phys. Rept. **362**, 193 (2002).

[60] S. Dalley and B. van de Sande, Phys. Rev. Lett. **82**, 1088 (1999).

[61] B. Lucini, M. Teper and U. Wenger, JHEP, **6** (2004).